VALIDITY OF THE COSSERAT THEORY FINITE ELEMENT IMPLEMENTATION FOR JOINTED ROCK MODELLING

Irina S. Korosteleva

Master of Science Thesis

Delft 2017

TU Delft Delft University of Technology

Challenge the future

Validity of the Cosserat theory finite element implementation for jointed rock modelling

MSc Thesis

by

Irina S. Korosteleva

to obtain the degree of Master of Science

at the Delft University of Technology,

to be defended publicly on 29 August 2017 at 13:30 PM.

Student number:	4508920	
Project duration:	November 1, 2016 – August 29, 2017	
Thesis committee:	Dr. P.J. Vardon,	TU Delft, supervisor
	Prof. dr. ir. L.J. Sluys,	TU Delft
	Prof. dr. M.A. Hicks,	TU Delft
	Ir. W.P. Kikstra,	DIANA FEA
	Dr. G.J. Schreppers,	DIANA FEA

TU Delft

Abstract

Significant part of geotechnical engineering projects involve the problems related to jointed rock masses. For example, construction of tunnels in rock or stability analysis of the rock slopes. In this framework, the finite element modelling is often used for problems with complex geometries or where the analytical solution is difficult to obtain. Finite element analysis for jointed rocks could be conducted by means of several techniques. For instance, the introduction of interface elements could be used to consider the stratified nature of a material (explicit joint model). Another possible approach is to employ an equivalent continuum, where discontinuities are included implicitly. In the current thesis, one of such equivalent continuum methods based on the Cosserat theory was explored. This method is characterised by two features: additional degrees of freedom, typically referred to a microrotations, and an internal length parameter. Microrotations provide information related to the orientation of the material layers, and the internal length parameter defines the size of the representative elementary volume, which depends on the layer thickness.

The purpose of this research is to evaluate the validity of the Cosserat finite element model for the modelling of joined rock. To do so, the Cosserat formulation for the analysis of elastic and plastic deformation was implemented in DIANA FEA software. As the Cosserat theory belongs to smeared models, the influence of the ratio between the geometric dimension of the model and the layer thickness was studied and compared with the explicit joint model. The convergence rate of the Cosserat finite element model was assessed and slower rate was observed under shearing conditions. Additionally, we studied the effect of different boundary conditions for the microrotations on the mechanical response of the model. The plastic analysis permitted to investigate the influence of the material parameters on the area of displacements localization. Furthermore, the performance of the tension cut-off algorithm based on mean stress was measured. Finally, the implemented formulation was applied for the slope stability assessment.

The conducted research confirmed the validity of the Cosserat finite element formulation. In order to make it fully available for the geotechnical applications, recommendations for further improvements were proposed. Mainly, they are related to the introduction of higher order shape functions for the microrotations and alternative tension cut-off algorithm.

Preface

This thesis is the final work of my studying at the Delft University of Technology, Geoengineering Program. During this period I was able to focus on a particular topic which subsequently filled in some missing pieces in my understanding of the numerical modelling bases. Throughout my studying in the TU Delft university I have gained not only extensive knowledge but also had a chance to be a part of the academic community again. This period certainly influenced the decision regarding my future occupation.

I would like to express my gratitude to university graduation committee, Phil Vardon, Michael Hicks, Bert Sluys for their collaboration and guidance during this time. I appreciate your sharing with me your knowledge and experience and your thoughts on what you would like to be included in the project.

Additionally, I would like to thank DIANA FEA company for the granted opportunity to see the "reality" of the numerical modelling and giving me the freedom to make my own choices during the work. I acknowledge the valuable comments and positive critic given by Dr. Gerd-Jan Schreppers. Wijtze Pieter, I admire your patience in answering all my questions and I appreciate your encouragement and support during that journey.

Irina S. Korosteleva
Delft, August 2017

Contents

1

Introduction

Numerical methods are a branch of mathematics which over the past years have found vast applications in solving engineering problems. Just to name few of them: structural mechanics, environmental engineering, geotechnics, etc. Numerical methods are usually presented in the form of finite element code and delivered to the final user as a commercial finite element software. It is usually used for the problems with complex geometries or where an analytical solution is difficult to derive. Additionally, continuing demand for resources saving requires a highly efficient and accurate technical design making sophisticated calculations method more competitive. At the same time, constantly growing computational power makes it possible to cover more problems which could be solved by the numerical methods due to the implementation of more complex algorithms and improvement of the existing ones.

Definitely, the area of geotechnics has a lot of tasks which often could be solved just with aid of numerical modelling. That is related to the inherent properties of the geomaterials, for instance, non-linear behaviour, heterogeneity and presence of imperfections. One such example is layered materials e.g. stratified materials or jointed rock. Usually, joint acts as a weakened zone governing the behaviour of the material. That is why it becomes crucial to introduce them in the numerical model. There are two main approaches including joints, either explicitly employing intact material and individual joints separately (explicit joint method) or adopting an equivalent continuum models where the joints are smeared across the rock mass (implicit method). The former method requires the usage of the interface elements to reproduce the deformation along the joints. The latter considers the joints implicitly, for instance by building the additional parameters which describe the dimension and material properties of layers in the constitutive model. Moreover, the suggested formulation should be able to provide with an ability to represent deformations caused by joints movement. One of the proposals on how to tackle that matter is to induce the Cosserat theory. Alternative solutions would be presented later on in the thesis.

Cosserat theory was formulated by the Cosserat brothers [11] at the beginning of the XX century. However, it was not appreciated at that time but was reappraised in the 1990s, resulting in extensive research which is still ongoing nowadays. It is also referred to as the micro-polar theory and included in the family of solutions used if localization phenomenon occurs. The essential feature of the Cosserat finite element formulation is the presence of the non conventional primary variables called microrotations. This characteristic brings additional advantage when a jointed rock is modelled since it coincides with the physical behaviour of the layers. More specifically, depending on

the layers dimension and stiffness they can bend, thus part of the load could be sustained by the layers bending resistance. That mechanism is not available in standard continuum formulation, but is a part of the Cosserat formulation.

1.1. Problem statement

The Cosserat theory was extensively applied for modelling of granular material. The development of the Cosserat theory in relation to granular materials has been carried out by Vardoulakis and Mühlhaus [30], De Borst [15], [14]; here it was mainly applied for the objective modelling of shear bands. Static and dynamic loading was considered by by De Borst and Sluys [17]. In the mentioned works, there is a detailed finite element derivation which makes it attractive for the implementation. Regarding the application of the Cosserat theory for the jointed rock modelling there are important works conducted by Mühlhaus [23], Adhikary and Dyskin [5]. Here, the modified constitutive relationship is introduced, essentially, it is based on the transverse isotropic model with additional coefficients for the curvatures. It is more advantageous to use the constitutive model with incorporated layers for models with a large number of joints, because it is unfeasible to model each of them separately. The elasticity matrix used in the present research is a function of intact rock elasticity parameters, joints normal and shear stiffnesses and joints spacing [34]. For the Cosserat model this constitutive relationship brings another advantage, namely, the layer thickness could be used as a internal length characteristic. Although it should be extended with additional relationship between curvatures and couple stresses in a way analogous to the plates theory.

Literature review has shown that the Cosserat finite element formulation is extensively presented for granular materials, but in less details for layered materials, especially the plastic formulation. Furthermore, examples which are used for the verification usually contain only horizontal layers. Models with inclined layers are considered by Riahi in [38] for the elastic case and in [37] for the plastic one. In these examples the non-linear behaviour was modelled, using the Mohr Coulomb failure criterion.

According to the author's knowledge which is based on the conducted literature review, there is a lack of numerical examples for models with inclined layers, especially examples which include a non-linear analyses. Additionally, the finite element formulation does not include all derivation details explicitly which are important for the jointed rock analysis. For example, the tension algorithm is addressed quite shortly. Essential uniqueness of the present research is a combination of the well-defined Drucker-Prager plasticity formulation, which was acquired by De Borst [15] and validated for granular materials, and transverse isotropic constitutive relationship. Drucker-Prager failure criterion is a fair approximation of the Mohr Coulomb criterion. On the one hand, it accounts for the pressure dependency and material dilatancy, on the other hand, it has less complicated for the implementation cone-shaped yield surface, which makes it attractive for the academic purposes. The Cosserat finite element formulation with the transverse isotropic constitutive model has just been employed in the model with the Mohr Coulomb failure criterion. The advantage of the relatively simple plasticity formulation with the Drucker-Prager yield criterion was taken to investigate the applicability of the Cosserat theory for the modelling of jointed rock. The aim of the present study is to investigate the aspects of the Cosserat finite element formulation which should be considered while applying it for the jointed rock analysis and the following research question was formulated:

Is Cosserat theory valid for modelling of jointed rock?

In order to guide the research two major sub-questions were highlighted:

- *What is the effect of the Cosserat parameters on the elastic numerical solution?*
- *Which aspects of the Cosserat formulation should be considered while conducting non-linear analysis?*

Essentially, answering to these questions would allow assessing the validity of the Cosserat theory for the jointed rock modelling.

1.2. Methodology

Currently there is no software where the Cosserat finite element formulation is open for external users. DIANA FEA software became the platform for its implementation, then it was used to answer the above questions. The present research has been carried out according to the following methodology:

- Develop and verify the elasticity Cosserat finite element formulation in the DIANA FEA software.
- Investigate the influence of the Cosserat finite element parameters on the numerical model.
- Implement the plastic Cosserat finite element formulation in the DIANA FEA software.
- Define the essential benchmark models for the plasticity code verification and confirm the validity of the Cosserat finite element formulation.
- Explore the effect of the Cosserat parameters while performing non-linear analysis.
- Consider relevant geotechnical problems with a jointed rock for the validation of the implemented Cosserat finite element formulation.

1.3. Report structure

The summary of the report structure is presented below. **Chapter 2** gives the brief introduction into existing methods for jointed rock modelling, together with alternative to the Cosserat theory localization techniques. Micro-polar continuum review with the governing equations and constitutive model explored in **Chapter 3**. In the same chapter Cosserat finite element formulation including plasticity used in this thesis is introduced. The verification of the elastic model and investigations regarding the Cosserat additional degrees of freedom and material parameters are presented in **Chapter 4**. **Chapter 5** shows the validation of the developed algorithm for Cosserat non-linear analyses using one element and jointed column models. Afterwards, the effect of material parameters on the localization zone is discussed. **Chapter 6** is dedicated to the application of the Cosserat formulation for the slope stability analysis. Furthermore, each chapter includes the description of the relevant issues and possible solutions. **Chapter 7** consists of conclusions drawn from the accomplished research and recommendations for the further improvements. The **appendices** include additional derivations and examples of the input files for DIANA FEA software.

2

Literature review

Long history of the formation and surrounding conditions make rock mass a complicated material for modelling. Rock is usually discontinuous, inhomogeneous, anisotropic and non-elastic (DIANE) [24]. It experiences constant changing of the properties and structure over time. For instance, the tectonic movements, weathering, porosity contribute not only to the overall non-linear behaviour but also originate the anisotropy, formation of discontinuities and fractures. Example of this rock type could be observed in Figure(2.1). The described material impurities often govern global structural behaviour, thus it is required to consider them in the numerical models. The aim of the current chapter is to give a brief review of the existing rock mass modelling techniques.

2.1. Rock mass modelling techniques

According to Jing [25] there are three main groups of numerical methods which are nowadays used for modelling of rock:

- Continuum methods - FDM (Finite difference method), FEM (Finite element method) , BEM (Boundary element method);
- Discrete methods - DEM (discrete element method), DFN (discrete fracture network) method;
- Hybrib continuum methods.

Among continuum methods, FEM is a widely applied method today. The most famous technique for the modelling of jointed rock was proposed by Goodman *et al.*[21]. The main idea of this method is the introduction of the additional elements called interfaces. This type of element has assigned normal and shear stiffnesses and considered to have infinity small thickness. It is still used to represent the joints in a material, however the model for a densely jointed rock mass could easily become complex due to a huge amount of elements. Furthermore, element size of the model is constrained by the dimension of the joint. For example, elements could not be larger than the layer thickness. Owing to the availability in most of the commercial software and rather simple handling, this method was used for the verification in the current research. Another continuum approach which considers a localized deformation field, which often occurs along the joints, is known as an equivalent continuum approach. Its main characteristic is that the localization of deformations is

Figure 2.1: Example of the rock mass with discontinuities, heterogeneous material and characteristics of the anisotropy

induced by means of enchantment of the standard continuum with additional features or by employment of generalised theories. One of them is called the Cosserat theory and it was used in the present research. A quick overview of another localization techniques is given below.

BEM is a numerical computation method where linear partial differential equation is formulated as an integral equation and then solved. It is not as efficient as FEM and has limited amount of applications. For instance, BEM has difficulties in dealing with heterogeneous materials and less efficient in simulating non-linear behaviour.

The main idea of the discrete methods is to represent the medium as a set of rigid or deformable bodies with defined and continuously updated contacts. It was originated by Cundall [13] and found extensive application in rock modelling, for instance UDEC code is based on that approach [12]. In the explicit version of DEM method a rock mass is considered as an assemblage of the non-deformable or deformable blocks which interact with each other. The DFN method is a discrete model that includes fluid flow. For more information about that technique, please see [27]. As for hybrid models, they are a combination of approaches, for instance FEM/BEM, to consider deformations and flow problems at the same time.

2.2. Smeared models

In the equivalent continuum approach discontinuities are smeared across the continuum. In order to define the representative elementary volume, the internal length parameter is introduced. There are three general approaches for enhancing the conventional continuum with the internal length characteristic [16]:

1. Non-local models or gradient continuum models;

2. Rate-dependent models (valid for high loading rates);

3. Micro-polar theory.

The concept of the non-local models is to introduce the influence of the neighbouring points to each point of the space. Theoretically, the stress at the point can be influenced by stress history of the entire body, but this effect alleviates with the distance from the point. In other words, the length parameter above which the behaviour of the material becomes non-local exists. Firstly, this theory was applied to model the behaviour of the fractured concrete [8]. The affected area acts as the characteristic length and defines the contribution of each element to the behaviour of surrounding elements. Schweiger *et al.* [41] pointed out that the element size and the internal length should be at least equal in all directions. Otherwise, if the internal length is smaller than the element size there is no contribution from the neighbouring elements. Non-local theory was applied to model jointed rock mass by Chen and Bažant [10] and was successfully validated for several triaxial test experiments.

Gradient dependent theories departure form non-local models and include the dependency of the yield stress on the gradients of internal variable, for instance plastic strain gradient. It is sufficient to consider the relationship between yield stress and plastic strain for a homogeneous material; but when shear bands or other localization of the plastic strains occur this dependency fails to capture the heterogeneous pattern [29]. Suggesting second-order derivatives, the yield function becomes dependant on the derivative of the plastic strain $f = f(\sigma, \gamma^p, \nabla^2\gamma^p)$. This gradient term supplies the conventional model with information on the material behaviour on the next smaller length scale. That is how the influence from neighbouring points is introduced. This approach is applicable for decohesion (Mode-I) and frictional (Mode-II) failures. Hence, the mentioned theory requires additional degree of freedom on the global level and additional material parameters, which cannot be directly derived from an elementary laboratory tests.

Rate dependant models allow introducing implicitly the length scale parameter without constitutive model modification. For the rate-independent solids the stress-strain relationship is usually defined in the incremental form. Furthermore, the material shear stiffness in the plastic region is a function of a strain. The consequence of that dependence was illustrated by Needleman [32]; he pointed out that if the bifurcation phenomenon occurs the condition for the solution being unique is the vanishing of the shear stiffness. The latter is the feature of the material softening which is not always the reason for the localization phenomenon [40]. In opposite, for the rate-dependant materials the plastic strain rate is formulated in aa way that it depends only on the absolute value of the stress and not on its increment. Taking into consideration this difference Needlman [32] has also shown that for the rate dependant models the initiation of the localization is possible for the positive shear stiffness and scale parameter (for instance, imperfection parameter) is used to ensure the uniqueness of the solution and determined shear band width.

Cosserat or micro-polar theory was firstly introduced in the beginning of the XX century by the Cosserat brothers [11]. Although, it was not appreciated at that time due to lack of natural interpretation of the microrotation variable which was an additional degree of freedom together with translational deformations. These microrotations do not always coincide with structural rotations and describe the orientation of the material particles which could change significantly under certain conditions. In the 1970s a new interest arose to the micro-polar theory again, a number of scientists such as Mühlhaus and Vardoulakis [30] Borst and Mühlhaus [16] based their analysis of material microstructure on it. Main features of that theory are the introduction of the internal length characteristic in the constitutive model and adding explicit equilibrium condition for the shear stresses. The latter is achieved with implementation of the micromoments also called couple stresses or moment stresses. Consequently, the Cauchy assumption that shear stress are symmetric vanishes. Con-

sequently, conventional kinematic variables such as displacements and strains are extended with microrotations and their gradients (curvatures). They have the physical meaning and referred to the ability of particles to rotate changing its orientation on the microscopic level. Another example comes from the stratified material where each layer is enabled to bend and twist. There are several successful examples of the jointed rock models using Cosserat theory, for instance Adhikary and Dyskin [5], Riahi and Curran [39]. It should be noted that micro-polar theory is valid for the failures where friction between particles determines the stability of the material making it inappropriate for Mode-I failures. As well as gradient theory it requires additional degree of freedom (rotation), however minor changes are required for finite element framework.

In the current work the Cosserat theory was used in order to model the jointed rock. Discontinuities thickness and elastic parameters were taken into account by means of the transverse isotropic constitutive model. Moreover, it was extended with additional coefficients in order to consider microrotations degrees of freedom.

3

Micro-polar continuum

3.1. Directed continuum review

Directed continuum is a generalized form of continuum mechanics which covers cases when classical continuum mechanics based on Cauchy assumptions is not valid. For instance, the generally accepted idea to represent the set of material points in Euclidean space fails for materials which tend to have the localized deformation field. Jointed rock is one of such materials, because displacements are often governed by weak zones. There were some scientists in the past e.g. Toupin [36], Koiter [26], Eringen [19] who specified the importance of generalizing the classical continuum mechanics approach.

The importance of microscopic material behaviour was considered when it was observed that global response depends on it. For instance, the development of shear bands in the soil. In Figure (3.2b) it is clearly seen that particles, which lay on the shear band determine the response of the specimen due to the loading. They are oriented and distributed in a distinct way form surrounding particles which are not involved in the shearing mechanism.

In classical continuum mechanics a body is a set of material points occupying a particular space at each moment in time. The assumption was made that each material point is infinitely small and homogeneous. That implies the fact that the material microstructure would not possible be to observe while zooming in this body. For a large class of materials this assumption is valid. For instance, if a homogeneous material is loaded in a way that excludes localized shearing, then the behaviour of each material point is similar to each other. In contrast to that, continua with microstructural “parameters" allows to distinct the microscopic order of particles. These parameters are called directors and were firstly used to describe deformable body by the Cosserat brothers [11]. Directors define the direction of each material point; it is able to stretch and rotate *independently*. Therefore, the deformation in directed continua consists of material point displacements and directors enchaining it with the ability to rotate. Before showing how directors work, the physical and mathematical bases for them would be emphasised.

In mechanics the motion is described by Euler’s balance of momentum and balance of moment of momentum:

$$F = \int_V \rho \mathbf{f} dV + \int_S \mathbf{t} dS \tag{3.1}$$

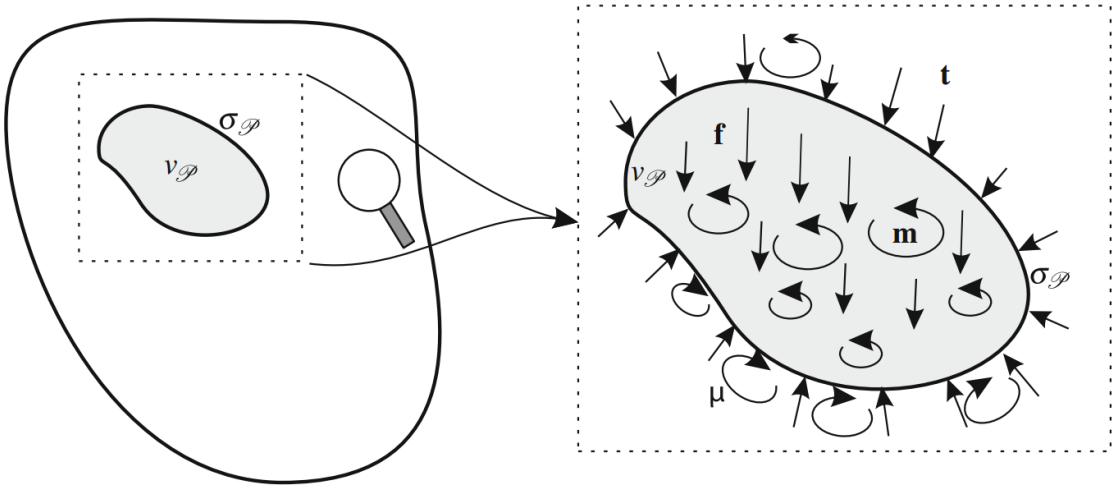

Figure 3.1: Forces and couples acting on a body part $\mathscr{P}$ [18]

$$M = \int_V ((\mathbf{r}-\mathbf{r}_0)\times\rho\mathbf{f}+\rho\mathbf{m})dV + \int_S ((\mathbf{r}-\mathbf{r}_0)\times\mathbf{t}+\boldsymbol{\mu})dS \tag{3.2}$$

where ρ is the material density, $\mathbf{r}$ is the position vector in the current configuration, $\mathbf{f}$ and $\mathbf{m}$ are body forces and couples per unit mass and $\mathbf{t}$ and $\boldsymbol{\mu}$ are traction and couple torque, graphical illustration is shown in Figure (3.1). The first step is to apply the divergence theorem to the symmetrical part of the stress term in equations (3.1) and (3.2):

$$\int_S (\mathbf{r}\times\mathbf{t})dS = \int_S (\boldsymbol{r}\times(\boldsymbol{\sigma}^{\boldsymbol{T}}\boldsymbol{n}))dS = \int_V (\boldsymbol{r}\times\nabla\boldsymbol{\sigma}^{\boldsymbol{T}}+\boldsymbol{\varepsilon}:\boldsymbol{\sigma})dV, \tag{3.3}$$

where in index form:

$$\boldsymbol{\varepsilon}:\boldsymbol{\sigma} = \varepsilon_{ijk}\boldsymbol{\sigma}_{jk}\boldsymbol{e}_i\otimes\boldsymbol{e}_j\otimes\boldsymbol{e}_k. \tag{3.4}$$

Secondly, the momentum equilibrium condition should be considered:

$$\nabla\boldsymbol{\sigma}^{\boldsymbol{T}}+\rho\boldsymbol{f} = 0 \tag{3.5}$$

Finally, by inserting the (3.3) and (3.5) into (3.2) the balance of moment of momentum could be expressed as:

$$\int_V (\rho\boldsymbol{m}+\boldsymbol{\varepsilon}:\boldsymbol{\sigma})dV + \int_S \boldsymbol{\mu}dS = 0 \tag{3.6}$$

Considering the fact that $\boldsymbol{\mu} = \boldsymbol{c}^{\boldsymbol{T}}\boldsymbol{n}$, where $\boldsymbol{c}$ is a couple stress, (3.6) could be written as follows:

$$\rho\boldsymbol{m}+\boldsymbol{\varepsilon}:\boldsymbol{\sigma}+\nabla\boldsymbol{c}^{\boldsymbol{T}} = 0 \tag{3.7}$$

It is seen that if body couples $\boldsymbol{m}$ and couple stresses $\boldsymbol{c}$ are not equal to zero than the term $\boldsymbol{\varepsilon}:\boldsymbol{\sigma}$ is also not necessarily zero implying the fact that the total stress tensor is non-symmetric. On the other hand, in classical continuum mechanics Cauchy assumption in the absence of couples and couple stresses is true and the only requirement for the equilibrium of moment of momentum is the symmetric stress tensor

$$\sigma_{ij} = \sigma_{ji}. \tag{3.8}$$

Body forces are related with body loads which act on each material point independently. For instance, the gravity load of the material or external load applied to the body. Couples are represented by a contact load which is referred to the interaction with remaining part of the body. The moment

generated by the parallel forces which have the same magnitude but applied in the opposite directions is the source of the couples. That implies the fact that they add only turning effect and does not contribute to the force balance. Hence, in the classical continuum mechanics it is assumed that all moments arise only from the forces and the body couples are neglected.

However, there are some cases when couples and couple stress should be considered. For instance, during shear band development the microscopic behaviour of a material plays the principal role. Oda *et al.* [33] has conducted the studying of material behaviour on microscopic level. Figure (3.2) shows the results of experiment. Experimental data reveals the significant rotation of the particles located into the shear band. Furthermore, it proves that not only forces but also moments were transmitted through the particles. It is clear, that reaching peak stress state Figure (3.2a), particles are mainly compressed without changing the orientation. Although, the material structure in residual state Figure (3.2b) shows that when particles start to roll over each other the reorientation along the shear band is observed. It should be mentioned that particles rotation takes place during shearing and becomes negligible under uniform compression. Another important remark made in [7] is related to the interpretation of this microrotations. In the above example and micro-polar theory itself two different levels of deformation exist: macrolevel where the translational deformation occurs on structural level and microlevel where the microrotations of particles happen on continuum level. To consider microrotations additional rotation degree of freedom together with translations should be added. That is where the directors mentioned in the beginning of this chapter is taken into account. Essentially, they provide information about the continuum orientation based on the micro-rotation of the particular material point. It should be emphasised that these micro-rotations are different from the classical mean rotation of the structure. In order to show that consider the deformation tensor as:

$$\gamma_{ij} = u_{i,j} - e_{ijk}\theta_k \tag{3.9}$$

where symmetrical part is identical to classical strain definition:

$$\gamma_{(ij)} = \frac{1}{2}(u_{i,j} + u_{j,i}) \tag{3.10}$$

and anti-symmetrical part as:

$$\gamma_{[ij]} = \frac{1}{2}(u_{i,j} - u_{j,i}) - e_{ijk}\theta_k \tag{3.11}$$

Classical definition of the rotation is distinguished in (3.11), $\omega_z = \frac{1}{2}(u_{i,j} - u_{j,i})$. Anti-symmetric part of the deformation tensor in vectorial notation is expressed as:

$$\boldsymbol{\gamma}^{\boldsymbol{A}} = \boldsymbol{\omega} - \boldsymbol{\theta} \tag{3.12}$$

pointing out the difference between classical structural rotation and microrotation. Finally, the equilibrium of forces and moments derived from (3.1) and (3.2) was used as governing equations in the finite element formulation:

$$\begin{aligned} \sigma_{ij,i} + f_i &= 0 \\ m_k + \mu_{kj,j} + e_{kij}\sigma_{ij} &= 0 \end{aligned} \tag{3.13}$$

where m is the body couple moment and μ is the couple stress (Cosserat couple stress). It should be noted that eq. $(3.13)_2$ introduces non-symmetric stress tensor.

3.2. Constitutive model

Except the governing equations (3.13) the constitutive relationship between stresses (σ) and strain (γ) and couple stresses (μ) and curvatures (κ) is required to set up the Cosserat finite element for-

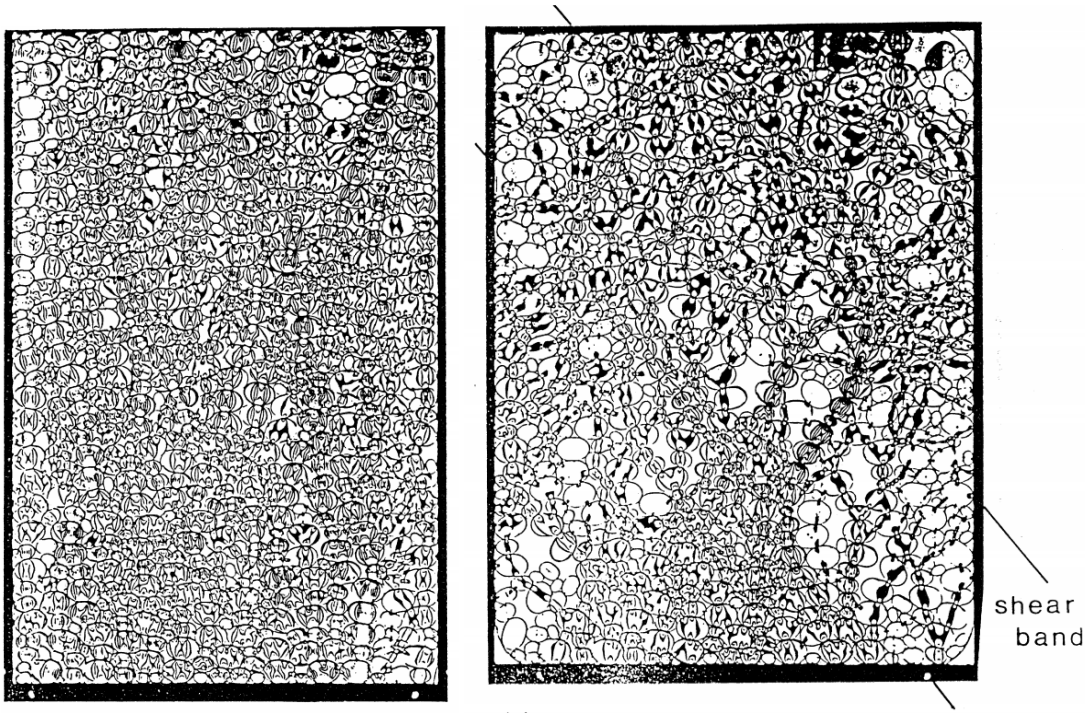

(a) Peak stress state (b) Residual stress state

Figure 3.2: Photoelastic pictures taken at the peak stress state and the residual stress state [33]

mulation. The measure of the strain in the Cosserat theory is expressed as:

$$\gamma_{ij} = u_{i,j} - e_{ijk}\theta_k \tag{3.14}$$

where θ is the rotations vector, u is the vector of displacements and γ is the strain vector. Volumetric strains have the same formulation as in the conventional continuum mechanics and the shear strains are added with rotations as follows:

$$\begin{aligned}
\gamma_{zy} &= \frac{\partial u_y}{\partial z} + \theta_x, \quad \gamma_{yz} = \frac{\partial u_z}{\partial y} - \theta_x \\
\gamma_{zx} &= \frac{\partial u_x}{\partial z} + \theta_y, \quad \gamma_{xz} = \frac{\partial u_z}{\partial x} - \theta_y \\
\gamma_{yx} &= \frac{\partial u_x}{\partial y} + \theta_z, \quad \gamma_{xy} = \frac{\partial u_y}{\partial x} - \theta_z
\end{aligned} \tag{3.15}$$

It should be noted that the assumption of symmetric shear strains is no longer applicable, instead it differs by the amount of microrotation. On the other hand, the equilibration mechanism involving microrotations is only activated when the shearing comes into place. Otherwise the formulation reduces to the conventional continuum theory with predominantly normal strains and symmetrical shear strains and stresses tensors. Curvatures are defined as first order derivatives of microrotation:

$$\kappa_{ij} = -\theta_{i,j} \tag{3.16}$$

The constitutive relationship proposed by Riahi [38] contains two main parts:

$$\boldsymbol{D} = \begin{bmatrix} \boldsymbol{D}_1 & 0 \\ 0 & \boldsymbol{D}_2 \end{bmatrix} \tag{3.17}$$

where $\boldsymbol{D}_1$ comes from the conventional transverse isotropic elasticity model with additional Cosserat parameters and $\boldsymbol{D}_2$ serves to establish the relationship between Cosserat micromoments and curvatures. Suggesting the case when the local coordinate system coincides with the global one the equivalent anisotropic material tensor enhanced with one joint set could be more clearly represented through the compliance tensor $\boldsymbol{C}_{eq}$ as follows:

$$\boldsymbol{C}_{eq} = \boldsymbol{C}_{cont} + \boldsymbol{C}_j \tag{3.18}$$

$$\boldsymbol{C}_{cont} = \begin{bmatrix} \frac{1}{E} & -\frac{\nu}{E} & -\frac{\nu}{E} & 0 & 0 & 0 \\ \frac{\nu}{E} & \frac{1}{E} & -\frac{\nu}{E} & 0 & 0 & 0 \\ \frac{\nu}{E} & -\frac{\nu}{E} & \frac{1}{E} & 0 & 0 & 0 \\ 0 & 0 & 0 & \frac{1}{G} & 0 & 0 \\ 0 & 0 & 0 & 0 & \frac{1}{G} & 0 \\ 0 & 0 & 0 & 0 & 0 & \frac{1}{G} \end{bmatrix} \quad \boldsymbol{C}_j = \begin{bmatrix} 0 & 0 & 0 & 0 & 0 & 0 \\ 0 & 0 & 0 & 0 & 0 & 0 \\ 0 & 0 & \frac{1}{hk_n} & 0 & 0 & 0 \\ 0 & 0 & 0 & \frac{1}{hk_s} & 0 & 0 \\ 0 & 0 & 0 & 0 & \frac{1}{hk_s} & 0 \\ 0 & 0 & 0 & 0 & 0 & 0 \end{bmatrix} \tag{3.19}$$

where $\boldsymbol{C}_{cont}$ is a continuum (intact) material matrix Young's modulus E and Poisson's ratio ν; $\boldsymbol{C}_j$ is a joint set matrix with joints which are normal in Z direction, have thickness h, normal stiffness k_n and shear stiffness k_s. Now the elasticity matrix $\boldsymbol{D}_1$ could be obtained by simple inversion of the compliance tensor $\boldsymbol{C}_{eq}$. Afterwards it was modified to take into account the non-symmetric component of the shear stresses as follows [38]:

$$\boldsymbol{D}_1 = \begin{bmatrix} A_{11} & A_{12} & A_{13} & 0 & 0 & 0 & 0 & 0 & 0 \\ A_{21} & A_{22} & A_{23} & 0 & 0 & 0 & 0 & 0 & 0 \\ A_{31} & A_{32} & A_{33} & 0 & 0 & 0 & 0 & 0 & 0 \\ 0 & 0 & 0 & G_{22} & G_{11} & 0 & 0 & 0 & 0 \\ 0 & 0 & 0 & G_{11} & G_{11} & 0 & 0 & 0 & 0 \\ 0 & 0 & 0 & 0 & 0 & G_{22} & G_{11} & 0 & 0 \\ 0 & 0 & 0 & 0 & 0 & G_{11} & G_{11} & 0 & 0 \\ 0 & 0 & 0 & 0 & 0 & 0 & 0 & G_{11} & G_{11} \\ 0 & 0 & 0 & 0 & 0 & 0 & 0 & G_{11} & G \end{bmatrix} \tag{3.20}$$

where

$$\begin{aligned} &A_{12} = A_{21}, A_{13} = A_{31} = A_{23} = A_{32} \\ &G_{11} = \frac{Ghk_s}{G + hk_s}, \quad G_{22} = G_{11} + G \end{aligned} \tag{3.21}$$

Here A_{ij} and G_{11} are results of (3.18) inversion. Joints normal and shear stiffnesses were calculated based on the infilling material properties E_0 and G_0 such as [3]:

$$k_n = \frac{E_0}{h}, \quad k_s = \frac{G_0}{h} \tag{3.22}$$

The limit case of the Cosserat formulation is for $(k_s, k_n) \to \infty$ or $h = 0$. If one of the conditions hold the layers disappear and the model converts to the conventional homogeneous continuum.

Matrix $\boldsymbol{D}_2$ is formed with elements which establish the relationship between curvature and couple stresses in a following way:

$$\begin{aligned} &\mu_{xy} = B(\kappa_{xy} + \nu\kappa_{yx}), \quad \mu_{yx} = B(\kappa_{yx} + \nu\kappa_{xy}), \quad B = \frac{Eh^2}{12(1-\nu^2)}\left(\frac{G - G_{11}}{G + G_{11}}\right) \\ &\mu_{xx} = (1-\nu)B\kappa_{xx}, \quad \mu_{yy} = (1-\nu)B\kappa_{yy}, \end{aligned} \tag{3.23}$$

here μ_{xy}, μ_{yx} are analogous to bending moments from plate theory, μ_{xx}, μ_{yy} are similar to twisting moments and B plays a role of flexural rigidity of the layers. Then the second part of material tensor $\boldsymbol{D}$ is formed as follows [38]:

$$\boldsymbol{D}_2 = \begin{bmatrix} (1-\nu)B & 0 & 0 & 0 & 0 & 0 & 0 & 0 & 0 \\ 0 & (1-\nu)B & 0 & 0 & 0 & 0 & 0 & 0 & 0 \\ 0 & 0 & 0 & 0 & 0 & 0 & 0 & 0 & 0 \\ 0 & 0 & 0 & 0 & 0 & 0 & 0 & 0 & 0 \\ 0 & 0 & 0 & 0 & 0 & 0 & 0 & 0 & 0 \\ 0 & 0 & 0 & 0 & 0 & 0 & 0 & 0 & 0 \\ 0 & 0 & 0 & 0 & 0 & 0 & 0 & 0 & 0 \\ 0 & 0 & 0 & 0 & 0 & 0 & 0 & B & \nu B \\ 0 & 0 & 0 & 0 & 0 & 0 & 0 & \nu B & B \end{bmatrix} \tag{3.24}$$

Material tensor $\boldsymbol{D}$ is valid when local and global coordinate systems are equal, otherwise a transformation should be applied. It is done, for instance, when a rock layers are inclined. The transformation is carried out with the rotation matrix $\boldsymbol{R}$ which consists of rotation about x, y, z axes and could be written as:

$$\boldsymbol{R} = \boldsymbol{R}_x(\phi)\boldsymbol{R}_y(\theta)\boldsymbol{R}_z(\psi)$$

$$\boldsymbol{R}_x(\phi) = \begin{bmatrix} cos(\phi) & -sin(\phi) & 0 \\ sin(\phi) & cos(\phi) & 0 \\ 0 & 0 & 1 \end{bmatrix} \boldsymbol{R}_y(\theta) = \begin{bmatrix} cos(\theta) & 0 & -sin(\theta) \\ 0 & 1 & 0 \\ -sin(\theta) & 0 & cos(\theta) \end{bmatrix} \boldsymbol{R}_z(\psi) = \begin{bmatrix} cos(\psi) & -sin(\psi) & 0 \\ sin(\psi) & cos(\psi) & 0 \\ 0 & 0 & 1 \end{bmatrix} \tag{3.25}$$

Now the global material tensor $\boldsymbol{D}^*$ could be obtained as:

$$\boldsymbol{D}^* = \boldsymbol{R}^T \boldsymbol{D} \boldsymbol{R} \tag{3.26}$$

For instance, the example of rotation matrix in two dimensions is [23], [5]:

$$\mathbf{R} = \begin{bmatrix} c^2 & s^2 & cs & cs & 0 & 0 \\ s^2 & c^2 & -cs & -cs & 0 & 0 \\ -cs & cs & c^2 & -s^2 & 0 & 0 \\ -cs & cs & -s^2 & c^2 & 0 & 0 \\ 0 & 0 & 0 & 0 & c & 0 \\ 0 & 0 & 0 & 0 & 0 & c \end{bmatrix} \tag{3.27}$$

where $c = cos\beta, s = sin\beta$, β is the layer inclination. It should be noted that three dimensional case requires two additional angles θ and φ as shown in Figure (3.3). Now the advantage brought by the micromoments for layered materials could be appreciated. Consider the beam which are loaded in the middle and supported vertically on the ends Figure (3.4). A load applied in the longitudinal direction produces moments, as a result both translations and rotations occur. The jointed rock could be interpreted as a stack of inclined beams which interact with each other and under certain conditions could introduce additional bending resistance. Therefore, the model should reproduce bending behaviour as well. Adhikary [4] pointed out the deficiency of ubiquitous joint model which does not include the bending mechanism. He has shown that when the shearing becomes a driving mechanism, displacements could be overestimated, because the slipping is allowed without considering the bending resistance of layers. The model based on the Cosserat theory contains micromoments and brings the ability to consider the bending contribution to the deformations. There are examples [39] which show, that for some layers orientation, better displacements estimation is achieved if the Cosserat formulation is used.

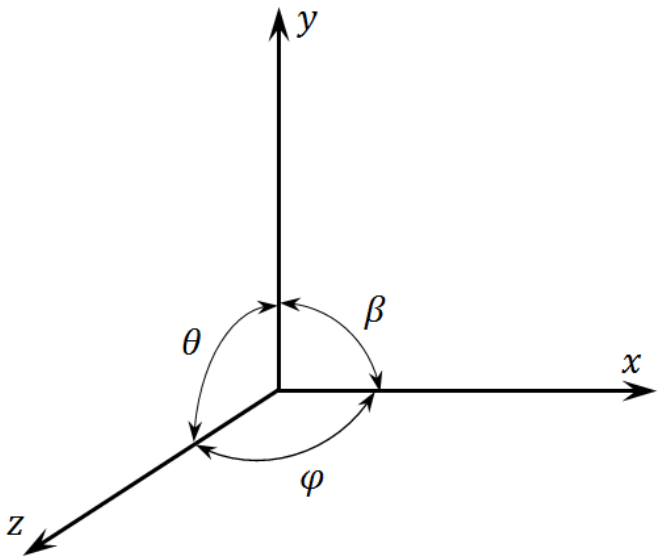

Figure 3.3: Input angles for the three dimensional rotation matrix ***R***

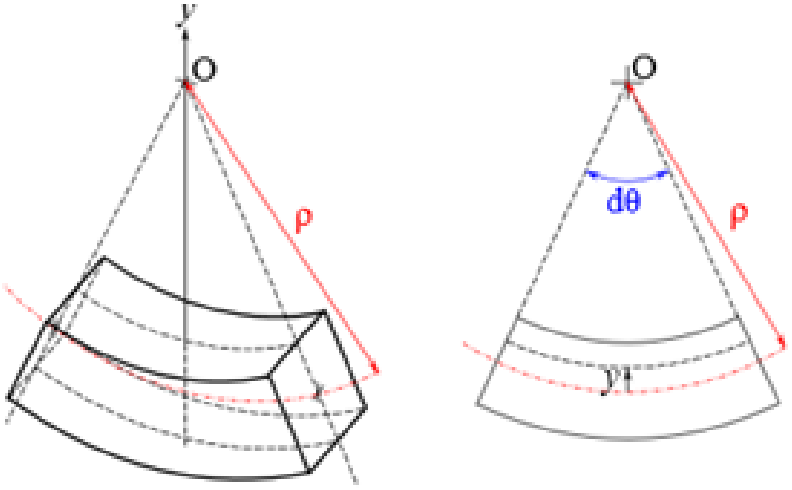

Figure 3.4: Bending due to load in Y direction

3.3. Finite element formulation

Generally, the framework for the Cosserat finite element formulation is similar to classical continuum with some differences due to additional degrees of freedom in each node (microrotations). The governing equations (3.13) and constitutive matrix (3.20), (3.24) were given in the preceding sections. Applying the principle of virtual work to (3.13) a modified $\boldsymbol{B}$ matrix emerges [37].

$$\boldsymbol{B} = \begin{bmatrix} \boldsymbol{B}_{N1} & \boldsymbol{B}_{N2} \\ 0 & \boldsymbol{B}_{N3} \end{bmatrix} \tag{3.28}$$

with

$$\boldsymbol{B}_{N1} = \begin{Bmatrix} \phi_{N,x} & 0 & 0 \\ 0 & \phi_{N,y} & 0 \\ 0 & 0 & \phi_{N,z} \\ 0 & 0 & \phi_{N,y} \\ 0 & \phi_{N,z} & 0 \\ 0 & 0 & \phi_{N,x} \\ \phi_{N,z} & 0 & 0 \\ 0 & \phi_{N,x} & 0 \\ \phi_{N,y} & 0 & 0 \end{Bmatrix} \boldsymbol{B}_{N2} = \begin{Bmatrix} 0 & 0 & 0 \\ 0 & 0 & 0 \\ 0 & 0 & 0 \\ -\phi_N & 0 & 0 \\ \phi_N & 0 & 0 \\ 0 & \phi_N & 0 \\ 0 & -\phi_N & 0 \\ 0 & 0 & -\phi_N \\ 0 & 0 & \phi_N \end{Bmatrix} \boldsymbol{B}_{N3} = \begin{Bmatrix} -\phi_{N,x} & 0 & 0 \\ 0 & -\phi_{N,y} & 0 \\ 0 & 0 & -\phi_{N,z} \\ 0 & -\phi_{N,z} & 0 \\ 0 & 0 & -\phi_{N,y} \\ -\phi_{N,z} & 0 & 0 \\ 0 & 0 & -\phi_{N,x} \\ -\phi_{N,y} & 0 & 0 \\ 0 & -\phi_{N,x} & 0 \end{Bmatrix} \tag{3.29}$$

where $\phi_{N,}$ is the shape function of the N^{th} node. For the three dimensional finite element formulation each node N is associated with three displacements and three rotations degrees of freedom. The vector of nodal degrees of freedom is determined as:

$$\boldsymbol{U} = [\boldsymbol{u}, \boldsymbol{\theta}] = [u_x \; u_y \; u_z \; \theta_x \; \theta_y \; \theta_z] \tag{3.30}$$

Using the global material tensor $\boldsymbol{D}^*$ (3.26) the stiffness matrix $\mathbf{K}$ for each integration point is formed as:

$$\boldsymbol{K} = \int_V \boldsymbol{B}_N^T \boldsymbol{D}^* \boldsymbol{B}_N \tag{3.31}$$

The element stiffness matrix is the summation of stiffness matrices from all integration points

3.4. Cosserat plasticity formulation

The theory of plasticity is used in order to describe material nonlinearities, due to reaching the yielding point. It includes the yielding function which defines if the material state belongs to elastic or plastic region. That function depends on the current stress state and the previous material history. Micropolar formulation involves the modifications of the plasticity formulation due to the presence of micromoments. General formulation of the elasto-plasticity was given by Steinmann in [42]. In the present work formulations of Von Mises (J_2) and Drucker-Prager theories derived by De Borst in [15], [14] were used. Originally the homogeneous material tensor with the internal length characteristic which is a function of particle size was used. That formulation was tested for the identification of the shear band thickness. Currently, the same plasticity algorithm but with the constitutive model containing layers was developed to apply it for the jointed rock analysis.

3.4.1. J_2 theory

One of the most simple yield functions is a Von Mises function. It has a shape of cylinder in stress space and does not depend on the mean stress (first stress invariant, I). That is why it is also called

J_2 flow theory, because it is controlled only by deviatoric stress and yield stress. This assumption holds, for instance, for metals, hence, is not sufficient for soils and rocks. In the present work the Von Mises plasticity formulation was used as a base for the further pressure dependant plasticity formulation. According to J_2 theory the yield function f can be written as [15]:

$$f = \sqrt{3J_2} - \overline{\sigma}(\kappa) \tag{3.32}$$

where $\overline{\sigma}$ is the yield stress which is a function of hardening parameter κ. J_2 is the second invariant of the deviatoric stress which should be modified generalizing it for a micro-polar continuum [15]:

$$J_2 = a_1 s_{ij} s_{ij} + a_2 s_{ij} s_{ji} + a_3 \mu_{ij} \mu_{ij} / l^2 \tag{3.33}$$

here s_{ij} is the deviatoric stress tensor, μ_{ij} is the couple-stress tensor and a_1, a_2, a_3 are material parameters. For the reason that anisotropic material tensor already contains the length scale parameter which is the layer thickness (h) the following form of J_2 was adopted:

$$J_2 = a_1 s_{ij} s_{ij} + a_2 s_{ij} s_{ji} + a_3 \mu_{ij} \mu_{ij} \tag{3.34}$$

In the matrix-vector notation the second invariant takes the shape:

$$J_2 = \frac{1}{2} \boldsymbol{\sigma}^T \boldsymbol{P} \boldsymbol{\sigma} \tag{3.35}$$

and leads to the following expression for the yield function:

$$f = \sqrt{\frac{3}{2} \boldsymbol{\sigma}^T \boldsymbol{P} \boldsymbol{\sigma}} - \overline{\sigma}(\kappa) \tag{3.36}$$

3.4.2. Drucker-Prager theory

The Drucker-Prager model is a pressure dependant model which considers the influence of the volumetric stress applied to the structure by means of additional component in the yield function. It is an approximation of the Mohr Coulomb failure criterion which takes into account only minimum and maximum principal stresses. This feature makes the yield function in the stress space cone-shaped and reduces the complexity of its implementation if compared with Mohr Coulomb. The expression for the yield function is given as [15]:

$$f = \sqrt{3J_2} + \alpha p - \overline{\sigma}(\kappa), \tag{3.37}$$

where α is a friction coefficient, p is the volumetric pressure. The vector-matrix form of the previous equation is:

$$f = \sqrt{\frac{3}{2} \boldsymbol{\sigma}^T \boldsymbol{P} \boldsymbol{\sigma}} + \alpha \boldsymbol{\sigma}^T \boldsymbol{\pi} - \overline{\sigma}(\kappa), \tag{3.38}$$

with $\boldsymbol{\pi}^T = [1/3, 1/3, 1/3, 0, 0, 0, 0]$. Basically, it is Von Mises yield criterion enhanced with the first stress invariant which is a function of compression stresses. Furthermore, for rocks it is recommended to use the non-associated flow rule otherwise, the plastic volume expansion is overestimated. The plastic potential function was considered as follows:

$$g = \sqrt{\frac{3}{2} \boldsymbol{\sigma}^T \boldsymbol{P} \boldsymbol{\sigma}} + \beta \boldsymbol{\sigma}^T \boldsymbol{\pi} - \overline{\sigma}(\kappa), \tag{3.39}$$

where β is a dilatancy factor.

The formulation of the strain hardening/softening behaviour is given in the Appendix (A.1).

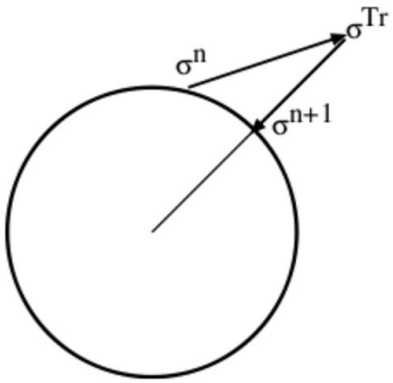

Figure 3.5: Schematic radial return mapping

3.4.3. Return mapping

According to Prager's consistency condition the plastic straining will occur if and only if the following two equations hold at the same time:

$$\begin{aligned} f &= 0 \\ \dot{f} &= 0 \end{aligned} \tag{3.40}$$

That implies the fact that physically possible stress must be on the yielding surface and has to be returned if out of the region. To keep the stress on the yielding surface ($f(\sigma) = 0$) the return mapping is used. Schematic radial return mapping is demonstrated in Figure (3.5). Here σ^n is the stress on the previous loading step; σ^{Tr} is the trial stress for the next loading step which is based in the elastic increment and falls out of yielding surface that is why it needs to be transferred back and σ^{n+1} is a new stress which was placed back to the yielding surface. Important ingredient of the returning algorithm is the direction of the mapping, essentially it is gradient of the yield function for the current stress state. If the yield surface has a relatively simple shape, for instance a circle like in Figure (3.5), then the return mapping is generally achieved in a single step. The return mapping for pressure independent Von Mises and pressure-dependent Drucker-Prager theories extended for Cosserat formulation are employed by De Borst in [15], [14].

The corrected stress state is derived based on the *Von Mises* yield function and in the end of the load step is expressed as:

$$\boldsymbol{\sigma_n} = \boldsymbol{\sigma_t} - \frac{3\triangle\lambda}{3\overline{\sigma}(\kappa)}\boldsymbol{D^e P \sigma} \tag{3.41}$$

where

$$\triangle\lambda = \frac{f(\boldsymbol{\sigma_t}, \kappa_0)}{h + \frac{\partial f^T}{\partial \boldsymbol{\sigma}}\boldsymbol{D^e}\frac{\partial f}{\partial \boldsymbol{\sigma}}}. \tag{3.42}$$

Here $\boldsymbol{P}$ is the projection matrix and $\boldsymbol{D^e}$ is the elastic material tensor which is the current research replaced with $\boldsymbol{D}^*$. The hardening modulus h is defined in the same manner as in classical plasticity theory:

$$h(\kappa) = \frac{\partial\overline{\sigma}}{\partial\kappa}. \tag{3.43}$$

Mathematically, by means of hardening modulus h the yielding surface $f(\sigma)$ is able to move depending on the current stress state and implicates the hardening or softening phenomenon. It should be noted that there is a linear dependency between updated stress state σ_n and plastic multiplier increment $\triangle\lambda$. This characteristic makes the algorithm relatively simple comparing with the Drucker-Prager plasticity.

The corrected stress state for the *Drucker-Prager* has more elaborative form:

$$\boldsymbol{\sigma_n} = \boldsymbol{\sigma_t} - \triangle\lambda \left[\frac{3\boldsymbol{D^e P \sigma_n}}{2\left[\overline{\sigma}(\kappa) - \alpha \boldsymbol{\pi^t \sigma_n}\right]} + \beta \boldsymbol{D^e \pi} \right] \tag{3.44}$$

In that equation the updated stress state depends on itself and requires iterative methods to solve it. Prior to that, the non-linearity in the denominator was relaxed by substituting the updated stress with the trial stress as follows:

$$\boldsymbol{\pi^t \sigma_n} = \boldsymbol{\pi^t \sigma_t} - \triangle\lambda\beta \boldsymbol{\pi^t D^e \pi} \tag{3.45}$$

Considering the yield condition ($f = 0$) the resultant nonlinear equation has the following form:

$$f(\triangle\lambda) = \sqrt{\frac{3}{2}\boldsymbol{\sigma_n^t P \sigma_n}} + \boldsymbol{\pi^t \sigma_n} - \overline{\sigma} \tag{3.46}$$

As it was proposed in the reference paper Regula Falsi method was used to find the solution.

Regula Falsi method

Regula Falsi is a method used to find the numerical estimate of the equation. The schematic representation of the root searching technique is shown in Figure (3.6). The necessary requirement to start the algorithm is that the examined function F intersects X axes; means the existence of real root. Additionally, that intersection point ($F(x) = 0$) must lie in the prescribed interval $[a_1; b_1]$; such as $F(a_1) > 0$ and $F(b_1) < 0$. Next root prediction is calculated based on the slope from the previous step and expressed as follows:

$$b_{i+1} = b_i - \frac{F(b_i)(b_i - a_i)}{F(b_i) - F(a_i)}, \tag{3.47}$$

where a_i and b_i is updated such as the condition $F(a_{i+1})F(b_{i+1}) < 0$ holds. Each iteration, one of the interval boundaries approaches the equation root and it stops when $F(b_i)$ is less than defined tolerance. Transferring it to the non-linear analysis the function F is the yield function and root of the equation is the increment of plastic multiplier $\triangle\lambda$. The initial a_1 value is equal to zero. Thus it corresponds to the yield function with respect to elastic stress predictor and places it in the plastic region. Substitution of ($\triangle\lambda = 0$) in the equation (3.46) proves the above statement. On the other hand, the parameter b_1 has to bring the yield function in the elastic region and provide the negative function F. During iteration process the increment of plastic multiplier is adjusted such as the yield function F is returned to the yield surface which is possible only if ($F(\triangle\lambda) = 0$).

It might be noticed that Regula Falsi method is similar to the bisection method [9], the difference is in the usage of the function itself for the calculation of the new root prediction. That fact is in favour of less iterations required to find the solution, thus generally speeding up the searching process.

3.5. Summary

This chapter presents fundamentals of the Cosserat theory revealing the difference from the standard continuum mechanics. To demonstrate the application of the Cosserat theory, the practical example from the literature was given. It is followed by the elasto-plastic finite element formulation of the Cosserat theory. In essence, each node should be enriched with additional degree of freedom, namely the microrotation, leading to the fundamental modifications in the programming code. Moreover, in order to consider the internal length parameter (in the current research it is the layer thickness) the constitutive model should be modified accordingly. Essentially, the transverse isotropic material model with additional coefficients for the micromoments was implemented. Inclined layers were considered by means of the rotated coordinate system with rotation matrix **R**.

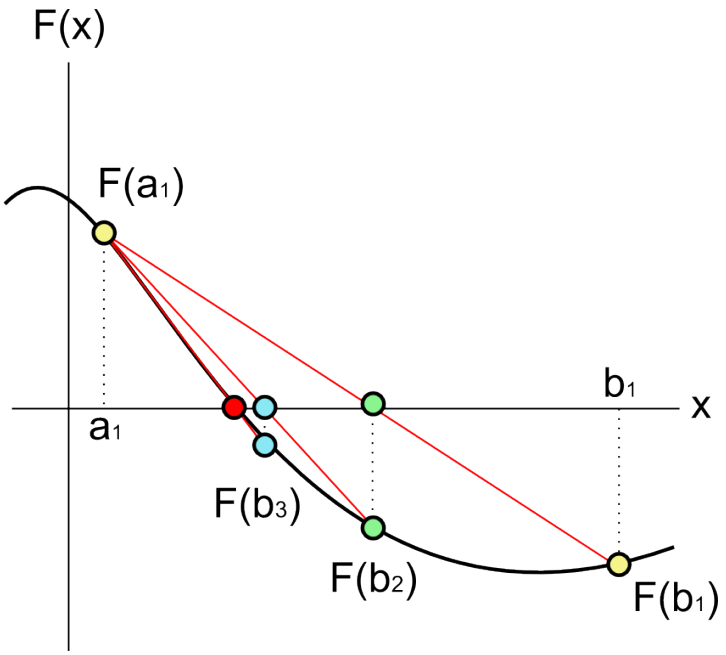

Figure 3.6: Schematic Regula Falsi method

Finally, Von Mises and Drucker-Prager formulations with the return mapping algorithm were given. The deviatoric stress invariant has to be modified due to the presence of micromoments.

4

Implementation of the elastic model

The implementation of the Cosserat finite element formulation was done in DIANA FEA software by introducing additional routines and modifying already existing ones. The elastic model is available for the two and three dimensional analyses. It includes four-node quadrilateral (Q12CO) and three-node triangle (T9COS) elements with linear shape functions. Three dimensional model is available for eight-node brick elements (HX48CO) with linear shape functions. The verification and performance analyses of the elastic formulation were carried out using the two dimensional jointed column model with inclined layers presented by Riahi [39]. This model was considered as an appropriate one because it has relatively simple geometry and replicates natural situation of the jointed media. Yet further, the model with explicit joints was constructed in Rocscience, RS2 [2] and DIANA FEA [1] applications to validate the results obtained with the Cosserat formulation. In the present work *the explicit model* or *explicit joint model* definitions refer to the model with standard continuum formulation and interface elements acting as joints. The detailed description of the geometry and material parameters are described below. Several questions have appeared while testing the elastic model. They are related to the internal parameter and numerical performance of the Cosserat formulation. The main goal of the current chapter is to address the artefacts and discuss possible solutions.

The first question is related to the distribution of layers. In the explicit joint model it was discovered that the displacement field depends on the spatial definition of the layers. Although, the layer thickness is the constant value. Since, layers are smeared in the Cosserat formulation their distribution is not possible to control. Then the first question could be formulated as follows: *What is the possible distribution of layers in the Cosserat formulation ?*

The second question is associated with the numerical convergence, one of the most essential features used to validate the obtained numerical results. Here, the definition “convergence” is used to describe the dependence of the result on the elements size. Results are assumed converged when further mesh refinement does not cause change in the final results. The studied literature shows the convergence test for homogeneous or horizontally layered materials. However, an inherent feature of the jointed rock is to be inclined. That is why the second question is: *Is there any influence of tilted layers on the numerical convergence?*

The final, third question, refers to the choice of boundary conditions. The Cosserat formulation includes non-conventional degree of freedom, microrotation. It is important to understand how

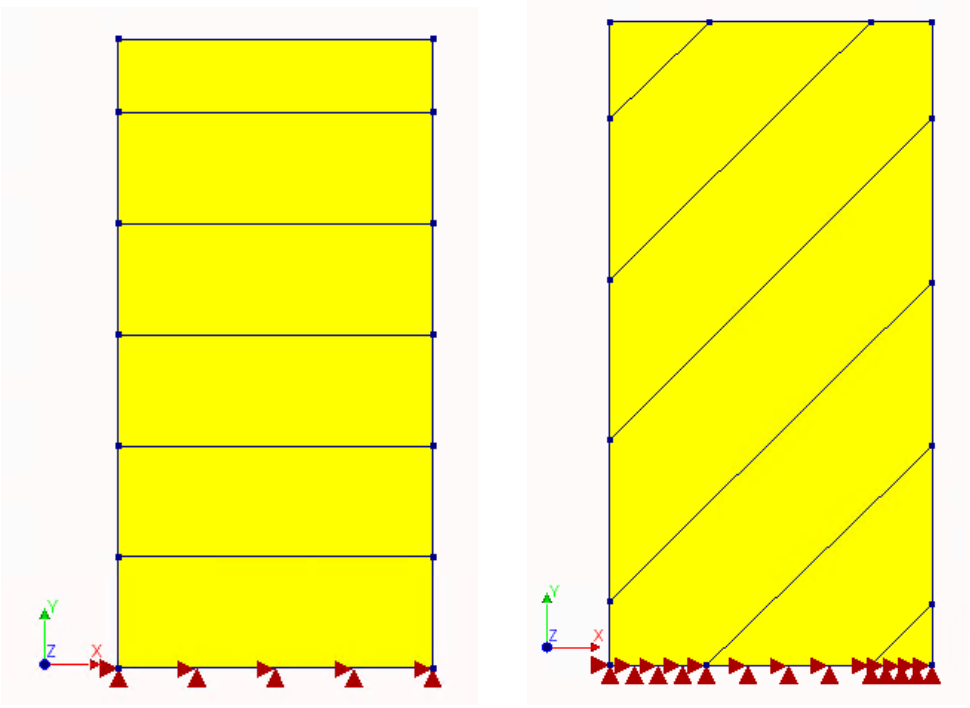

(a) (b)

Figure 4.1: Geometry of two dimensional jointed column with boundary conditions and load

to choose the appropriate boundary conditions for the former variable. Thus the third question is: *What is the influence of microrotation boundary condition?*

Suggested jointed rock column geometry is shown in Figure (4.1); left and right consists of horizontal and inclined layers respectively. The height of the column is 2 m, the width is 1 m and layer thickness is ($h = 0.35m$).Elastic parameters for intact rock are Young;s modulus ($E = 10GPa$), Poisson's ratio ($\nu = 0.25$) and for the joints there are normal stiffness ($k_n = 1000GN/m^3$) and shear stiffness ($k_s = 546MN/m^3$). Here relatively high normal stiffness was selected in order to reduce its influence and activate the shearing mechanism. In the conventional continuum each layer is defined explicitly by the interface element. In the Cosserat formulation joints are smeared along the column and the layers thickness (h) implicitly establishes the layers dimension in the constitutive matrix $\boldsymbol{D}$. The inclined layers are modelled by means of the rotation matrix $\boldsymbol{R}$ applied to the constitutive matrix $\boldsymbol{D}$ producing $\boldsymbol{D}^*$. In both cases the bottom movement was constrained in all directions. Additionally, the rotation of the bottom elements was fixed for the Cosserat formulation. Distributed vertical load is ($F_y = -5MPa$) applied on the top of column.

4.1. Column with horizontal layers

4.1.1. Vertical compression

Questions stated in the beginning of this chapter have appeared during the verification of the implemented Cosserat formulation versus explicit joint model. Firstly, the test with horizontally stratified column under vertical compression was conducted. In Figure (4.2) and Figure (4.3) vertical and horizontal displacements graphs for conventional continuum with explicit joints against the Cosserat continuum are presented. These graphs were constructed only for one edge of the model, since

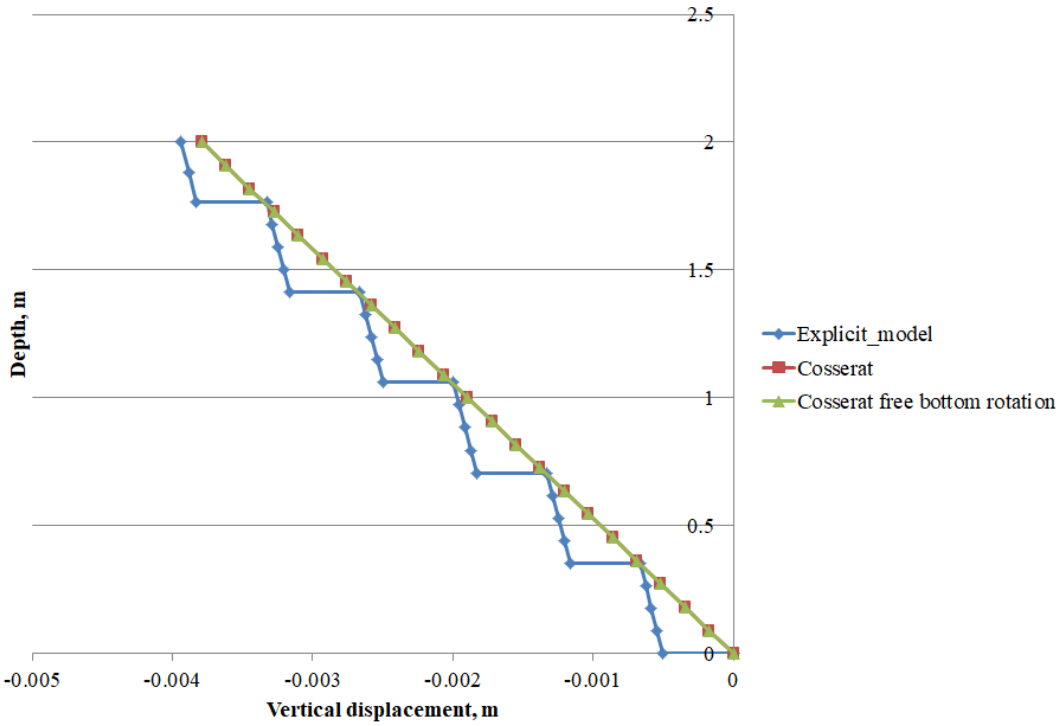

Figure 4.2: Verification of the vertical displacement, column with horizontal layers

the model is symmetric. The staircase shape of the vertical displacements produced by the explicit model was explained by the presence of interfaces, which allow higher shear strains in the interface elements, and lead to the discontinuous displacement field. Opposed to explicit joint model the Cosserat formulation is able to reproduce the continuous deformations due to additional rotation degree of freedom, which assists in handling the displacements due to shearing along the weak joints. Horizontal displacements for the right and left edges of the column are equal for the explicit and Cosserat models. In Figure (4.4) the microrotation evolution of the right column edge is shown; the left edge has the same results but with the opposite sign due to the symmetrical behaviour of the column. The maximum microrotation value is attained in the element next to the boundary. This is the result of the shearing mechanism, which was provoked by the constrained movement of the column bottom. In other words, the force close to the bottom is transferred through the microrotations and not via compression or expansion of the elements. Additionally, it should be noted, that for the suggested case no significant difference in results was detected between the model with fixed and free bottom rotations.

The total displacements field is shown in Figure (4.5). Both models have equal values and direction of deformations. On the top of the column the predominant direction is vertical, however approaching the bottom displacement field is oriented slightly towards the edges. Explicit joints model experiences jumps on the edge of interface. Staircase behaviour was explained by "penetration" of layers into each other due to the presence of interface elements. In other words, these interfaces acts as discontinuities and make possible that separate blocks move independently. On the other side, the Cosserat formulation considers layers implicitly and provide continuous deformation field. There is a difference in magnitude of maximum displacements ($\approx 4\%$) between the Cosserat and explicit joints model. That is the first evidence of the influence of layers distribution on the final result. This phenomenon would be covered in a detailed way for the case with inclined layers.

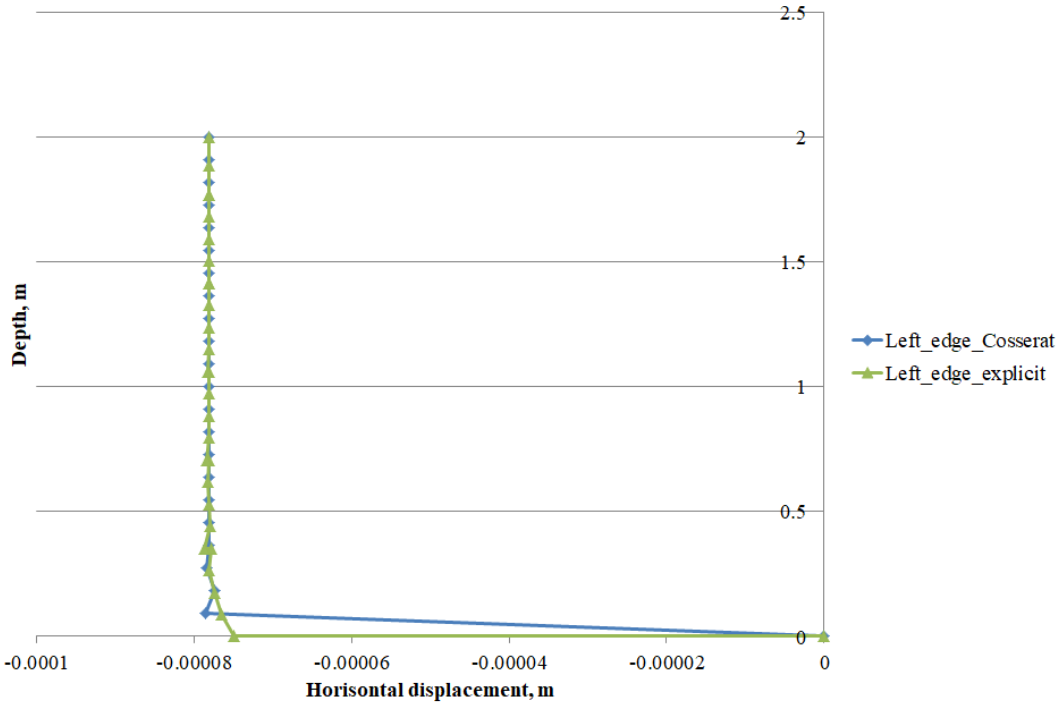

Figure 4.3: Verification of the horizontal displacement, column with horizontal layers

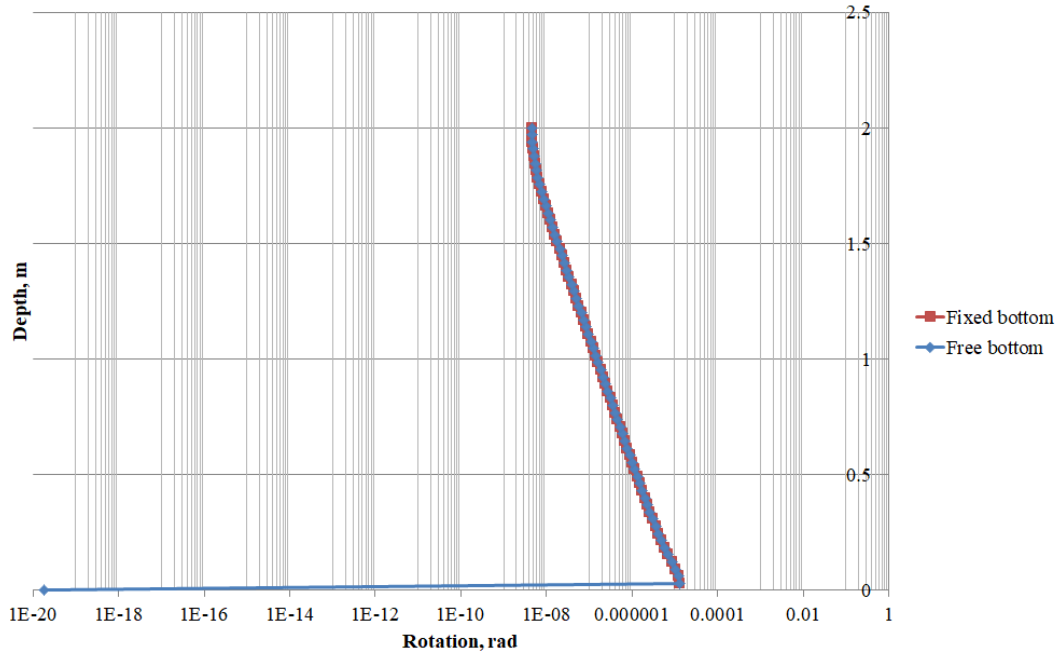

Figure 4.4: Cosserat microrotations on the right edge of the column, column with horizontal layers

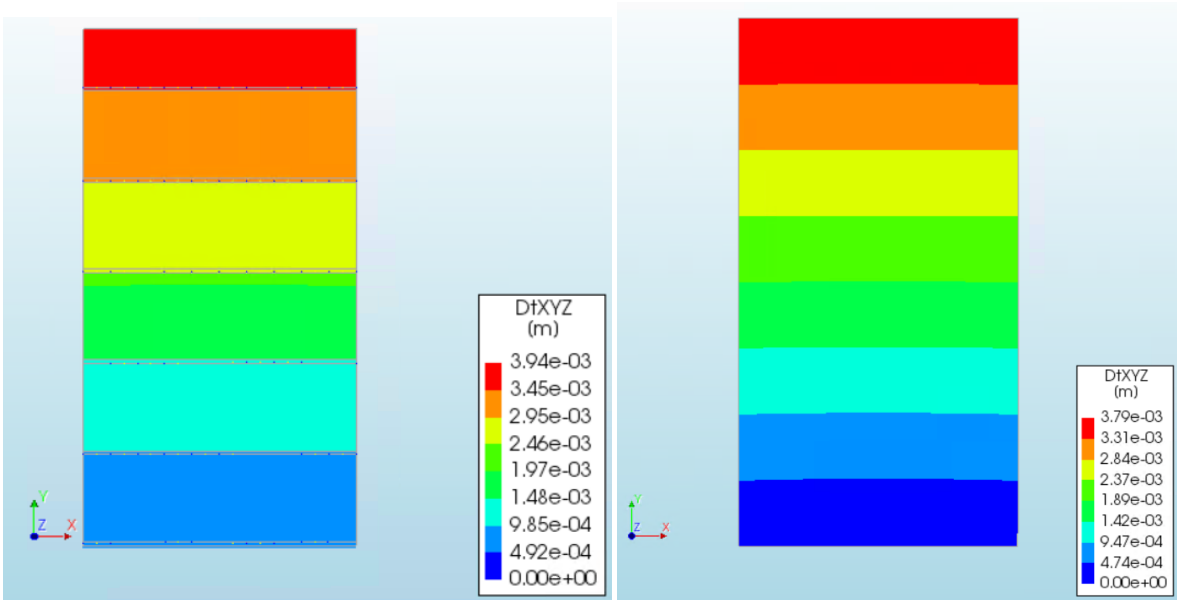

(a) Conventional continuum with explicit joints (b) Cosserat continuum

Figure 4.5: Total displacements field of the column with horizontal joints

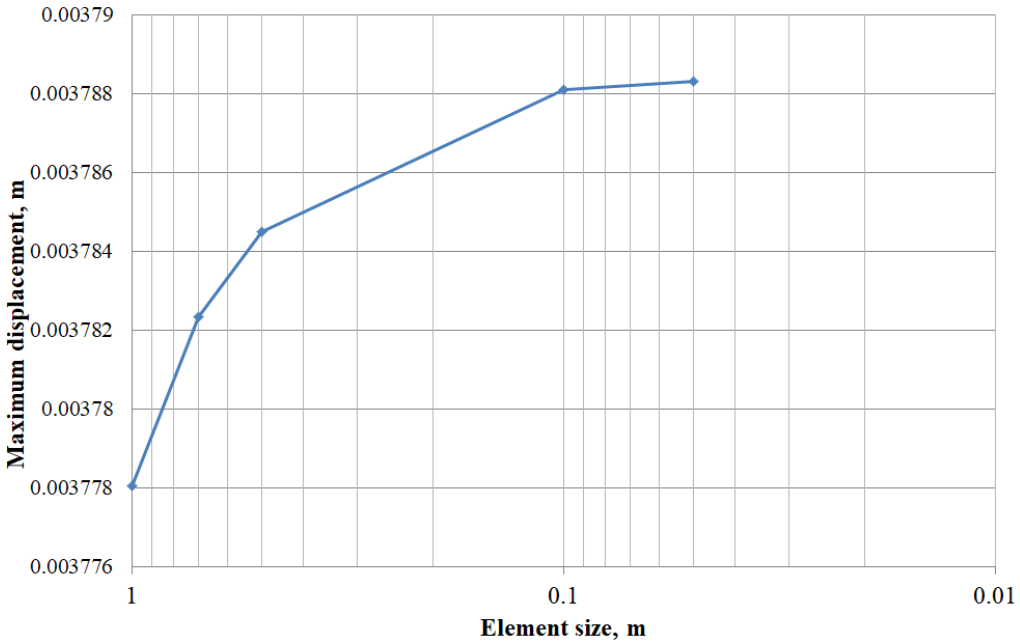

Figure 4.6: Maximum displacement convergence graph, horizontal layers h = 0.35m

Now the convergence rate of the model with horizontal layers would be discussed. Generally, the literature review shows that the convergence test is available for homogeneous [15] or horizontally layered materials [37] and claims promising results with elements which are quite large in relation to the internal length parameter. Similar behaviour was obtained for the case considered above. Figure (4.6) demonstrates that already for the element size equal to 1x1 m accurate displacements are obtained. Further mesh refinement does not bring significant changes and leads to the conclusion that results are converged.

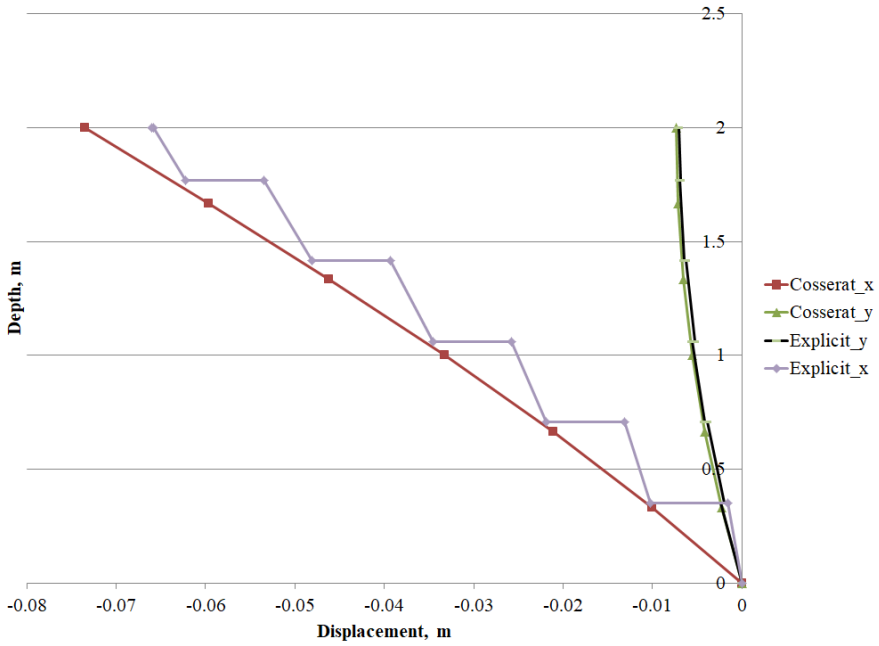

Figure 4.7: Vertical and Horizontal displacements Explicit joint model vs. Cosserat model

4.1.2. Horizontal load

The activation of microrotation was initiated by the horizontal load on the same column with horizontal layers as in the previous example. Distributed force load ($F_x = -5MPa$) was applied horizontally only to the column top nodes. Exactly like in the previous case horizontal and vertical displacements are equal for both Cosserat and explicit joint models Figure (4.7). Due to symmetric condition, the displacement profile only for one side of the model is presented. In contrast to the vertical compression example, the staircase deformation shape is more pronounced in lateral direction and remains continuous in vertical direction. That happens due to predominant displacements along interfaces in horizontal direction which do not cause major vertical deformations as it occurs when the column is loaded vertically.

The graph in Figure (4.8) allows to draw the following conclusions. Firstly, comparing with the test with vertical compression, column loaded horizontally produces larger microrotations marking noticeable shearing mechanism which requires higher microrotations to reach the equilibrium. Secondly, microrotations increase when the joint shear stiffness decreases due to higher flexibility of the material.

4.2. Column with inclined layers

In the current section a jointed column with inclined layers and different layer thickness was modelled. Following stiffness parameters were used for the joints ($k_n = 1000GN/m^3$), by changing the layer thickness k_s was adjusted such as the product ($k_s h = 194.3MPa$) is constant. By doing that the property of infilling material (shear modulus) per meter does not change and the influence of the layer thickness could be studied. Therefore it should be noted that smaller layer thickness requires higher shear stiffness. It is also revealed by the equation (3.22). Constant layers angle ($\beta = 45°$) was suggested in the current analysis. In Figure (4.9) displacements field for different layer thickness is presented. It was observed that the layer inclination and thickness control the direction and magni-

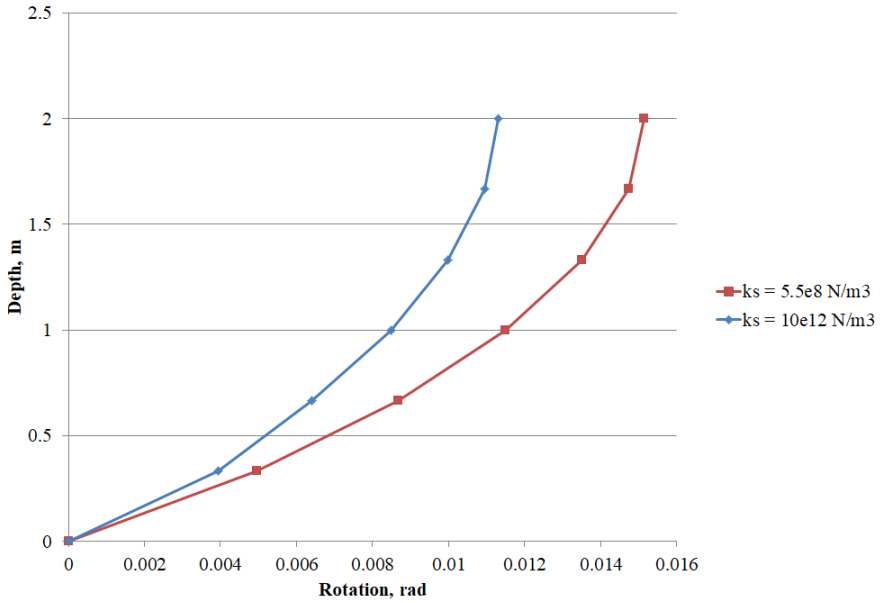

Figure 4.8: Micro-rotation variation with joint shear stiffness

tude of deformations. In general, if the deforming process is mainly governed by the shearing, that is attained by considering large joint normal stiffness k_n, displacements are larger for thicker layers. Additionally, the thickness defines the volume of material affected by the layering. For instance, in Figure (4.9d) it is seen that thick layers mobilize asymmetric deformations almost through the entire column, in opposite, thin layers Figure (4.9b) almost has no influence on the deformation field and behaviour is similar to the intact rock Figure (4.9a).

The validation of results was conducted by comparing maximum column deformations produced with the Cosserat formulation and explicit joint model Figure (4.10), showing fair agreement. That means that the Cosserat formulation is able implicitly to take into account the presence of joints by means of internal characteristic length parameter.

The comparison between the Cosserat formulation and the explicit joint model with inclined layers revealed the results dependence on the layers distribution. In Figure (4.11) columns on the right and on the left have the same material parameters including layer thickness, hence, their spatial spreading varies. That inequality causes the difference in resultant displacements. It could be easily spotted and adjusted according to the user requirements, when the explicit joint model is used, but it is less straightforward in the Cosserat formulation. That is why a side study was conducted in order to understand possible range of discrepancy between Cosserat and explicit joint models.

The procedure was as follows: construct several models with different first layer offsets considering at least two thickness values. Then scale up the geometry of each model and investigate if the influence of the distribution persists. In Figure (4.12) maximum displacement graph versus joint spacing for the Cosserat and three variants for explicit models are presented. The difference between three is the distribution of the layers. It is either equal to the projection of entire thickness (v_1) or just half of it (v_3) of third of it (v_3). First of all, it is clearly seen that the displacement field changes together with layers distribution and the Cosserat solution does not show the tendency towards one of the particular explicit models. More tests should be conducted to confirm if there is one. On the other hand, closer agreement between Cosserat and explicit joint models was found for larger models Figure (4.13). That observation implies the diminishing of the distribution effect when the geometry

becomes much larger than the layer thickness. For example, according to the graph in Figure (4.13) when the ratio between column height and layer thickness is equal to 60, the relative difference between Cosserat and explicit result is less than 2 %. Moreover, further ratio augmentation will lead to the case when the column could be considered as homogeneous material with reduced shear modulus and that is why the case with zero thickness does not vary in the conducted experiment.

Based on the performed analyses the following conclusion was made. When the dimension of the problem is comparable with the thickness of the layers there is a chance of descriptiveness between Cosserat and explicit model formulations within the same order. That happens because the Cosserat formulation smears displacements over the model based on the internal length parameter and the distribution of the layers is difficult to control. On the other hand, for geotechnical applications, for instance for the jointed slope analysis, exact distribution is not known and approximate layers spreading is used.

Carrying out the analysis with inclined layers, an important characteristic related to numerical convergence was discovered. It was noticed that comparing with Figure (4.6) where the convergence graph for the model with horizontal layers is presented, in Figure (4.14) the displacements variation for smaller element remains significant. The major difference between two models with horizontal and inclined layers is the amount of shearing activated. Model with horizontal layers loaded vertically does not produce non-symmetric shear stresses and seems has faster convergence rate. The convergence behaviour similar to the model with inclined layers was discovered by Ramèzani *et al.* [35] while conducting the torsion test for a cylindrical bar. There quadratic shape functions were used for displacement vector and linear shape functions for microrotations. Analysing stiffness-based torque and stiffness-based curvatures components Ramèzani *et al.* have concluded that the reason for slow convergence rate is the usage of linear shape functions for curvatures interpolation. It was also mentioned by Godio *et al.* [20] that the employment of quadratic shape functions for both deformations and microrotations improves the accuracy on coarse mesh. On the current implementation only linear shape functions were deployed. Switching to the higher order shape functions a least for the curvatures interpolation is considered as a worth improvement for the future.

4.3. Loading of the jointed rock column 3D case

The extension of the 2D formulation to 3D requires following modifications:

1. use the full constitutive model $\boldsymbol{D}_e$ (3.17);
2. extend the transformation matrix $\boldsymbol{R}$, considering three directions of rotation.

The verification of the three dimensional model was performed, using the same example as for the 2D case extruded in the third direction for 1m. For the explicit model shear stiffness values in both horizontal directions (x,y) are equal and were adjusted following the same methodology as in 2D analysis such as ($hk_s = 194.3MPa$); normal joint stiffness is high ($k_n = 1000GN/m^3$). The inclination of the layers is 45° . Additionally, the translational movement was fixed in X direction together with microrotation in Y direction in the same plane. Similar to the two dimensional case Cosserat formulation shows continuous deformation field Figure (4.15). In Figure (4.10) the maximum displacement for both two and three dimensional models are compared with explicit model revealing fair correspondence. Layers were also inclined in X direction displaying the same deformation values but directed in X direction.

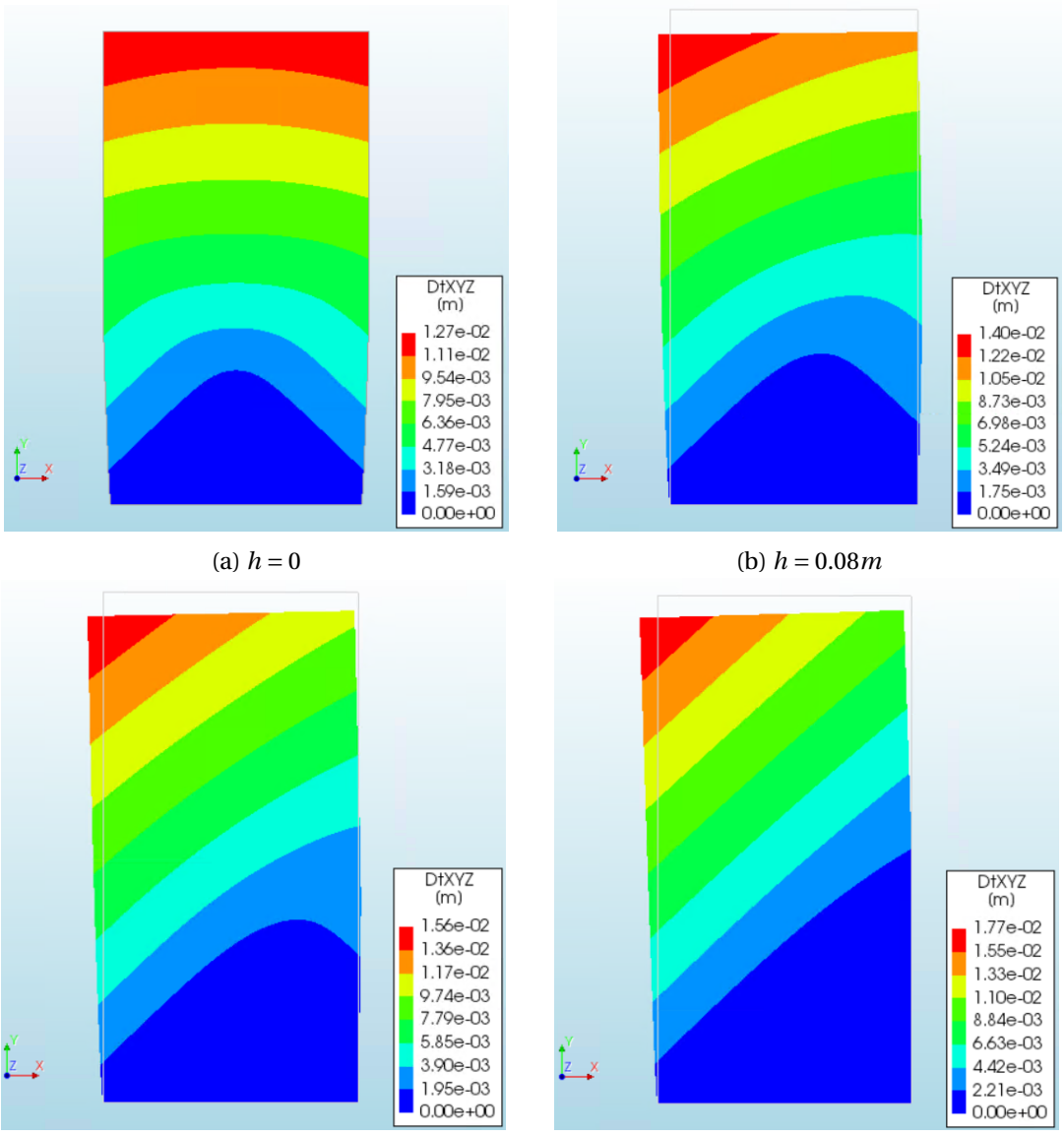

(a) $h = 0$ (b) $h = 0.08m$

(c) $h = 0.17m$ (d) $h = 0.35m$

Figure 4.9: Total displacements field of column with different joint thickness, 2D Cosserat model

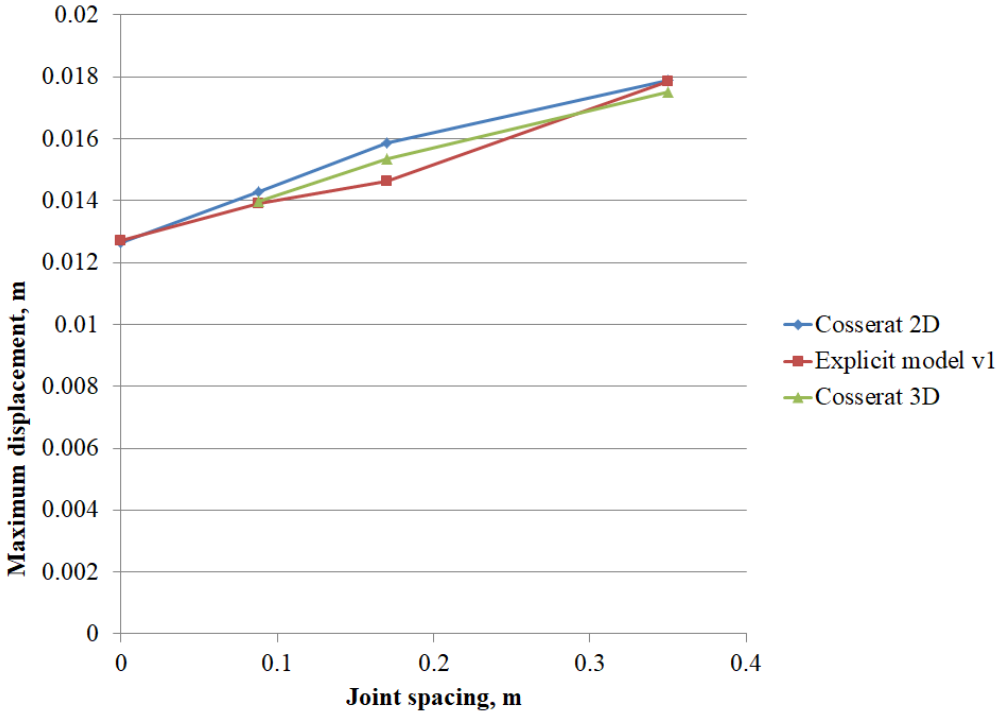

Figure 4.10: Maximum displacements of the jointed column vs. layer thickness

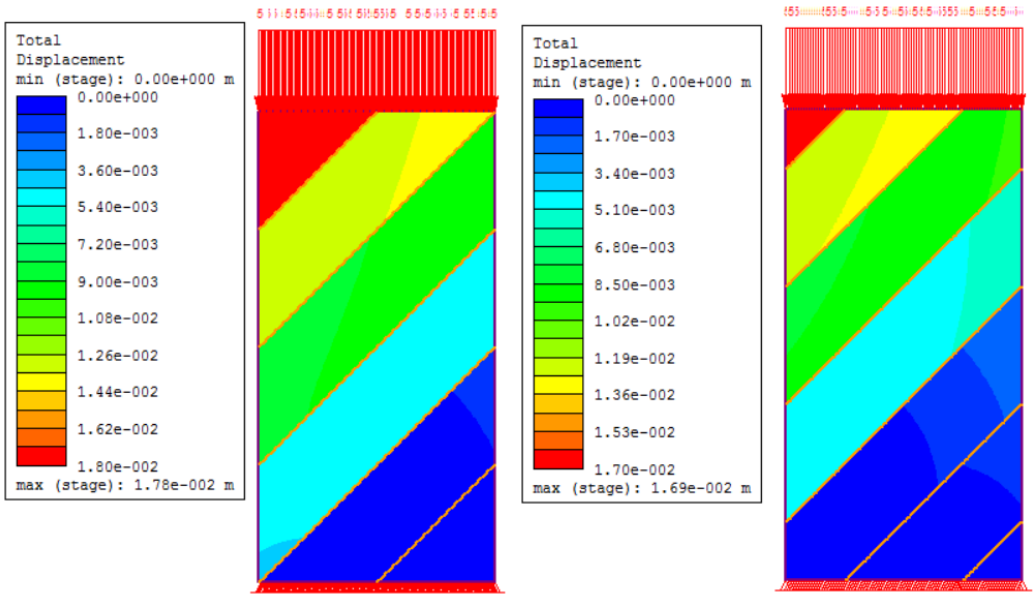

(a) First layer offset, 0.5 m (v_1) (b) First layer offset, 0.25 m (v_3)

Figure 4.11: Variation of total displacements field obtained with explicit joint model, h = 0.35m, RS2

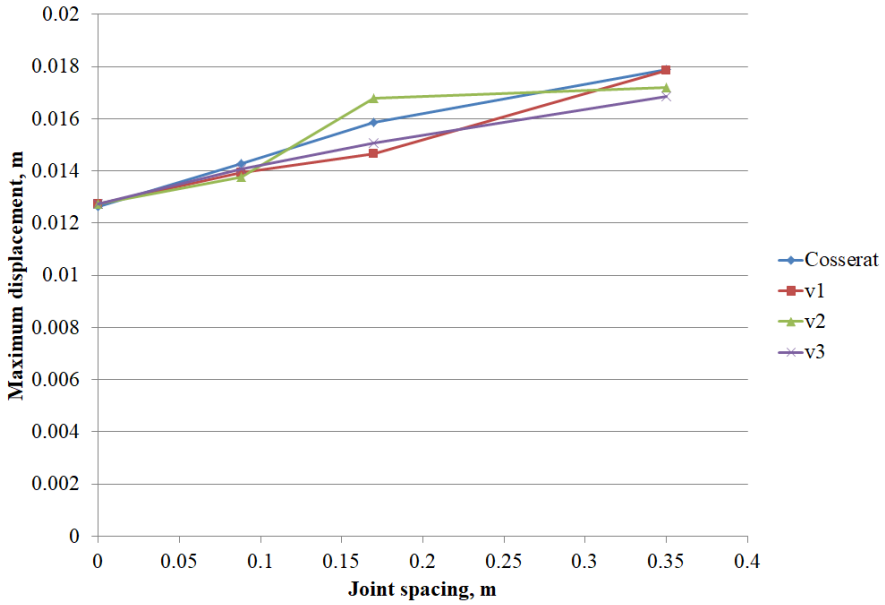

Figure 4.12: Maximum displacement versus joint spacing, Cosserat and three explicit models

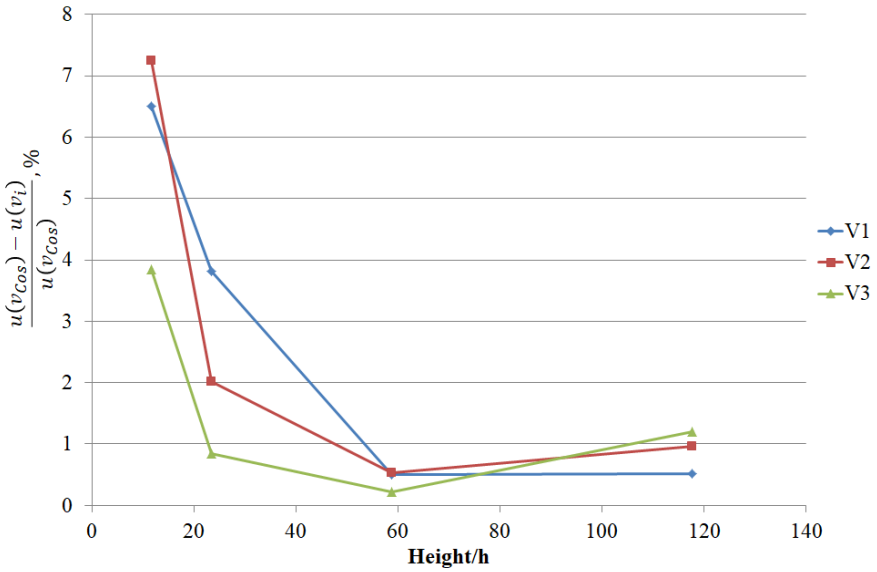

(a) h = 0.17m

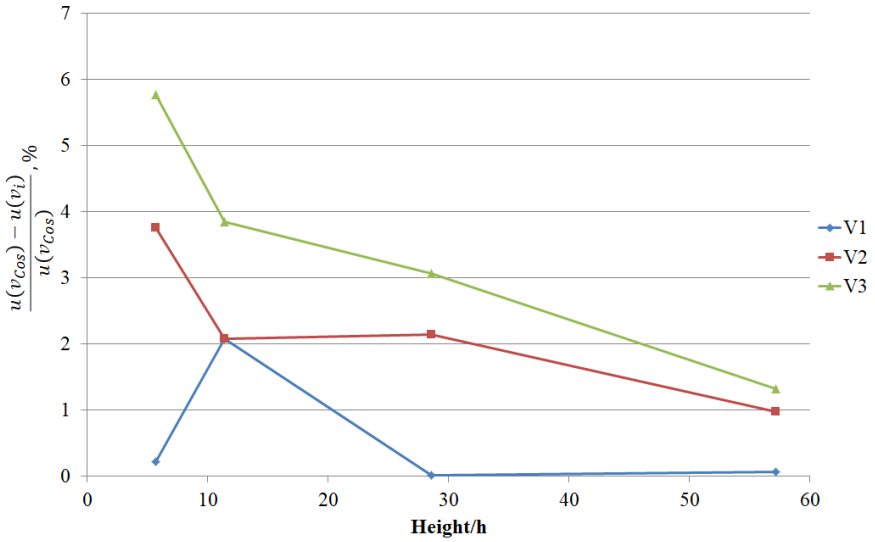

(b) h = 0.35m

Figure 4.13: Relative error between Cosserat and explicit model for different layers distribution

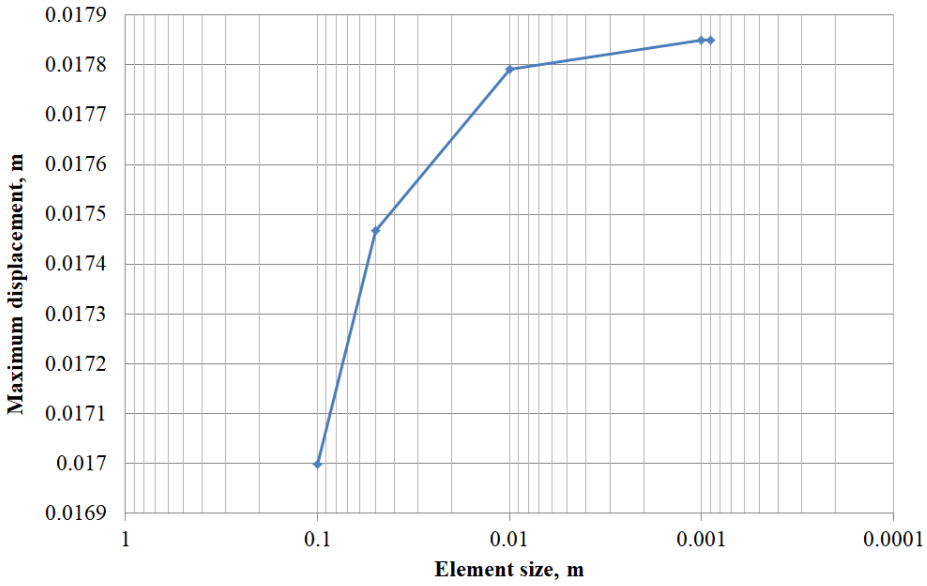

Figure 4.14: Convergence graph, inclined layers h = 0.35 m

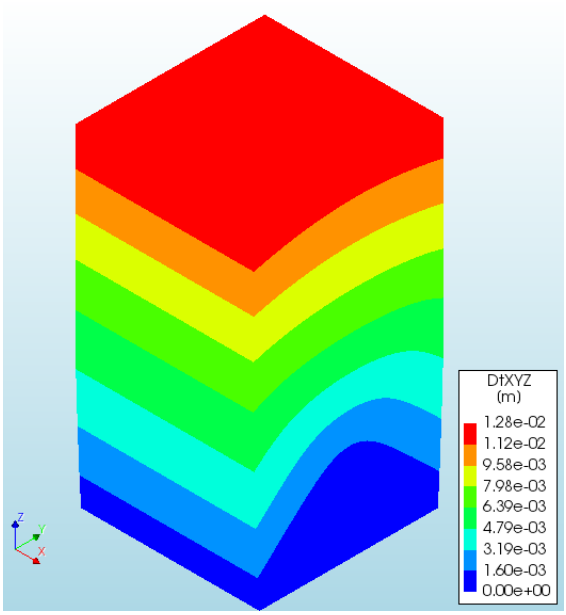

(a) h = 0

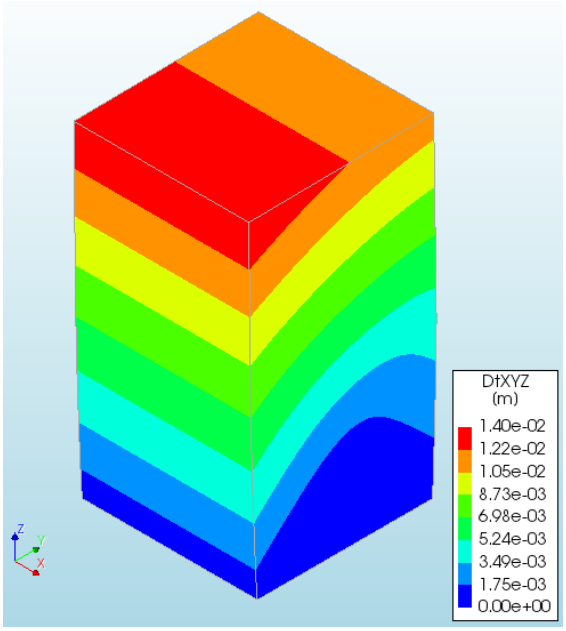

(b) h = 0.088m

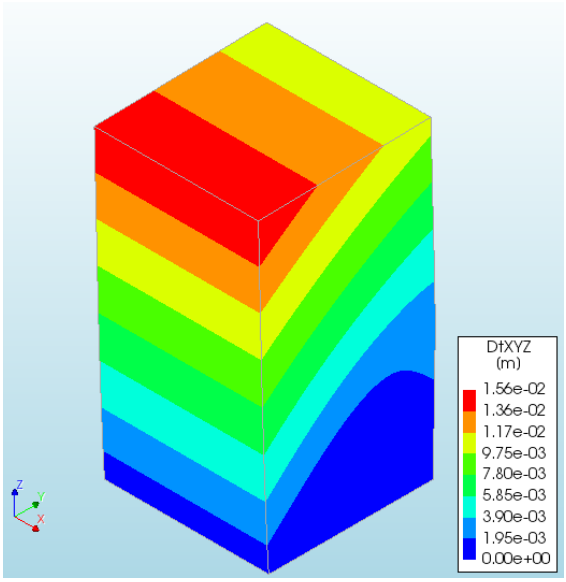

(c) h = 0.17m

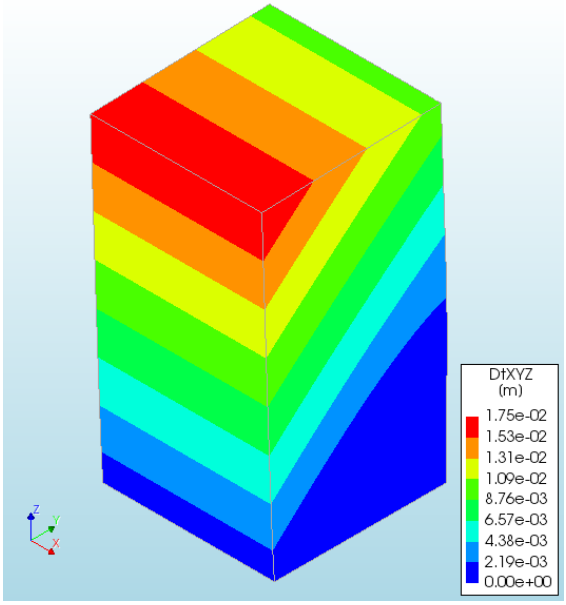

(d) h = 0.35m

Figure 4.15: Total displacements field of the jointed column with various layers thickness h, loaded vertically 3D Cosserat model

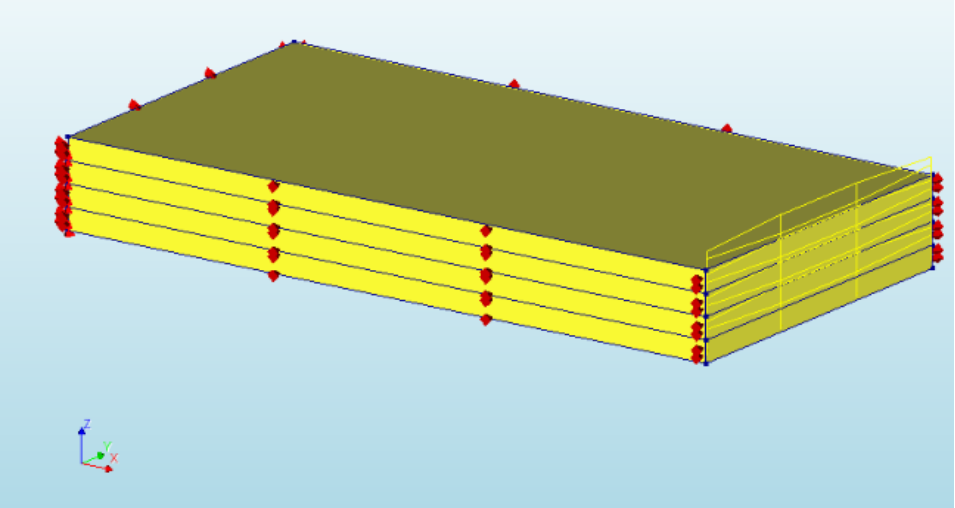

Figure 4.16: Boundary conditions of the slab, explicit joint model

4.4. Boundary conditions investigation: Slab example

Micro-rotations are additional degrees of freedom incorporated on the Cosserat formulation and often require prescribed boundary conditions. However, it is not straightforward choice and should be treated with care. The aim of the present subsection is to demonstrate the influence of the boundary conditions on the solution. Standard cantilever plate loaded with transverse traction on the end was chosen due to available analytical solutions for limit cases and same example was used for the verification of elastic model [39]. The plate has the following dimensions: the length is 2 m, the width is 1 m, the height is 0.25 m and the applied load is τ = -1 MPa. Geometry together with boundary conditions are shown in Figure (4.16). The beam is divided into 4 layers, each layer has the thickness h = 0.0625 m. The Cosserat model consists of 291081 elements; vertically there are 21 elements or 5.25 elements per layer. In the Cosserat formulation the layers thickness is considered as an internal length parameter. The Young's modulus and Poisson's ratio of the layers are 20 GPa and 0.3 respectively. Normal stiffness of the interfaces was chosen relatively high (k_n = 1e15 N/m^3) to prevent it's influence on the behaviour and shear stiffness was varied in the range (0 ÷ 1e15 Pa N/m^3). Suggested example has two limit cases which could be verified with analytical solution for beam. Based on Timoshenko theory vertical displacement is defined as follows: [43].

$$u_3(l) = \frac{4\tau l^3}{Eh^2}(1-\nu^2) \tag{4.1}$$

The first limit case implies high shear stiffness (k_s = 1e15 N/m^3) and reproduces the case when beam behaves as a homogeneous plate with height h = 0.25 m. On the other hand if the shear stiffness becomes negligible (k_s = 0 N/m^3) plate behaves as a stack of separate plates and each has the height 0.0625 m.

Translation boundary conditions are applied on the fixed end of the plate, where the movement is constrained in all directions. Additionally, the horizontal deflection in Y direction is specified to allow the deflection only in X and Z directions. Having done that mentioned above analytical solution could be used. On top of that three variations for microrotation constraints were considered:

1. no microrotations constraint;
2. microrotations are not allowed on the fixed end;

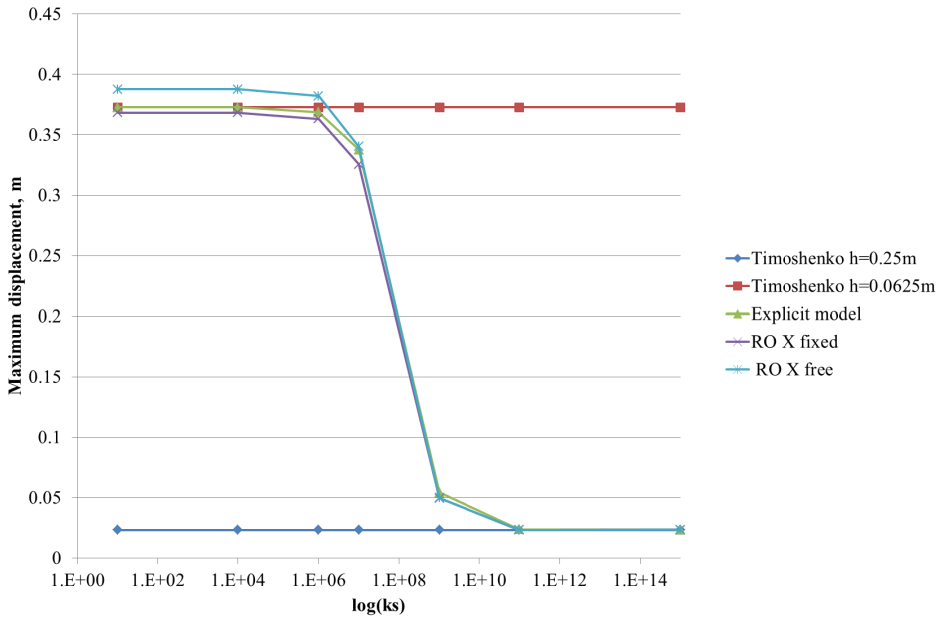

Figure 4.17: Maximum vertical displacement of the beam under vertical load on the tip, $\tau = -1MPa$

3. microrotations are not allowed on the fixed end and in X direction on the place of translation horizontal constraints.

On the first case no convergent or poor unrealistic results were obtained and only one limit case (with high shear stiffness) was satisfied. That example clearly shows the necessity of considering extra boundary conditions for microrotations and it was also pointed by Adhikary *et al.* [4]. Results for next two examples are compared with explicit joint model and displayed in Figure (4.17). The first observation is that all results are bounded between two analytical solutions. Second one is that both models have fair match with analytical solution when the shear stiffness is high (comparing with normal stiffness). The reason for that is the Cosserat continuum approaches the conventional continuum with symmetrical shear stress. Implying the fact that there is almost no micromoments evolution, then microrotations boundary conditions are irrelevant. However, the situation is different when the shear stiffness is lower than normal one. When this is the case, micromoments start to develop evoking the non-symmetrical part of the shear stress and interaction between layers. Lack of additional microrotations constraint in X direction leads to the result deviation from the explicit joint model. For instance, when the shear stiffness is very low the difference is approximately 5 %. The case without additional microrotation boundary condition in X direction was considered as less realistic, thus the twisting mechanism is possible. Nevertheless, for the example with suggested load direction and distribution mainly bending mechanism is expected. That is why the fixing the microrotations on X direction was considered as a more appropriate boundary conditions.

4.5. Summary

The Cosserat elastic formulation was implemented for both two and three dimensional problems. On the verification and debugging stages several findings were discovered and described in the preceding section. They refer the influence of the layers distribution, convergence rate and effect of the microrotations boundary conditions. The Cosserat formulation is the smeared model where internal length characteristic is a layer thickness. As a consequence, it is able to model the entire model

with the same element type comparing with the explicit model which requires introduction of interface elements. The verification shows fair match with the explicit model revealing some deviation due to dependency on layers distribution along the geometry. This descriptiveness decreases for larger geometries. The physical meaning of microrotations could bring additional complexity while choosing boundary conditions. Exploring that matter the following conclusion was declared: the additional constraint for the microrotation should be analysed for the particular problem since it effects the final result. More precisely, if the shearing mechanism is activated the additional degree of freedom becomes of importance since, it controls the non-symmetric part of shear stress. Additionally, the numerical efficiency related to the convergence rate was studied. It was found out that in the absence of shearing mechanism the convergence is achieved with elements with a size larger than the internal length characteristic. On the other hand, it slows down drastically if shearing takes place. Similar result were found in the literature. Possible solution is to switch to the higher-order shape functions for both translation and curvatures variables. However, it was not implemented in the current study due to time shortage.

5

Implementation of plasticity model

The plasticity algorithm was introduced in the DIANA FEA software for the quadrilaterals and triangle element types. The Cosserat formulation requires the modification of stress invariants, due to additional micromoment terms. The modification was derived in [15]. However, in some formulations [37] micromoments were considered implicitly, being a part of the shear stress, and revealed promising results. In the current research two yield criteria were implemented: Von Mises and Drucker-Prager. Special attention was given to the tension behaviour, because it is very common in the soils and rock behaviour and could not be fully described only by regular failure surface. The aim of this chapter is to introduce the development of non-linear behaviour and conduct tests to verify the correctness of the obtained results. Prior to applying the developed algorithm to a complicated geometries, one element model, reduced to homogeneous conditions, was used to enable the verification versus standard continuum mechanics formulation. Here, by the standard continuum formulation the most common finite element formulation based on the momentum equilibrium with the Cauchy assumption for shear stresses is called. Having done one element model validation two dimensional jointed column similar to the one used for the elasticity verification was suggested. Since layers are present in that model non-conventional Cosserat components are activated. Thus the influence of the material parameters on the localization zone could be studied. All plasticity analyses are carried out with non-accosiative plasticity and dilatancy angle zero. The aim of the current chapter is namely to answer the questions: *Which aspects of the plasticity implementation based on the Cosserat theory should be considered applicable the jointed rock analysis?* and *How do additional Cosserat components influence the results?*

5.1. Verification with one element model

The most simple benchmark for the non-linear algorithm is the one element model ($1x1m$) with homogeneous material. The following elastic and strength parameters were used: the Young's modulus is $10Gpa$, the Poisson's ratio is 0.25, the cohesion and the friction angle are $10kPa$ and 20° respectively. For the Cosserat formulation joint normal and shear stiffnesses ($k_n = 1e15N/m^3, k_s = 1e15N/m^3$) were chosen high enough to prevent their influence and make the material homogeneous. Moreover, boundary conditions were selected in a way that ensures that only vertical (top nodes) and one direction horizontal movements are possible. The deformation controlled compression/tension load was applied on the top nodes. Geometry and boundary conditions are shown in Figure (5.1).

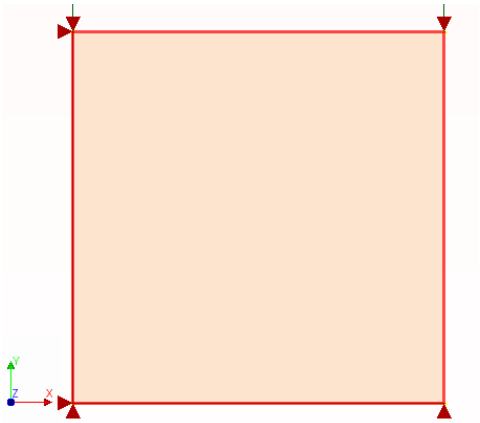

Figure 5.1: One element model, dimension 1x1 m

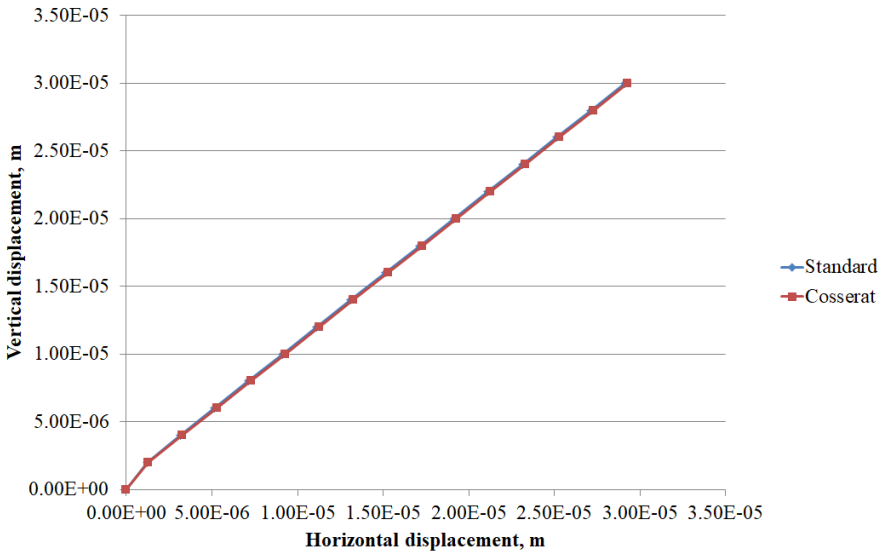

Figure 5.2: Verification of Von Mises implementation for the one element model under vertical compression, vertical displacement versus horizontal displacement

Vertical compression

Horizontal displacement components for the Von Mises perfectly plastic model obtained with standard continuum mechanics formulation and with the Cosserat formulation are in Figure (5.2). In general, fair correlation between two models was observed, revealing the fact that the Cosserat model could be reduced to the standard finite element formulation. Von Mises yield criterion enhanced with mean stress invariant transforms into Drucker-Prager yield function. In Figure (5.3) f-u graph for vertical displacement component, horizontal component of displacements and equivalent plastic strains verification are presented and shows perfect correspondence between two formulations.

Previous verification is valid for the shearing part of the yield envelope, in Figure (5.4) it is denoted as a Regular failure surface. Hence, special treatment is required if the tension takes place. That conclusion was made based on the tension test conducted for the same one element model. If the mean stress calculated based on the trial stress is higher than the apex value, then the numerical error occurs in the Regula Falsi method. Specifically, the function value on both Regula Falsi boundaries be-

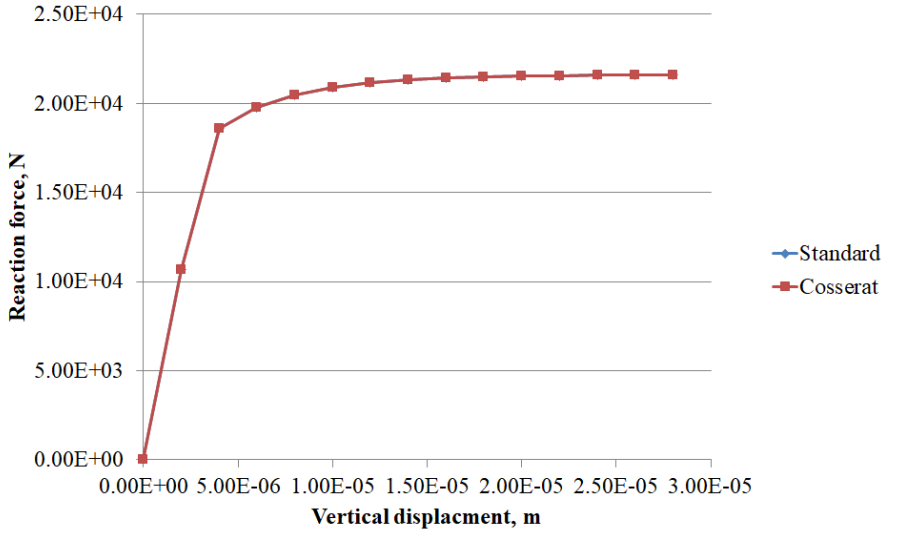

(a)

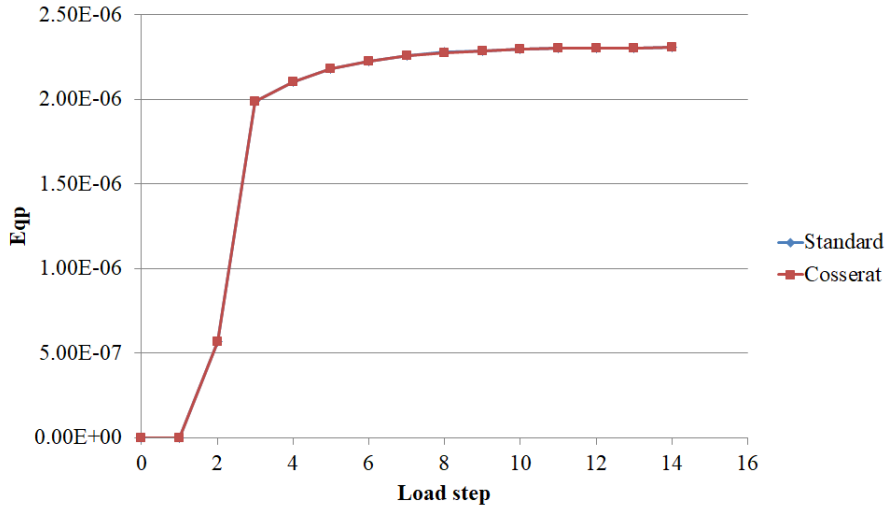

(b)

Figure 5.3: Verification of Drucker-Prager implementation, one element model under vertical compression (a) force-displacement curve, (b) Equivalent plastic strain versus load step

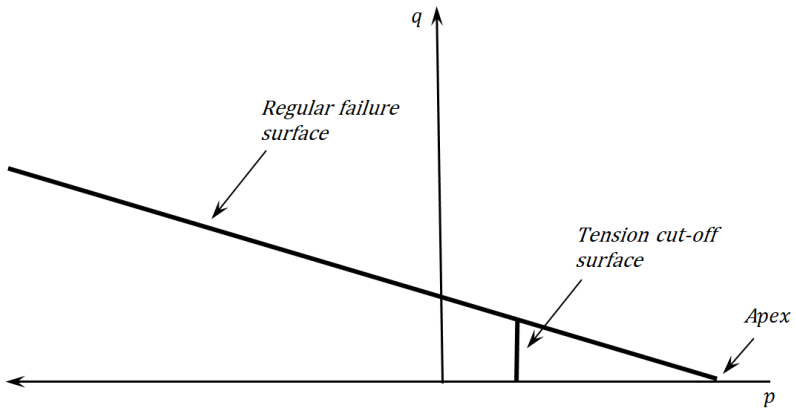

Figure 5.4: Drucker Prager yield surface in p-q space

comes positive, placing it outside of the yield surface and make it impossible to find the increment of plastic multiplier. As a consequence, the returned to the the yield surface stress state remains undefined. It was explained by the undetermined direction when it drops outside of the apex. In order to solve that problem for the one element model, load step was reduced, such as mean trial stress is always lower than the apex, however it is not easy to control for more complicated models. Another possible solution is to introduce the tension cut off algorithms. In the present research two of them were implemented and tested: cut off with returning to the apex point in the absence of prescribed maximum tensile strength and the tension cut-off based on the prescribed maximum means stress in tension. In Figure (5.4) both options are illustrated.

Apex returning

The following condition was used to identify if the trial stress is beyond the apex point:

$$I(\sigma_{tr}) > \eta, \tag{5.1}$$

where η is the apex value and $I(\sigma_{tr})$ is the first stress invariant. Literature studying shows [28] that the following condition could be used in order to modify the stress state if the mean pressure is beyond the apex point.

$$\boldsymbol{\sigma_n} = \{\eta, \eta, \eta, 0, 0, 0, 0\}, \tag{5.2}$$

In should be noted that micromoments are also equal to zero, because there is no shear stress at that point. Again the same homogeneous one element model with opposite to the compression deformation load was used for the verification. Results are very similar with the mean stress tension cut-off which would be explained next. For that reason, results are presented only for the latter.

Mean stress tension cut-off

Another way to handle the tension behaviour is to prescribe maximum mean stress for the tensile region. Opposite to the previous method, the suggested one has non-zero shear stresses and micromoments. The the entrance condition for the tension cut-off is:

$$I(\sigma_{tr}) > p_{cut}, \tag{5.3}$$

where p_{cut} is the prescribed mean pressure; after that the stress state could be returned to the point where two failure surfaces intersect with or parallel the cutting surface. For the verification, the

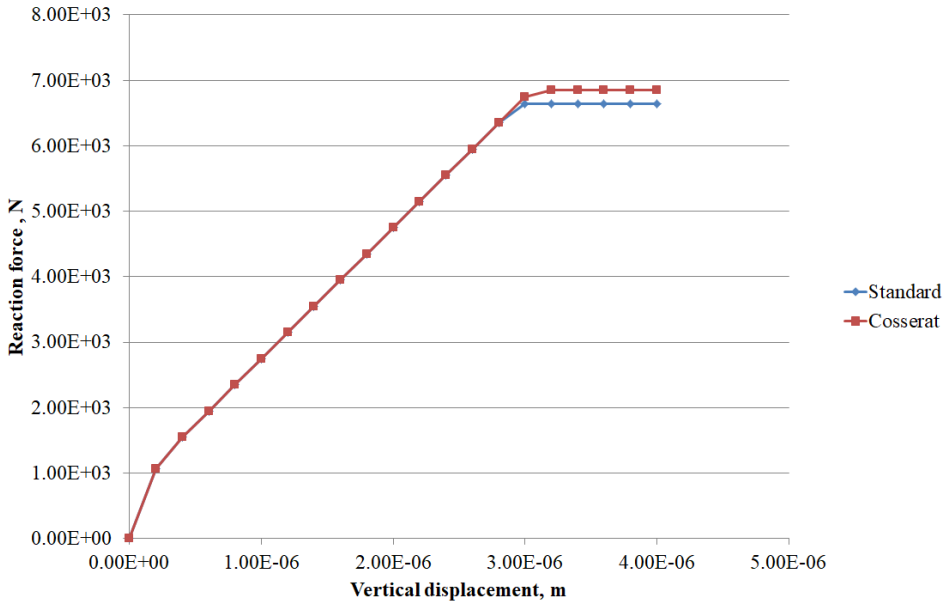

Figure 5.5: Verification of Drucker-Prager implementation for the one element model with mean stress tension cut-off exposed to tension, force-displacement curve

mean stress was selected equal to $1kPa$, the obtained results are presented in Figure (5.5). It could be observed for the picture that the first step drops into elastic regime allowing the compression in the horizontal direction (negative value). Starting from the second step the behaviour becomes plastic gradually reaching the peak strength. The shortcoming of the proposed method is that the new stress state is formed only based on the condition that the mean stress must be equal to the prescribed value. That implies the possibility for stress component(s) becoming highly in tension (even higher than the prescribed value) unless it is equilibrated with other negative component(s).

5.2. Jointed column under vertical compression

Having done the verification of the non-linear analysis for the homogeneous one element model, the following step is to consider more complicated geometry with inclined layers. For that purpose the jointed column from the elastic verification step with modified boundary conditions and load was adopted and could be found in Figure (5.6). The suggested model includes bottom and top translational constraints and compressed with displacement control manner. These boundary conditions were chosen to provoke the localization of the shear strains into shear bands. It should be mentioned that the Cosserat model has free microrotation in all boundaries. The material has the following strength parameters: cohesion is equal to 10 kPa and friction angle is 43° for both intact rock and joints. Firstly, the column with homogeneous material was tested. Secondly, layers were introduced and the influence of yield surface material parameters (a_1, a_2, a_3) and the layer thickness on the shear band was studied.

5.2.1. Homogeneous column

In order to appreciate the advantage of the Cosserat model it was compared with the standard homogeneous model. One of the crucial differences between two models is the presence of internal length characteristic in the Cosserat model. In the current implementation that role is played by

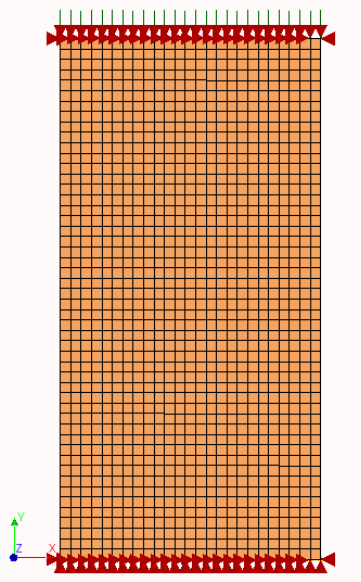

Figure 5.6: Two dimensional jointed column with displacement control load on the top, the Cosserat model

the layer thickness and for the present analysis it is equal to 0.35m with high joint shear and normal stiffnesses $k_s = k_n = 1000GN/m^3$. Two equal shear bands are expected to be developed due to symmetry conditions. Equivalent plastic strain profile for the standard homogeneous model is presented in Figure (5.7). Here two loading steps could be observed: on the left there is one step before the failure where the concentration of the plastic strain along the shear band is initiated, while out of the localization zone the material tends to deform elastically; on the right the specimen is at failure. The computation remains stable until strong strain gradient between material inside and out of the shear band develops. Further load leads the the divergence due to the shear band development which orientation approaches commonly used in practise Coulomb angle $\pi/2 + \varphi/2 = 66.5°$. The small deviation in orientation ($\sim 6°$) was explained by boundary conditions preventing any movement on the top and bottom of the specimen. That is why the band is shifted out of the corners. At that point the standard continuum mechanics governing equation fails due to loosing the ellipticity. This is the point where alternative techniques such as the Cosserat formulation appeal to model the localization phenomenon. The review of these techniques could be found in the beginning of presented research.

Same experiment was conducted for the Cosserat model and the equivalent plastic strain profile is shown in Figure (5.8a). Computation remained stable during shear band development, taking into account the fact that the final load is higher than for the previous model and equals to -0.014m. Two symmetric shear bands orientated toward 60° developed on the specimen. Homogeneous material and the absence of any imperfections evoked equal strain magnitude in both bands without triggering to the predominant direction. Looking at curvatures interesting detail was found, notably that they predominantly have developed on the shear band edges. It was explained by the inherent characteristic of the microrotation degree of freedom which servers to represent non-homogeneous straining. In the suggested example, the largest strain difference is on the band borders exactly where curvatures evolved. Furthermore, the activation of the microrotation degree of freedom could be observed in Figure (5.9), where components of the shear strain are presented. It is clearly seen that shearing mechanism leads to non-symmetric shear strains ε^{pl}_{xy} and ε^{pl}_{yx} and the Cosserat model is able to reproduce that behaviour due to microrotations degree of freedom.

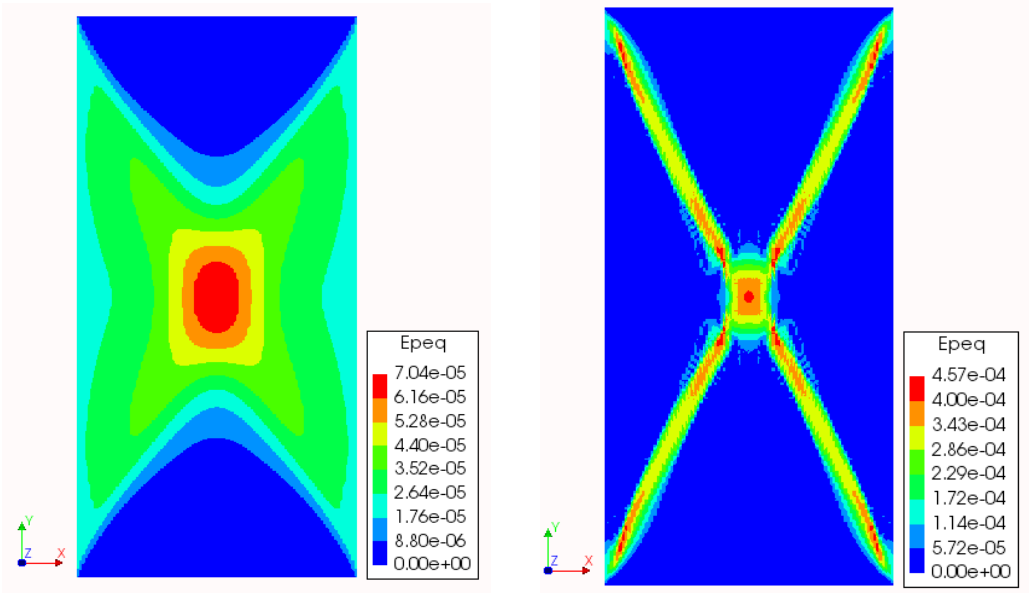

(a) Load -0.0001m (b) Load -0.00012m

Figure 5.7: Equivalent plastic strain field, one load step before failure (a) and failure of the specimen (b) under displacement control vertical load, standard continuum formulation

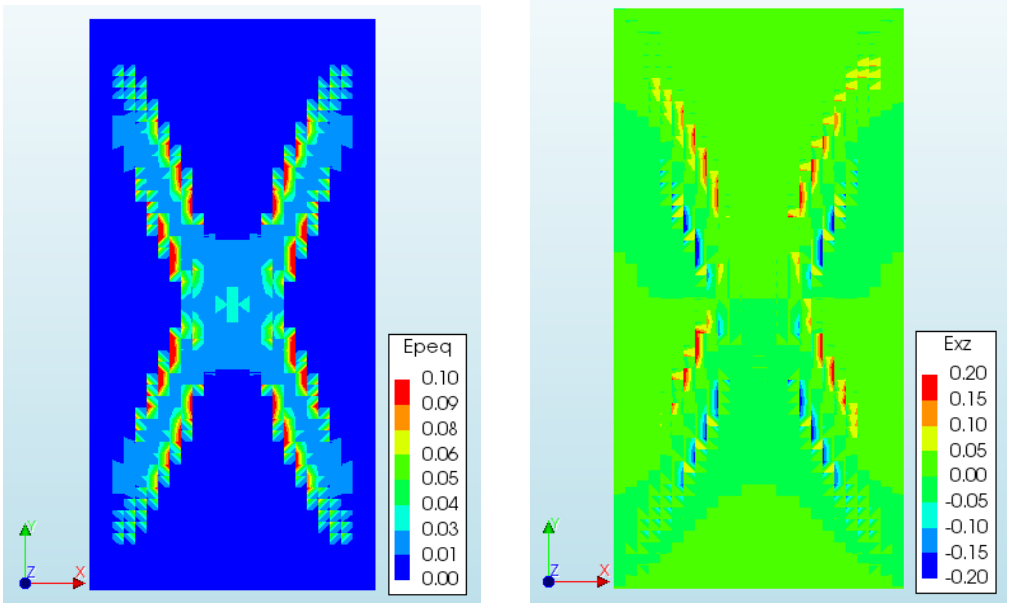

(a) Epeq (b) κ_{xz}

Figure 5.8: Equivalent plastic strain profile of the vertically compressed homogeneous column obtained with the Cosserat formulation, load -0.014 m

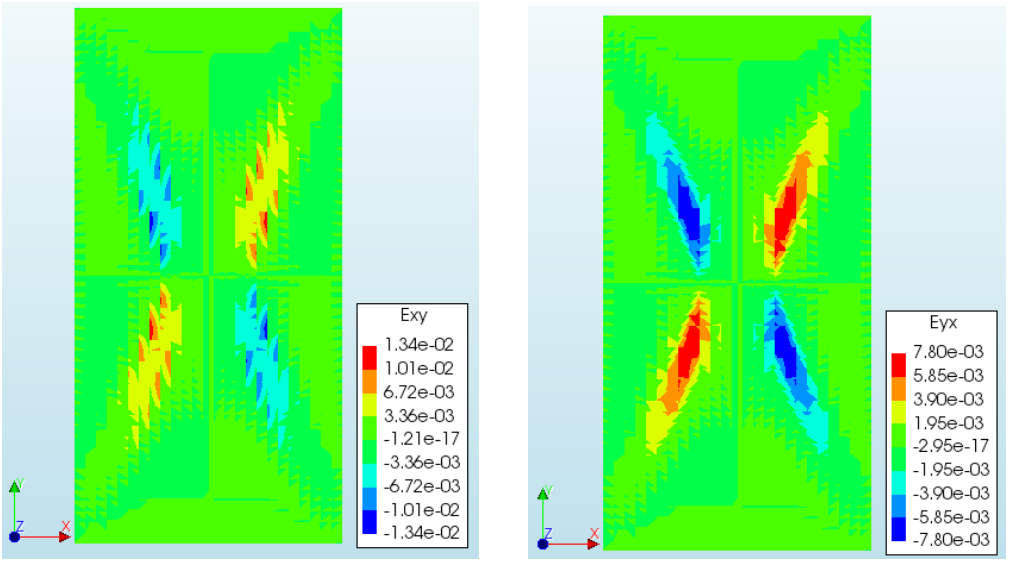

(a) ε_{xy}^{pl} (b) ε_{yx}^{pl}

Figure 5.9: Plastic shear strain components of the vertically compressed homogeneous column obtained with the Cosserat formulation, load -0.014 m

5.2.2. Layered column

The main goal of the experiment with layered column under vertical displacement load is to understand the influence of internal length parameter (the layer thickness) and yield surface material coefficients on the displacements localization area. In the proposed example layers inclination is 30 degrees tilting counter-clockwise from the horizontal and the shear stiffness was fixed to $k_s = 2207 MN/m^3$ in all calculations. In Figure (5.10) numerical experiments for the different layer thicknesses are presented. It could be observed that thicker layers (h = 0.35m) generate thicker shear band and the opposite for the thinner layers (h = 0.088m). Since the thickness sets "intrinsic length" it defines the scale of the stress and couple stresses thus smaller thickness induces less influence of the far material. That is why the material with a thinner thickness has a thinner shear band but higher concentration of the deformation on it. In contrast, the specimen with a larger internal length parameter experiences a thicker shear band, providing more space to redistribute the deformations inside the shear band and results in their overall reduction.

Next, the studying of the material parameters of the Drucker-Prager yield criterion was conducted. In the literature [31], [30] mainly three options for these parameters are considered: static ($a_1 = \frac{3}{4}$ $a_2 = -\frac{1}{4}$ $a_3 = \frac{1}{8}$), kinematic ($a_1 = \frac{3}{8}$ $a_2 = \frac{1}{8}$ $a_3 = \frac{1}{4}$), standard ($a_1 = \frac{1}{4}$ $a_2 = \frac{1}{4}$ $a_2 = \frac{1}{2}$) sets. Figure (5.11) shows the components of the plastic curvatures κ_{xz} revealing that the standard set favours larger curvatures and implies more pronounced influence of the micromoments. At the same time the horizontal plastic strain component ε_{xx}^{pl} increases in the opposite way, causing higher localization in the shear band Figure (5.12). The thickness of shear band hardly changes for three sets. The influence of the parameters is clearly seen on the horizontal displacement profiles shown in Figure (5.13). Here, the displacements are lower for the case with higher curvatures. It was explained by the contribution from the micromoments, such that they provide additional bending resistance and sustain part of the load.

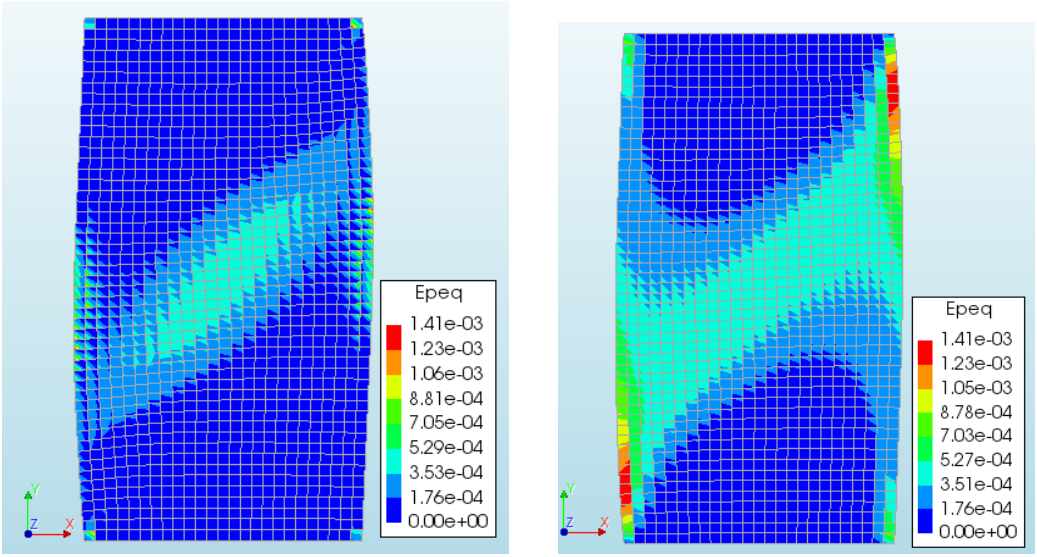

(a) $h = 0.088m$ (b) $h = 0.35m$

Figure 5.10: The influence of the thickness parameter on the shear band, horizontal plastic strain component of the Cosserat model under vertical displacement load -0.002m

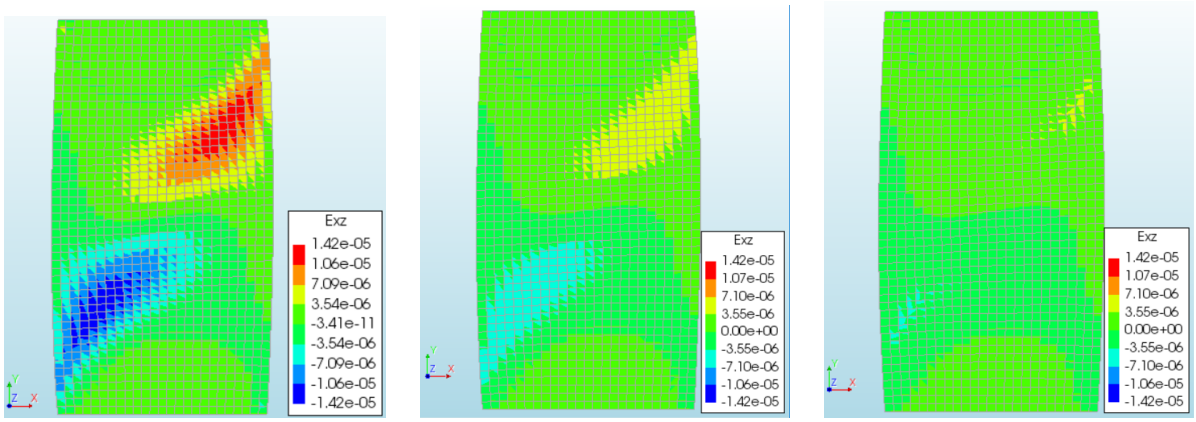

(a) Standard set (b) Kinematic set (c) Static set

Figure 5.11: Micro-curvatures plastic component, the Cosserat model

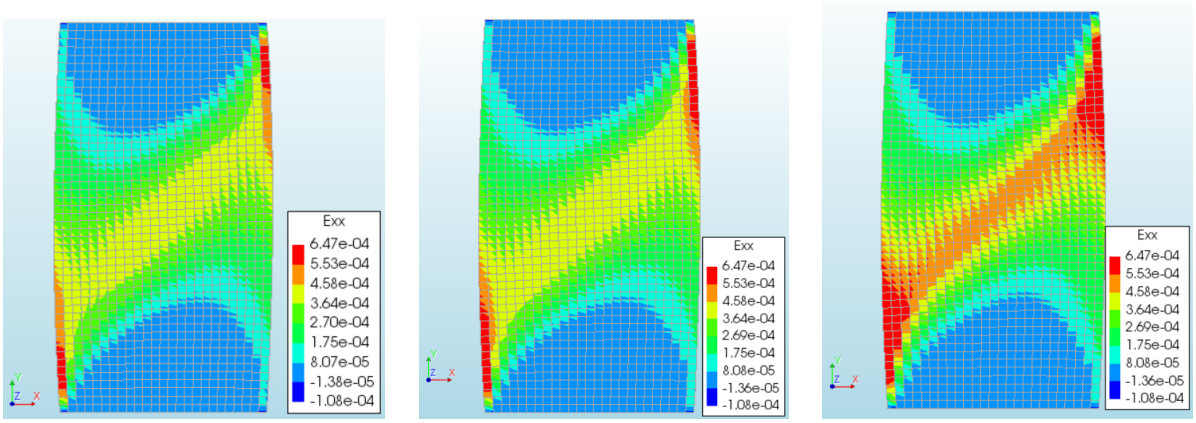

(a) Standard set (b) Kinematic set (c) Static set

Figure 5.12: Horizontal component of the plastic strain, the Cosserat model

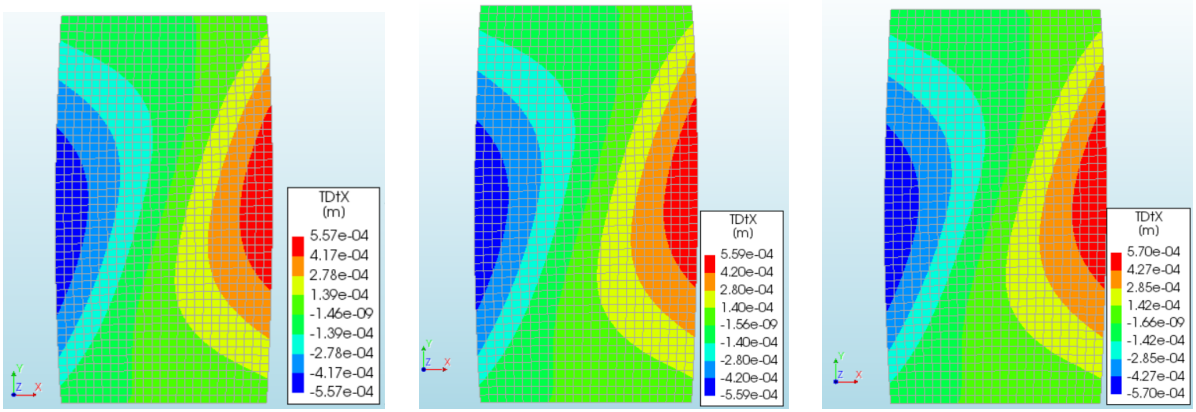

(a) Standard set (b) Kinematic set (c) Static set

Figure 5.13: Horizontal displacements profile, the Cosserat model

5.3. Summary

In the current chapter the plasticity algorithm verification for the one element model and two dimensional jointed column were presented. In general, the commercial software packages do not include the Drucker-Prager yield criterion for the interfaces. That is why the first benchmark was to prove that when reduced to the homogeneous limit case, the Cosserat plasticity formulation corresponds with the standard continuum formulation. Both Von Mises and Drucker-Prager models have demonstrated fair match with the standard model applying it for the one element model. Additionally, two possible methods to introduce the tension are presented and tested, showing promising results. However, even though results are positive for the one element model, it is not necessarily the same for more complicated models with complex geometry and activated layers. Thus, additional numerical experiments were conducted for the two dimensional jointed column model. It was found that the homogeneous standard formulation fails when the bifurcation occurs. The model based on the Cosserat formulation does not suffer that problem and numerically stable shear bands development was observed. Furthermore, the influence of the Cosserat parameters reveals that the thickness of the layer controls the shear band thickness and deformations magnitude concentrated inside the band. Essentially, thinner layers generate a thinner shear band with higher deformations. Yield surface parameters regulate the contribution of the micromoment component in the material resistance. Smaller horizontal displacements were found for the higher curvatures, due to additional bending resistance.

6

Slope stability analysis

The following chapter presents the application of the implemented Cosserat formulation to the slope stability analysis. One of the parameters which influences the stability of the slope and defines the type of failure is the direction of discontinuities. That is why, the layers inclination was selected such as three main mechanisms could be studied: planar, circular and toppling. All of them are the combination of friction and tension failure modes. The aim of the following chapter is to apply the developed formulation for the slope stability analysis, detect possibilities and limitations. The procedure was organised as follows: firstly, the elastic model versus explicit model was verified; secondly, homogeneous plastic model was verified versus standard continuum model; thirdly, the stability analysis of jointed slope was carried out with the strength reduction method. This method involves the reduction of the strength parameters each step while applying self weight. The stop criteria is the maximum allowable parameter for instance maximum displacements or when lack of convergence occurs.

For the verification of stability analysis the explicit model constructed in Rocscience (RS2) was used. The Drucker-Prager yield criterion for the joints is not available in this package. That is why the Mohr Coulomb criterion was selected for both intact and joints materials. This assumption makes impossible the quantitative comparison between the Cosserat and explicit models, only qualitative can be done. In general, higher displacements are expected for the Mohr Coulomb because Drucker-Prager is the circumscribed around Mohr Coulomb surface cone, allowing more stress states to drop into elastic region.

The geometry was chosen, based on the example discussed in [22]. In the current work, it was scaled down to reduce the number of elements and computation time, moreover the base was extended to prevent the influence of the base border to the results. The geometry with suggested boundary conditions is illustrated in Figure (6.1). The material parameters for the intact rock were also derived based on the mentioned source Table(6.1). In the present formulation single failure criterion for the smeared material was considered with zero tensile strength modelled with mean stress tension cut-off algorithm. That implies the same strength parameters for the intact rock and joints. All plasticity analyses are carried out with non-accosiative plasticity, dilatancy angle zero and standard set of the yield criterion material parameters. The presence of joints was accounted in the constitutive model with assigned normal and shear stiffnesses, the layers thickness and their inclination Table (6.2).

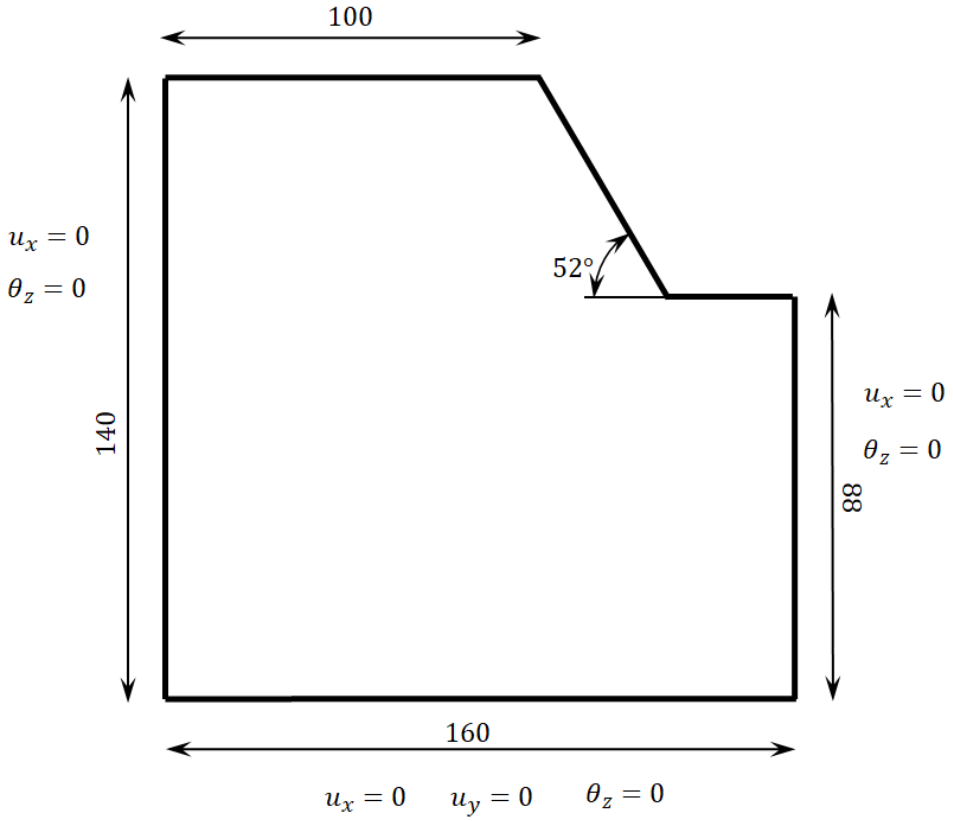

Figure 6.1: Slope geometry with boundary conditions

Material	E, GPa	ν	c, MPa	$\varphi,^\circ$	$\psi,^\circ$
Intact rock	9.072	0.26	1	43	0

Table 6.1: Continuum material parameters

Material	$k_n, GN/m^3$	$k_s, GN/m^3$	c, MPa	$\varphi,^\circ$	$\psi,^\circ$	h, m
Joint	1	0.01	1	43	0	5

Table 6.2: Joint material parameters

6.1. Elastic analysis of the slope

Before proceeding with non-linear analysis, the elastic solution was validated versus an explicit model constructed in the Rocscience package. Results of total displacement field for different layer inclinations are shown in Figure (6.2). In general, the displacement pattern of the Cosserat model coincides with the explicit joint model results. Further decreasing of element size led to small changes in displacements, that is why it was decided to proceed with the same amount of elements (about 20220 elements), to reduce the calculation time. In Figure (6.2a, 6.2b) the characteristic features for the planar failure could be observed. Since, the inclination of the layers is lower than the slope inclination, the top rock mass slides down along the discontinuity and produces the maximum displacements on the moving part. Circular failure usually starts close to the slope toe and then propagates as a shear band into the slope across the weakest path. That type of failure usually occurs if the inclination of layers is higher than the slope, here discontinuities play a secondary role. The initial behaviour of that type of failure with concentrated displacements close to the toe could be seen in Figure (6.2c, 6.2d) for both models. Toppling failure is one of the most complicated failure modes to model. It is mainly driven by the tension resistance of the material and involves the rotation like behaviour of layers. Elastic behaviour does not show the expected deformation pattern which was explained by the influence of boundary conditions Figure (6.2e, 6.2f) . However, the prediction for the non-linear analysis is the gradual movement of maximum displacements to the right top corner due to higher tension and lower side support.

6.2. Non-linear analysis of homogeneous slope model

The implementation of plasticity formulation was first tested for the homogeneous material versus the standard formulation with Drucker-Prager yield criterion. Gravity load analysis was used to activate the non-linear behaviour. In total 10 additional to the self weight steps were applied, each one equals to half of the self weight. Consequently, the highest applied load is five times more than the self weight. The plasticity was activated from the first step. Figure (6.3) reveals a fair match between two models in total displacements and normal stress. Additionally, in Figure (6.4) two shear stress σ_{xy}, σ_{yx} are presented. Due to the homogeneous material they are almost equal in both directions.

6.3. Slope stability analysis

Strength reduction analysis was conducted in order to evaluate the stability of the jointed slope. Strength parameters were reduced each step by the coefficient of 0.1 and the weight load was applied in several steps. The obtained results indicate adequate qualitative correspondence between the two models for the three suggested slopes as it could be observed in Figure (6.5), Figure (6.6), Figure (6.7).

Circular failure

Displacement components of the slope with layers steeper than the slope angle display the development of circular failure. It starts from the toe and propagates along the weakest zones of the material. Often joints present less resistance playing a major role in the failure guiding. It was observed that the Cosserat model is able fairly reproduce failure mechanism, showing the concentration of deformations on the slope toe and further development similar to the explicit joint model. However, the Cosserat model presents lager area with high deformations. Possible reasons for that are:

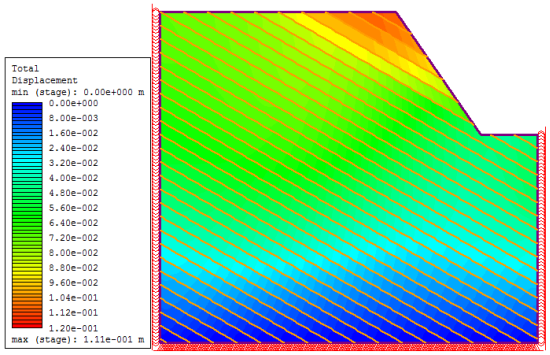

(a) $\beta = 30°$, Explicit model RS2

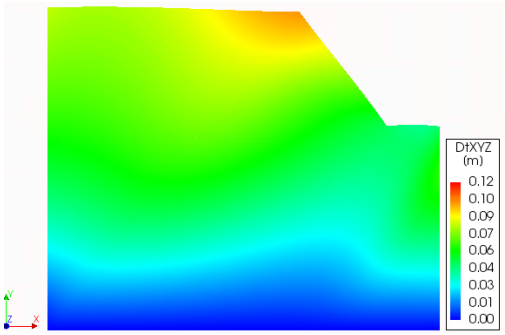

(b) $\beta = 30°$, Cosserat DIANA FEA

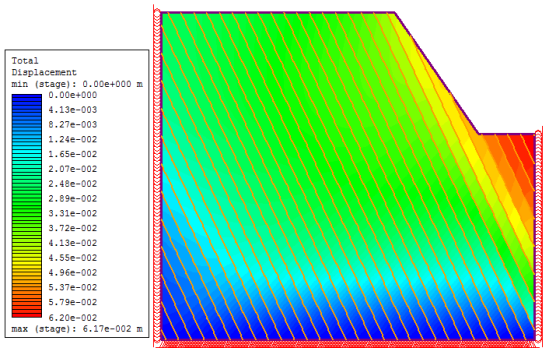

(c) $\beta = 65°$, Explicit model RS2

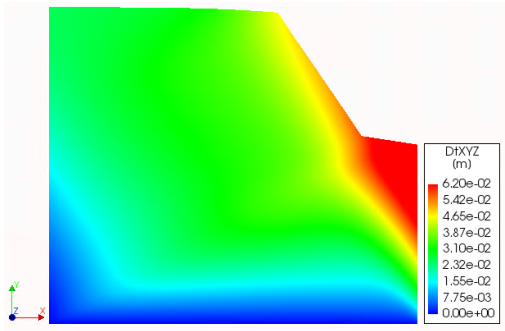

(d) $\beta = 65°$, Cosserat DIANA FEA

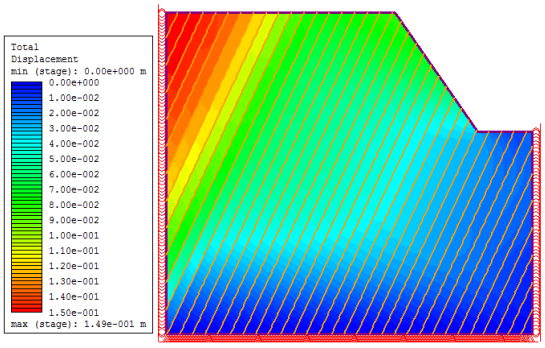

(e) $\beta = 65°$(toppling), Explicit model RS2

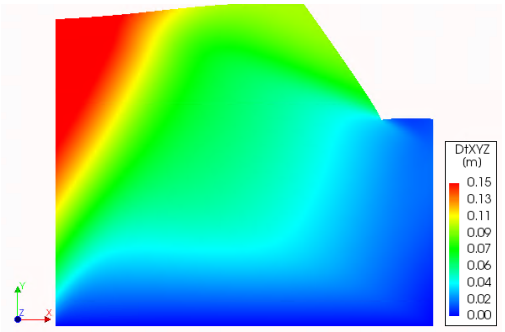

(f) $\beta = 65°$(toppling), Cosserat DIANA FEA

Figure 6.2: Slope elastic model verification explicit model (RS2) versus Cosserat model (DIANA FEA), total displacements field

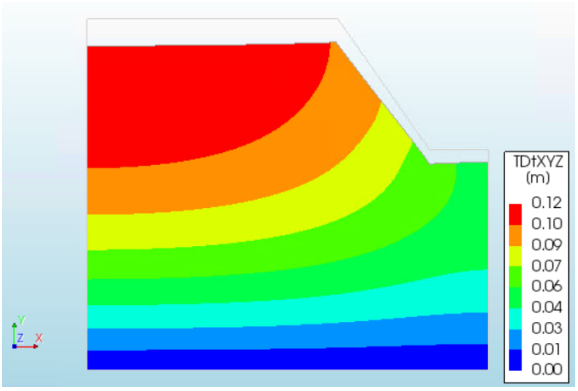

(a) Standard formulation, total displacements profile

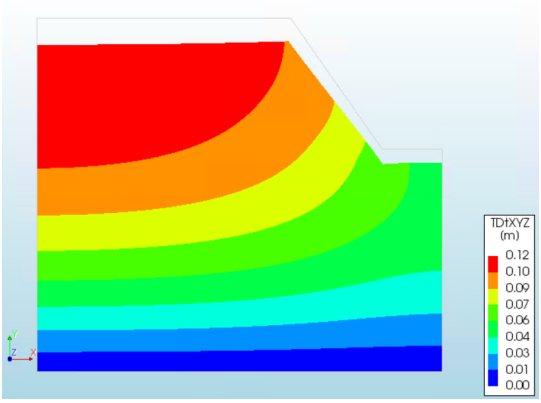

(b) Cosserat formulation, total displacements profile

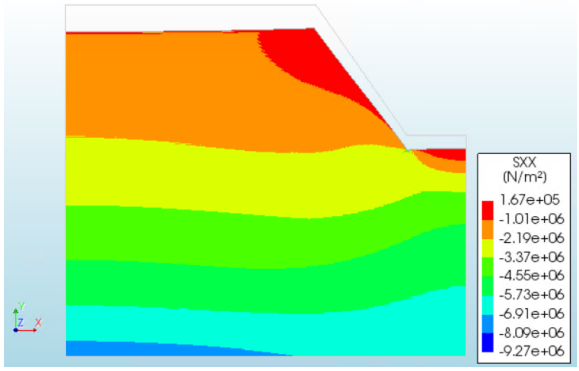

(c) Standard formulation, horizontal stress

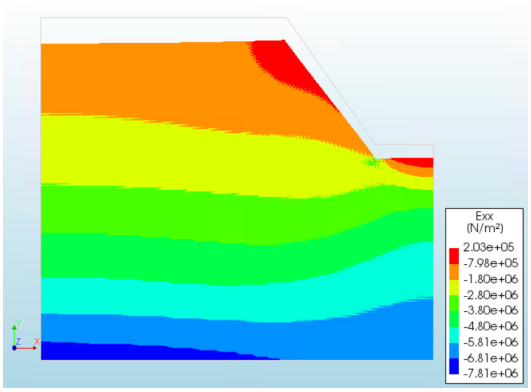

(d) Cosserat formulation, horizontal stress

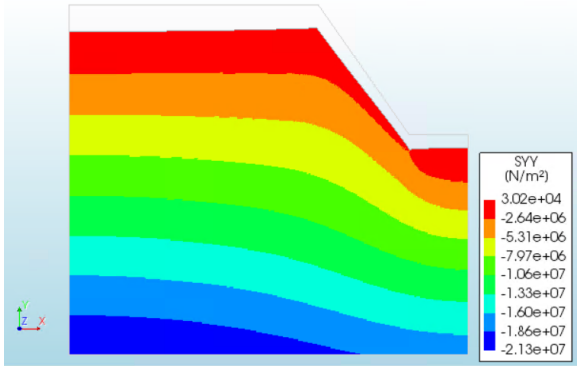

(e) Standard formulation, vertical stress

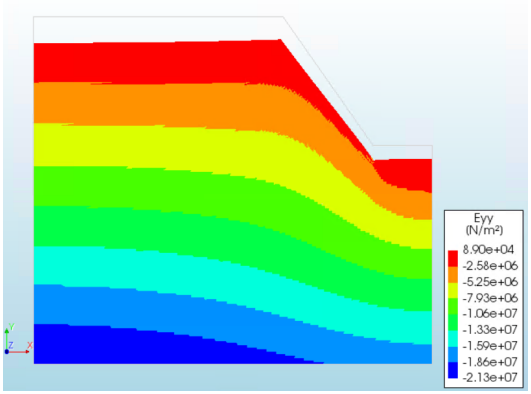

(f) Cosserat formulation, vertical stress

Figure 6.3: Verification of the Drucker-Prager implementation, homogeneous slope under gravitational load.

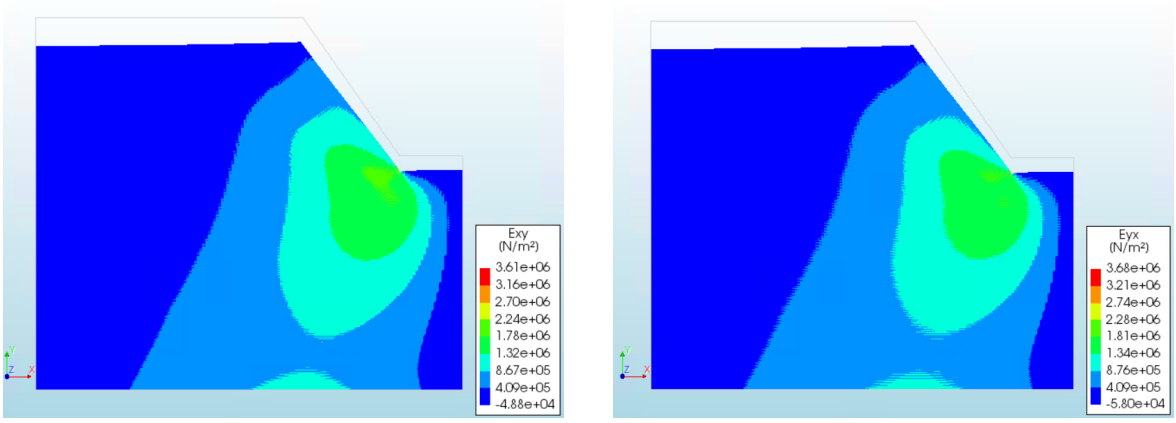

(a) σ_{xy} (b) σ_{yx}

Figure 6.4: Cosserat formulation, shear stresses

the Cosserat formulation smears some local effects over the larger area; in the explicit model zero tension cut-off based on principle stresses is considered. The later ensures less capacity comparing with mean stress tension cut-off employed in the Cosserat formulation. The consequences would be covered in details later on.

Planar failure

The required condition for the planar failure is the daylighting joints which under certain conditions, for instance excessive water pressure in the infilling material, could lead to the slippage of rock blocks. It was observed that the explicit model shows the combination of toe failure and tension damage in the top caused by layers sliding down. The Cosserat model has the capacity to localise the failure zone thus part of the rock mass subjected to movement. In contrast with the explicit model there is no major displacements in the toe observed, hence the equivalent plastic strain profile revealed initiation of the failure on the toe similar to explicit model. Additionally, that layers direction does not present significant layers bending and the Cosserat formulation should not bring important difference in results.

Toppling failure

Among three suggested cases the Cosserat contribution is the most pronounced when the toppling failure occurs. It involves the bending of interacting rock columns formed by the steeply dipping layers or joints fixed on the base. Under their own weight these columns start to bend transferring the load on underlying material and initiate the compressive and tensile bending stresses. If the load exceeds material tensile resistance the failure takes place. The Cosserat theory could be advantageous for that type of failure, since it is capable to consider the bending mechanism thus brings the additional resistance. That is why toppling failure was selected for more detailed analysis.

The non-linear slope stability analysis has enabled to investigate the effect of Cosserat non-conventional components. Due to curvatures and couple stresses are the conjugate pairs only one of them was chosen to be presented. For example, initially high couple stresses reduce while reduction factor increases; the evidence could be observed in Figure (6.8) where couple stress μ_{zy} profiles for two reduction factors are presented. That implies the diminishing of the bending resistance of material due to lower strength capacity. Consequently, the layers with degraded bending resistance lose their ability to bend and transfer their weight on layers below. Finally, the bending stress exceeds

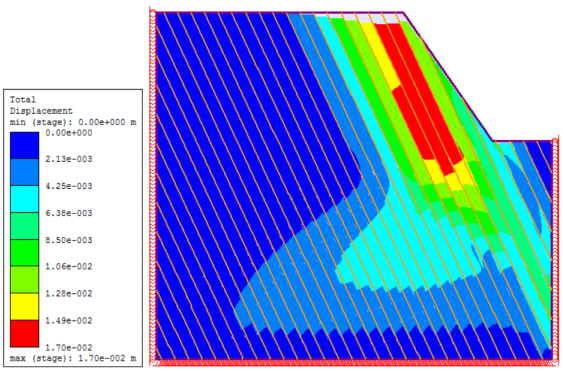

(a) Total displacement explicit model, RS

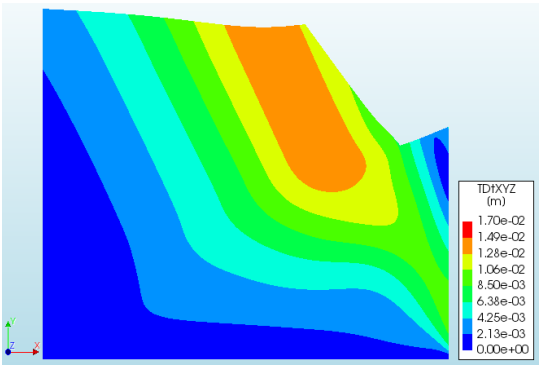

(b) Total displacement Cosserat model, DIANA FEA

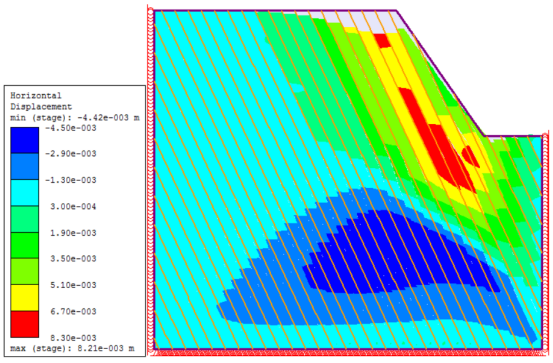

(c) Horizontal displacement explicit model, RS

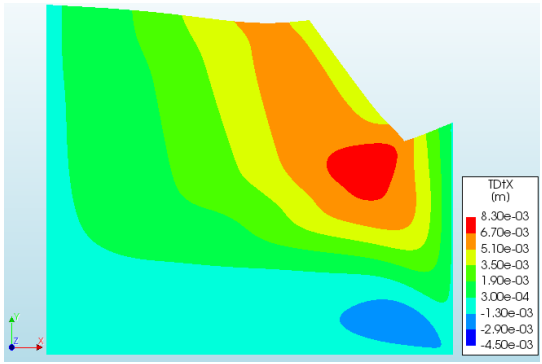

(d) Horizontal displacement Cosserat model, DIANA FEA

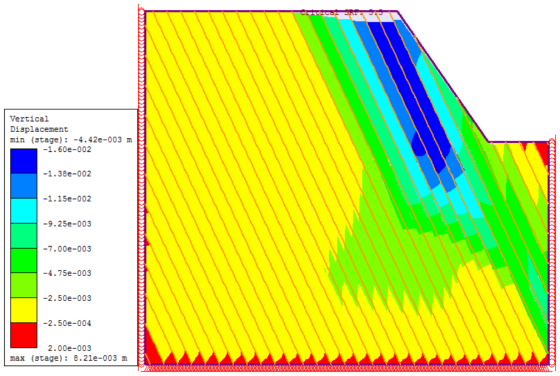

(e) Vertical displacement explicit model, RS

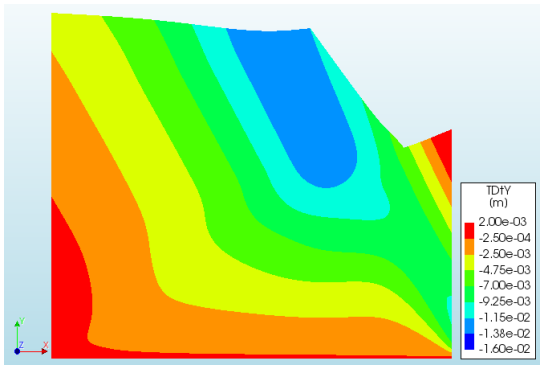

(f) Vertical displacement Cosserat model, DIANA FEA

Figure 6.5: Slope stability analysis, $\beta = 65°$, strength reduction factor 3

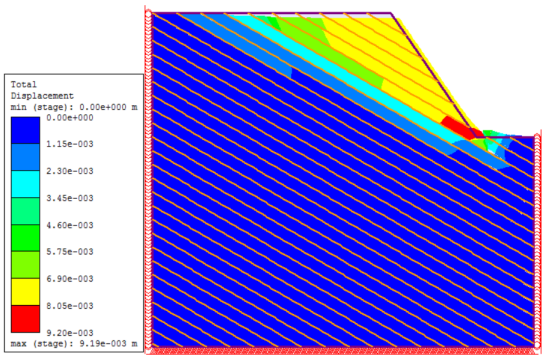

(a) Total displacement explicit model, RS

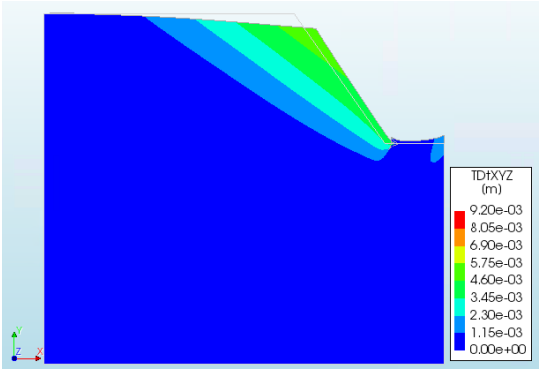

(b) Total displacement Cosserat model, DIANA FEA

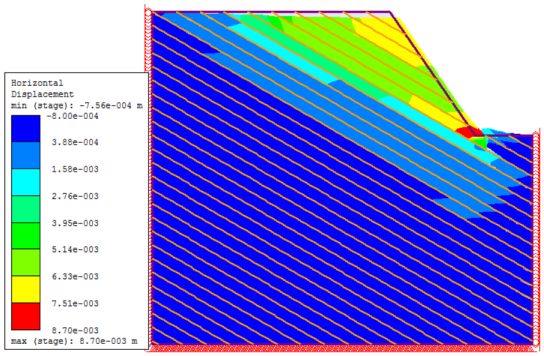

(c) Horizontal displacement explicit model, RS

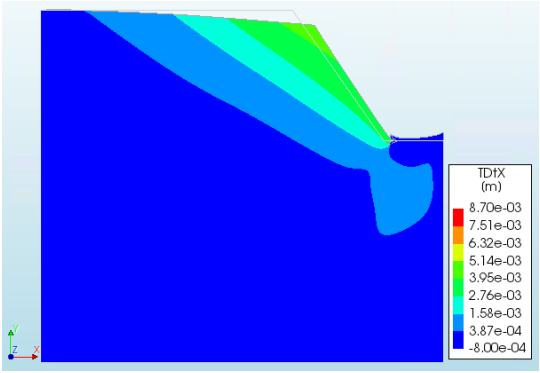

(d) Horizontal displacement Cosserat model, DIANA FEA

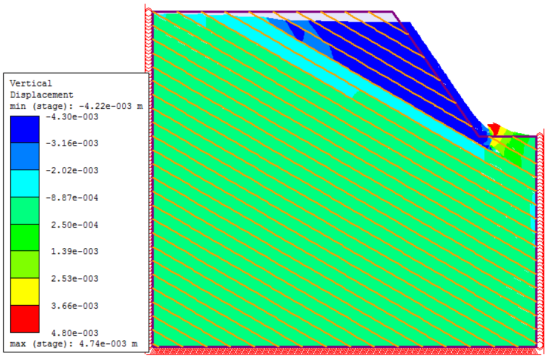

(e) Vertical displacement explicit model, RS

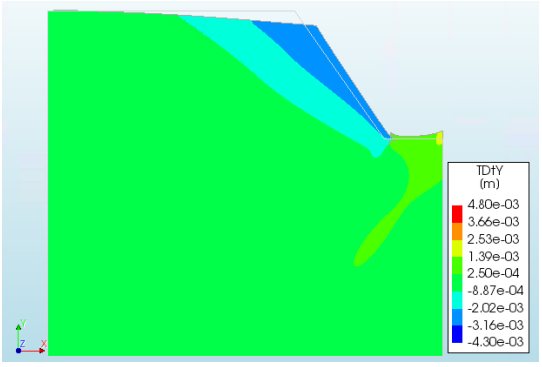

(f) Vertical displacement Cosserat model, DIANA FEA

Figure 6.6: Slope stability analysis, $\beta = 30°$ strength reduction factor 1.5

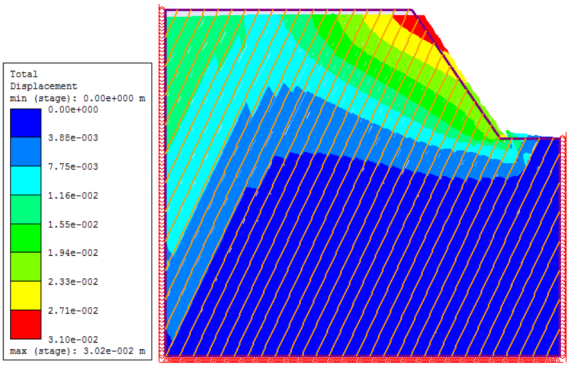

(a) Total displacement explicit model, RS

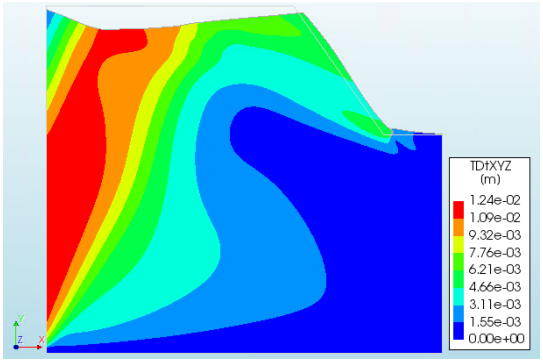

(b) Total displacement Cosserat model, DIANA FEA

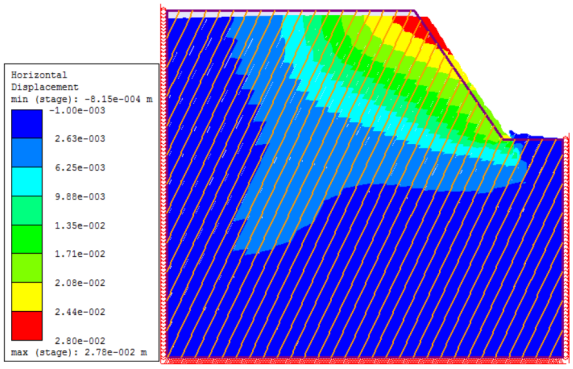

(c) Horizontal displacement explicit model, RS

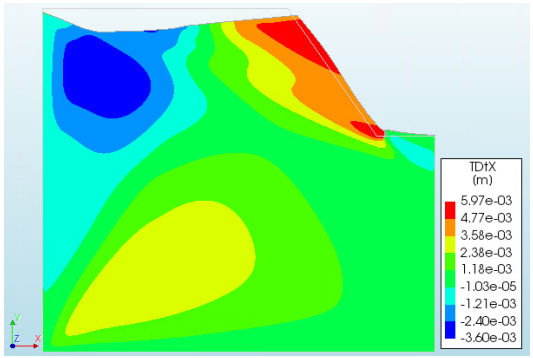

(d) Horizontal displacement Cosserat model, DIANA FEA

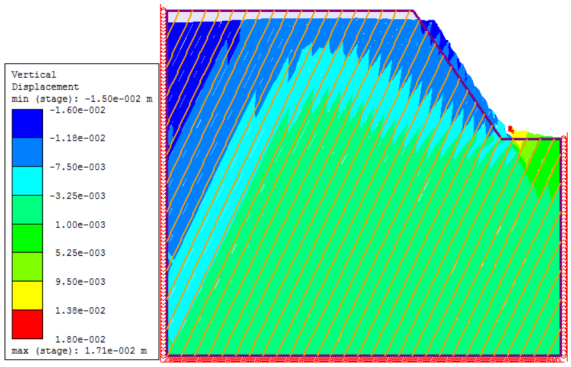

(e) Vertical displacement explicit model, RS

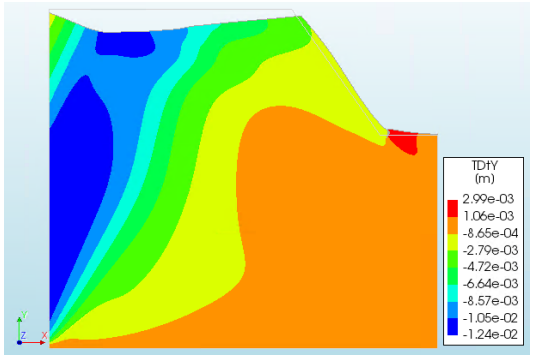

(f) Vertical displacement Cosserat model, DIANA FEA

Figure 6.7: Slope stability analysis, $\beta = 65°$(toppling) strength reduction factor 2.1

the material tensile strength, as a result large displacements start to develop on the toe and initiate the failure as it is shown in Figure (6.9). Similar behaviour was discovered by Adhikary *et al.*[6], there toppling failure was reproduced through the centrifuge experiments. This example revealed that by means of the Cosserat microrotations degrees of freedom the important mechanism influencing the stability of the structure could be captured.

It was not always possible to obtain the same as for the explicit model maximum safety factor due to the numerical failure while computing plastic multiplier. The reason of mentioned above short-

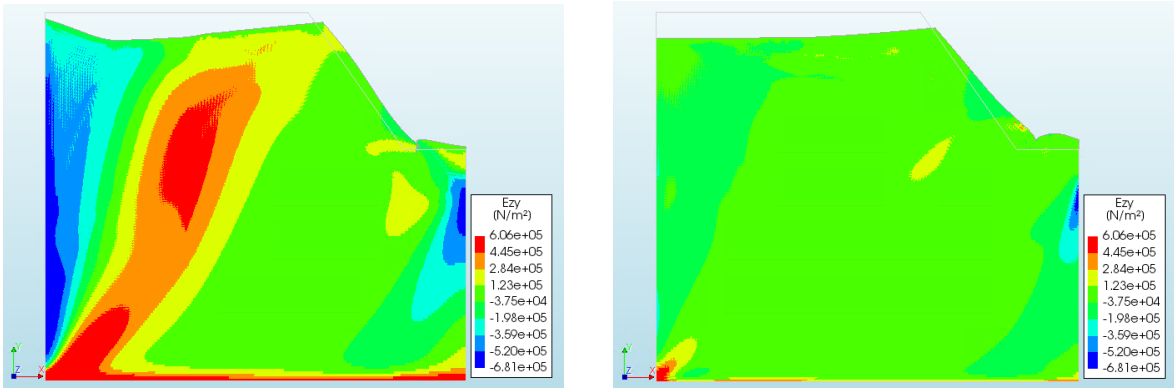

(a) Reduction factor 2.6 (b) Reduction factor 5.7

Figure 6.8: The couple stress component μ_{zy} for different reduction factors

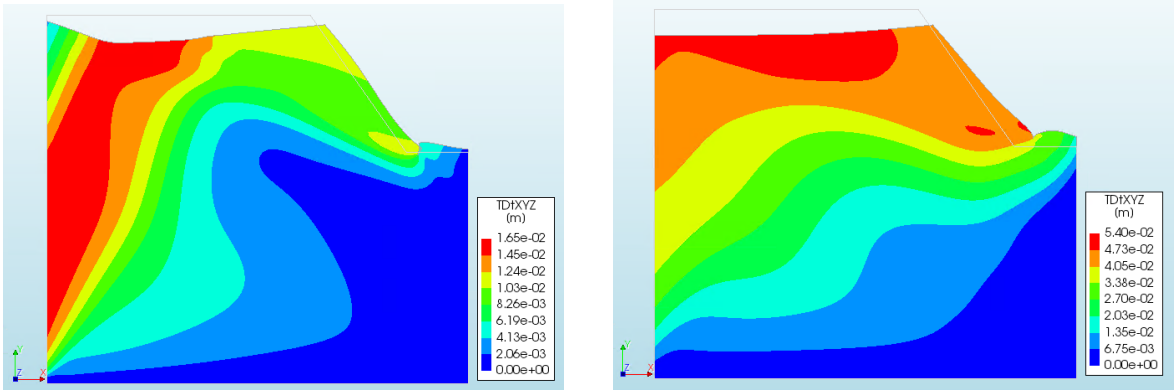

(a) Reduction factor 2.6 (b) Reduction factor 5.7

Figure 6.9: The development of total displacements field for different reduction factors

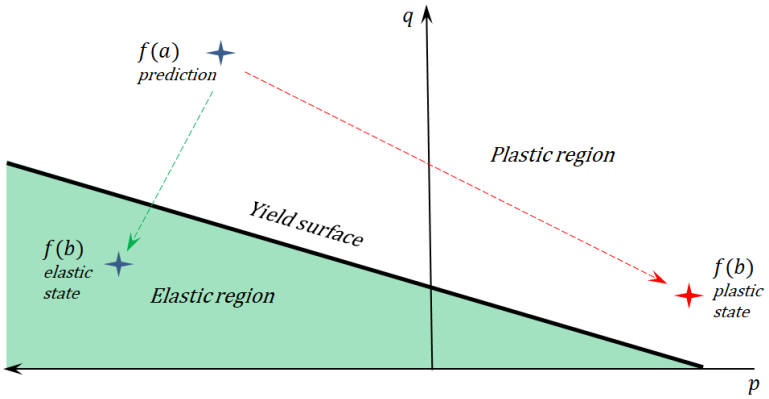

Figure 6.10: Schematic presentation of the Regula Falsi numerical failure

coming was analysed in details. The load steps were reduced as a first attempt - to simplify the problem for the computation. That solution was able to push the analysis further especially for the slope with layers inclined at 65° but not far enough. On the other side, the use of small load steps is not feasible, since it increase the computational time drastically.

Further investigation released that all three models have the same problem, which is the numerical failure in the Regula Falsi method. This method was explained in chapter 2, here is was used to compute the increment of plastic multiplier. To be specific, the yield function on both interval boundaries falls outside of the elastic region. The proof for that statement was confirmed by calculating the yield function in the integration points where Regula Falsi numerical error has occurred. Schematically, the problem is illustrated in Figure (6.10). Here, stress elastic predictor $f(a)$ brings the yield function in the plastic region and must be returned to the yield surface in the direction of the stress state where the yield function $f(b)$ becomes elastic. It is clearly seen that if $f(b)$ is placed in the plastic region it is impossible to find the intersection with the yield function, which results in the failure to return the stress on the yield surface. The first hypothesis was the wrong choice of the $\triangle\lambda$ for the point b which should bring the yield surface in the elastic region in the Regula Falsi method. However it was proved that it plays an insignificant role in the computation. The evidence is presented in Figure (6.11), here the yield function was evaluated for one of trial stress states where the failure occurs against the range of $\triangle\lambda$. It is seen that the yield function is always positive for that particular stress state. Based on the presented analysis the wrong point b choice in the Regula Falsi method was discarded.

Further investigation revealed the condition for the failure. It was discovered that one or more stress components are always in tension when the failure occurs. Additionally, the confirmation of the mean stress tension cut-off shortcoming was discovered. That type of tension treatment ensures that the mean stress is equal to or lower than the prescribed value and does not control separately each stress component. In general, corrected by mean stress tension algorithm the resultant stress vector has included components with unrealistically high tension values in one or more directions. Consequently, even though the new stress state satisfied the yield criterion it caused future numerical problem in the Regula Falsi algorithm.

The conducted investigation proofs that the alternative tension control algorithm should be considered in order to improve the results. The vital requirement is the ability to control stress components separately and not by the variable which relates all them (mean stress). Possible solution is to transform the stresses into principal directions and check if any of the components undergoes the tensile strength. In the current work that method was not implemented due to time shortage.

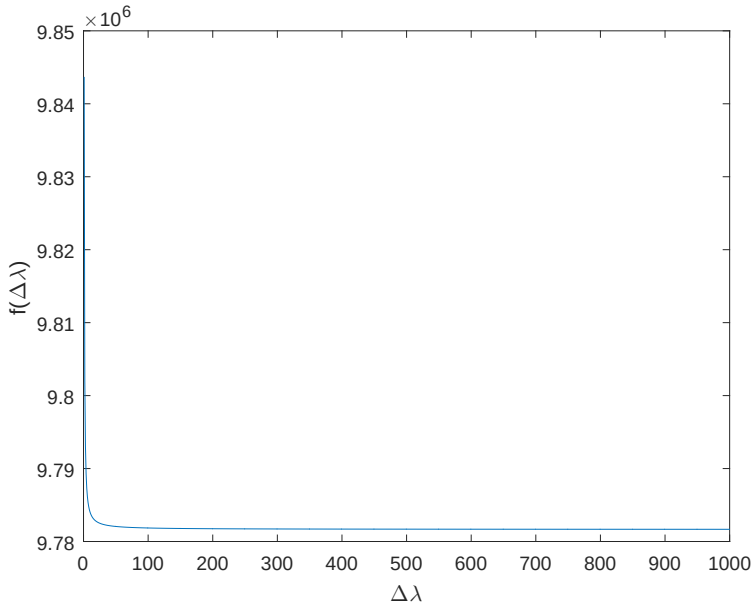

Figure 6.11: Yield function $f(b)$ versus different point b guess in the integration point where the failure in Regula Falsi occurred.

6.4. Summary

Non-linear Cosserat formulation was used for the stability analysis of jointed slope. Three layers inclinations were considered: 30° , 65° and 65° (toppling). These three examples were selected based on different failure mechanisms induced in each case. Analyses have shown fair correspondence between explicit and Cosserat models. The most pronounced effect of the Cosserat additional degrees of freedom was found for the toppling failure mechanism. The Cosserat model demonstrates the additional bending resistance due to micromoments. However, fully stability analysis was not possible to conduct due to numerical failure in the Regula Falsi method. Closer investigation revealed that a potential reason for the mentioned problem is the inefficient tension cutting algorithm. In the presented formulation the mean stress tension cut-off was implemented. The severe shortcoming of the proposed method is the inability to control each stress component separately, only by means of prescribed mean stress. An alternative approach is based on the principle stress cut-off and could have improved the results.

7

Conclusions and discussion

7.1. Conclusions

The Cosserat theory validity for the modelling of jointed rock was analysed in this thesis. The methodology that was used in order to assess the applicability includes the implementation of the Cosserat finite element formulation into the DIANA FEA software and its verification for the relevant geotechnical problems. The Cosserat theory belongs to the directed continuum theory and can consider the material microstructural order. It is achieved by means of additional "parameters" which are called directors. Directors enhance each material point of the continuum with the additional mode of movement - rotation. In the numerical formulation of the Cosserat theory it is induced by the non conventional degree of freedom, microrotation. Moreover, the supplementary governing equation and recasted constitutive relationship have to be incorporated, invoking the fundamental modifications in the finite elements formulation. The microrotation variable should not be confused with the conventional rotation degree of freedom as it is rather related to the order of the material particles ten to the global rotation of the structure.

Due to its inherent feature of the microrotations, the Cosserat theory found the application for the modelling of jointed rock e.g. [5]. Another important characteristic of the Cosserat theory is the "characteristic" length parameter which reflects the scale of the material heterogeneity. When jointed rock is the area of interest that role is simply played by the layer thickness. The particular interest of the present research was to explore the possibilities and limitations of the Cosserat theory for the jointed material modelling. Therefore, in this thesis a significant amount of time was dedicated to the implementation of the Cosserat formulation into existing finite element code DIANA FEA. Main findings were discovered during the development and test stages. They are presented below and could be generally divided into two main groups regarding elastic and plastic analysis.

Conclusions for elastic analysis

The Cosserat formulation is a smeared model which produces the continuous solution for the deformation field. However, the actual distribution of the layers is hidden from the user. In the present thesis the effect of the layers distribution was studied based on the elasticity model. Revealing the conclusion that the geometry of the suggested model should be several times larger (e.g. for conducted experiments 60) than the layer thickness in order to exclude the influence of the spatial layers distribution. For the geotechnical application this assumption is relevant, because the exact strati-

fication is not often available and usually the global behaviour of the structure is of importance. For instance, if the stability of the slope or tunnel has to be assessed then the main goal is to understand the entire contribution of the joints and estimate maximum deformations which is possible with the Cosserat formulation. The important advantage of the Cosserat formulation comparing with the explicit join model is that the coarser mesh could be used without compromising the accuracy. In the current research it was confirmed that, indeed, there are cases when layered models with elements much larger than the internal length show precise final results. Hence, it was discovered that the activation of the shearing mechanism requires to reduce the element size such that it becomes much smaller than the layer thickness. Since, the shearing involves the activation of the microrotations degree of freedom, it was concluded that the source of the problem is the inefficient representation of the non-conventional Cosserat variables in the formulation. The supporting evidences were found in the literature pointing out that the usage of the linear shape functions for microrotations requires a finer mesh. To overcome that issue the quadratic shape functions for both translations and microrotations are recommended. Another important consideration that should be accounted for the Cosserat formulation is the choice of boundary conditions. In the current thesis it was proved that there is a negligible effect of the boundary conditions in the absence of shearing. Opposite to that the final result varies in the absence/presence of microrotations boundary conditions if the shearing is activated. Due to non-trivial physical meaning of the microrotations it is not always straightforward to select the suitable boundary conditions. In general, if the symmetry takes place then the micro-rotations should be fixed across the symmetry axis.

Conclusions for plastic analysis

Together with the linear analysis the non-linear formulation was developed in the DIANA FEA software. In this thesis the Drucker-Prager plasticity formulation developed by De Borst [15] was combined with the transverse isotropic constitutive model which was proposed in the literature while applying the Cosserat theory for the modelling of jointed rock. This approach was considered by the author in order to simplify the development stage, while still having a representative behaviour of the material. The one element model was successfully verified versus standard continuum formulation, when the Cosserat parameters were adopted such that the model behaves as being homogeneous. While conducting non-linear experiments admissible for the geotechnics, two types of studies were carried out. The first one is related to the effect of material parameters. It was found that, similar to the granular material experiments, the layer thickness (internal length parameter) predominately controls the the localization region and the magnitude of the displacements in it. It was confirmed that thicker layers form wider localisation zones. Secondly, the effect of the material parameters from the yield function was investigated. Based on the preformed analyses, the following conclusion was arrived at; if the contribution from the micromoments is weighted with higher coefficient then the resistance due to bending increases. Therefore, the overall resistance of the structure grows revealing lower deformations.

Slope stability analyses considering three main failure mechanisms (planar, circular, toppling) were conducted. In order to do that the direction of the layers was adjusted accordingly. The Cosserat model shows fair correspondence with the explicit model. The effect of bending resistance were demonstrated for the slope where the toppling failure occurs.

The validation of the Cosserat theory for the modelling of jointed rock requires that the non-linear algorithm is able to correctly govern major yielding mechanisms. At least two essential of them should be considered: shearing/slipping and tension. The formulation for the former is presented in the literature, hence the latter is just mentioned briefly. In the present thesis, two possible solutions were considered: returning to apex or tension cut-off based on the mean stress. These meth-

ods were examined because they are available in the DIANA FEA software for the standard continuum formulation, thus the verification could be easily conducted. The extensive studying has manifested that the proposed solutions fail to satisfy zero tension condition. That condition means that the material does not represent tension resistance which is rather common for the geomaterials. In other words, if positive stress (positive tension convention) occurs in any of the directions, it should be equalled to nil. However that is not possible with the suggested methods, since both of them allow the existence of positive stress. The reason for that in details is explained in chapter 5. The proposed solution involves the modification of the tension cut-off algorithm which includes switching to the principal stresses space.

The achievement of the present research is the pilot implementation of the Cosserat formulation in the DIANA FEA software which could extend the range of the problem solved by that software. Furthermore, the conducted experiments allowed revealing aspects e.g convergence rate issue which should be considered to optimize computations. In addition to the identification of the problems, the explanation and possible solutions were proposed. Finally, the conducted research allows concluding that the Cosserat formulation is capable of jointed rock modelling. In order to make it fully available for the analysis, additional elaboration is necessary.

7.2. Discussion and further research

Based on the performed research the following suggestions were made for the further improvement of the existing project:

- The introduction of higher-order shape functions at least for the microrotations should improve the convergence rate when the contribution from shearing becomes significant.
- Alternative tension cut-off algorithm will better reproduce the behaviour of the rock in the tensile zone.
- Further understanding of material parameters from the Drucker-Prager yield criterion is required. Another option is to implement Mohr Coulomb yield criterion which does not consist these parameters. However, it is more elaborative and tedious.

The exiting project could be extended for more applications. As it was mentioned in the literature review, the Cosserat theory was successfully applied to prevent the mesh dependency when the strong localization occurs and the governing equation solution is not unique any more. The example of such behaviour is the softening plasticity. The incorporating of the softening algorithm will provide the capacity to study post peak behaviour in the material and estimate the residual strength of the structure.

In the present study the Drucker-Prager failure criterion is considered for the entire continuum. However, further development could be conducted if an additional failure criterion with separate strength parameters for joints is introduced. That will allow a better representation of the material itself with different parameters for the intact rock and joints.

A

A.1. Hardening/Softening parameter formulation

The formulation of the strain hardening/softening behaviour is based on the following strain-hardening hypothesis [15],

$$\dot{\boldsymbol{\kappa}} = \sqrt{\frac{\mathbf{2}}{\mathbf{3}} \dot{\boldsymbol{e}}^{\boldsymbol{p}}_{\boldsymbol{ij}} \dot{\boldsymbol{e}}^{\boldsymbol{p}}_{\boldsymbol{ij}}}, \tag{A.1}$$

where $\dot{e}^p_{ij}$ is the plastic deviatoric strain-rate tensor. Then the hardening parameter was devised in a way similar to (3.33)

$$\dot{\kappa} = \sqrt{\frac{2}{3}\left[(\dot{e}^p_{xx})^2 + (\dot{e}^p_{yy})^2 + (\dot{e}^p_{zz})^2\right] + b_1(\dot{\epsilon}^p_{xy})^2 + 2b_2\dot{\epsilon}^p_{xy}\dot{\epsilon}^p_{yx} + b_1(\dot{\epsilon}^p_{yx})^2 + b_3\left[(\dot{\gamma}^p_{xz}l)^2 + (\dot{\gamma}^p_{yz}l)^2\right]}. \tag{A.2}$$

Introducing the matrix

$$\mathbf{Q} = \begin{bmatrix} \frac{2}{3} & -\frac{1}{3} & -\frac{1}{3} & 0 & 0 & 0 & 0 \\ -\frac{1}{3} & \frac{2}{3} & -\frac{1}{3} & 0 & 0 & 0 & 0 \\ -\frac{1}{3} & -\frac{1}{3} & \frac{2}{3} & 0 & 0 & 0 & 0 \\ 0 & 0 & 0 & \frac{3}{2}b_1 & \frac{3}{2}b_2 & 0 & 0 \\ 0 & 0 & 0 & \frac{3}{2}b_2 & \frac{3}{2}b_1 & 0 & 0 \\ 0 & 0 & 0 & 0 & 0 & \frac{3}{2}b_3 & 0 \\ 0 & 0 & 0 & 0 & 0 & 0 & \frac{3}{2}b_3 \end{bmatrix} \tag{A.3}$$

enables the following form of the rate of the hardening parameter

$$\dot{\boldsymbol{\kappa}} = \sqrt{\frac{2}{3}(\dot{\boldsymbol{\epsilon}}^{\boldsymbol{p}})^{\boldsymbol{t}}\boldsymbol{Q}\dot{\boldsymbol{\epsilon}}^{\boldsymbol{p}}}. \tag{A.4}$$

Next step is to introduce the derivative of plastic strain rate

$$\dot{\boldsymbol{\epsilon}^{\boldsymbol{p}}} = \dot{\lambda}\left[\frac{\mathbf{3}\boldsymbol{P}\boldsymbol{\sigma}}{\mathbf{2}\sqrt{\mathbf{3/2}\boldsymbol{\sigma}^{\boldsymbol{t}}\boldsymbol{P}\boldsymbol{\sigma}}} + \beta\boldsymbol{\pi}\right], \tag{A.5}$$

into (A.2)then the rate of the hardening parameter $\dot{\kappa}$ is given as:

$$\dot{\kappa} = \dot{\lambda}\sqrt{\frac{\boldsymbol{\sigma}^{\boldsymbol{t}}\boldsymbol{P}\boldsymbol{Q}\boldsymbol{P}\boldsymbol{\sigma}}{\boldsymbol{\sigma}^{\boldsymbol{t}}\boldsymbol{P}\boldsymbol{\sigma}}}. \tag{A.6}$$

If the parameters a_1, a_2, a_3 and b_1, b_2, b_3 are chosen such that $\boldsymbol{PQP} = \boldsymbol{P}$ then (A.6) reduces to:

$$\dot{\boldsymbol{\kappa}} = \dot{\boldsymbol{\lambda}}. \tag{A.7}$$

B

In the presented section data and command DIANA FEA files are presented.

One element model for the Cosserat formulation

```
'DIRECTIONS'
   1   1.00000E+00   0.00000E+00   0.00000E+00
   2   0.00000E+00   1.00000E+00   0.00000E+00
   3   0.00000E+00   0.00000E+00   1.00000E+00
'MODEL'
DIMENS PLANESTRAIN
GRAVDI 2
GRAVAC  -9.81000E+00
'COORDINATES'
   1   1.00000E+00   1.00000E+00   0.00000E+00
   2   0.00000E+00   1.00000E+00   0.00000E+00
   3   0.00000E+00   0.00000E+00   0.00000E+00
   4   1.00000E+00   0.00000E+00   0.00000E+00
'MATERI'
   1 NAME "Material DP"
     MCNAME SOLROC
     MATMDL DRUCKP
     YOUNG    1.00000E+10
     POISON   0.25000E-00
     DENSIT   2.5000E+03
     POROSI   0.00000E+00
      crackb  1.0
      dsny     1e15
      dssx     1e15
      DECLIN   0.0
      AZIMUT   0.
     YIELD  DRUCKE
     TENTYP NOCTOF
```

```
     ISOHAR   1.00000E+00
     PHI      0.3400000
     PSI      0.00000E+00
     COHESI   1.00000E+04
     KAPCOH   0.00000        1.00000E+04   1.00000E+00   1.00000E+04
'GEOMET'
    1  thick  0.1
      xaxis  1. 0. 0.
'DATA'
   1 NAME   "Element data 1"
'ELEMENTS'
SET  "Sheet 1"
CONNECT
   1 Q12CO  1 2 3 4
MATERIAL 1
GEOMETRY 1
DATA 1
'LOADS'
CASE 2
NAME "Top"
DEFORM
/ 1 2 / TR 2  -2.00000E-03
'SUPPOR'
NAME "Bottom"
/1 2 3 4/ TR 2
/ 2 3 / TR 1
'END'


*FILOS
INITIA
*INPUT
*NONLIN LABEL="Structural nonlinear"
  BEGIN EXECUT
    BEGIN LOAD
      LOADNR 2
      BEGIN STEPS
        BEGIN EXPLIC
          SIZES  0.00100000(15)
        END EXPLIC
      END STEPS
    END LOAD
    BEGIN ITERAT
      MAXITE 50
      METHOD SECANT
      LINESE
      CONVER SIMULT ON
    END ITERAT
  END EXECUT
  SOLVE PARDIS
```

```
:  BEGIN OUTPUT TABULA
    BEGIN OUTPUT
    TEXT "Output"
    BINARY
    SELECT STEPS ALL /
    DISPLA TOTAL TRANSL GLOBAL
    STRAIN PLASTI VONMIS
    STRAIN PLASTI GREEN VONMIS INTPNT
    FORCE REACTI TRANSL GLOBAL
    FORCE EXTERN TRANSL GLOBAL
    STRAIN TOTAL LOCAL INTPNT
    STRAIN PLASTI LOCAL INTPNT
    STRAIN ELASTI LOCAL INTPNT
    STRESS TOTAL CAUCHY LOCAL INTPNT
  END OUTPUT
*END
```

2D homogeneous column for standard continuum

```
'DIRECTIONS'
   1   1.00000E+00   0.00000E+00   0.00000E+00
   2   0.00000E+00   1.00000E+00   0.00000E+00
   3   0.00000E+00   0.00000E+00   1.00000E+00
'MODEL'
DIMENS PLANESTRAIN
GRAVDI 2
GRAVAC  -9.81000E+00
'COORDINATES'
1   1.00000E+00   2.00000E+00   0.00000E+00
 ...
20301   1.00000E-02   1.99000E+00   0.00000E+00
'MATERI'
   1 MCNAME SOLROC
     MATMDL DRUCKP
     ASPECT
     YOUNG    1.00000E+10
     POISON   2.50000E-01
     DENSPC DRYDEN
     DENSIT   2.66000E+03
     POROSI   0.00000E+00
     YIELD  DRUCKE
     TENTYP MEANST
     ISOHAR   1.00000E+00
     COHESI   1.00000E+04
     PHI      7.50000E-01
     PSI      0.00000E+00
     TENSTR   0.00000E+00
'GEOMET'
   1 GCNAME SHEET
```

```
     GEOMDL PLSTRA
'DATA'
   1 NAME   "Element data 1"
'ELEMENTS'
SET  "Sheet 1"
CONNECT
   1 Q8EPS  2 303 601 302
   ...
20000 Q8EPS 20301 600 4 5
MATERIAL 1
GEOMETRY 1
DATA 1
'LOADS'
CASE 1
NAME "Load"
DEFORM
/ 1 4 502-600 / TR 2  -2.00000E-03
'SUPPOR'
NAME "Bot"
/ 2 3 204-302 / TR 1
/ 2 3 204-302 / TR 2
NAME "Top"
/ 1 4 502-600 / TR 1
/ 1 4 502-600 / TR 2
'END'


*NONLIN LABEL="Structural nonlinear"
  BEGIN EXECUT
    BEGIN LOAD
      LOADNR 1
      STEPS EXPLIC SIZES 0.0100000(20)
    END LOAD
    BEGIN ITERAT
      MAXITE 50
      METHOD SECANT
      CONVER SIMULT ON
    END ITERAT
  END EXECUT
  SOLVE PARDIS
  BEGIN OUTPUT
    TEXT "Output"
    BINARY
    SELECT STEPS ALL /
    DISPLA TOTAL TRANSL GLOBAL
    STRAIN TOTAL GREEN GLOBAL
    STRAIN ELASTI GREEN GLOBAL
    STRAIN PLASTI GREEN GLOBAL
    STRAIN PLASTI GREEN VONMIS
    STRAIN PLASTI GREEN VOLUME
```

```
    STRESS TOTAL CAUCHY GLOBAL
    FORCE REACTI TRANSL GLOBAL
    FORCE RESIDU TRANSL GLOBAL
  END OUTPUT
*END
```

2D homogeneous column for the Cosserat continuum

*In order to activate layers the inclination was defined by means of DECLIN parameter.

```
'DIRECTIONS'
   1   1.00000E+00   0.00000E+00   0.00000E+00
   2   0.00000E+00   1.00000E+00   0.00000E+00
   3   0.00000E+00   0.00000E+00   1.00000E+00
'MODEL'
DIMENS PLANESTRAIN
GRAVDI 2
GRAVAC  -9.81000E+00
'COORDINATES'
   1   1.00000E+00   2.00000E+00   0.00000E+00
...
1326   4.00000E-02   1.96000E+00   0.00000E+00
'MATERI'
   1 MCNAME SOLROC
     MATMDL DRUCKP
     ASPECT
     YOUNG    1.00000E+10
     POISON   2.50000E-01
     DENSPC DRYDEN
     DENSIT   2.66000E+03
     POROSI   0.00000E+00
     crackb  0.35
     dsny     1e12
:      dssx     2207.95e6
     dssx     1e12
:      DECLIN   -.2618
      DECLIN   0.0
      AZIMUT    0.
     YIELD  DRUCKE
     TENTYP NOCTOF
     ISOHAR   1.00000E+00
     COHESI   1.00000E+05
     PHI      7.50000E-01
     PSI      0.00000E+00
     KAPCOH   0.00000       1.00000E+05   1.00000E+00  1.00000E+05
'GEOMET'
    1  thick  0.1
        xaxis   1.0 0.0 0.0
'DATA'
```

```
   1 NAME   "Element data 1"
'ELEMENTS'
SET  "Sheet 1"
CONNECT
   1 Q12CO  2 78 151 77
...
1250 Q12CO  1326 150 4 5
MATERIAL 1
GEOMETRY 1
DATA 1
'LOADS'
CASE 1
NAME "Load"
DEFORM
/ 1 4 127-150 / TR 2  -2.00000E-03
'SUPPOR'
NAME "Bot"
/ 2 3 54-77 / TR 1
/ 2 3 54-77 / TR 2
NAME "Geometry support set 1"
/ 1 4 127-150 / TR 2 TR 1
'END'


*FILOS
INITIA
*INPUT
*LINSTA LABEL="Structural linear static"
  SOLVE PARDIS
  BEGIN OUTPUT
    TEXT "Output linear static analysis"
    BINARY
    SELECT LOADS ALL /
    FORCE REACTI TRANSL GLOBAL
    FORCE EXTERN TRANSL GLOBAL
    DISPLA TOTAL TRANSL GLOBAL
    STRAIN TOTAL LOCAL
  END OUTPUT
:*END
*NONLIN LABEL="Structural nonlinear"
  BEGIN EXECUT
    BEGIN LOAD
      LOADNR 1
      BEGIN STEPS
        BEGIN EXPLIC
         SIZES 0.05(20)
           ARCLEN OFF
        END EXPLIC
      END STEPS
    END LOAD
```

```
    BEGIN ITERAT
      MAXITE 80
      METHOD SECANT
      BEGIN CONVER
      SIMULT ON
      FORCE TOLCON 0.01
      END CONVER
    END ITERAT
  END EXECUT
  SOLVE PARDIS
  BEGIN OUTPUT
    TEXT "Output"
    BINARY
    SELECT STEPS ALL /
    FORCE REACTI TRANSL GLOBAL
    FORCE EXTERN TRANSL GLOBAL
    DISPLA TOTAL TRANSL GLOBAL
    STRAIN TOTAL LOCAL
    STRAIN PLASTI LOCAL
    STRAIN ELASTI LOCAL
    STRESS TOTAL CAUCHY LOCAL
    STRAIN PLASTI VONMIS
  END OUTPUT
*END
```

Bibliography

[1] DIANA FEA v10.1. URL https://dianafea.com/.

[2] Roscience Inc. RS^2 v2.9. URL https://www.rocscience.com/rocscience/products/rs2.

[3] RS^2 (*Phase^2*), Estimating joint stiffness. URL https://www.rocscience.com/help/phase2/webhelp9/theory/Estimating_Joint_Stiffness.htm.

[4] Deficiencies in the Ubiquitous joint model of layered rocks. In *"Rock Mechanics in Civil and Environmental Engineering"*, pages 165–168. CRC Press, 2010.

[5] D. P. Adhikary and A. V. Dyskin. A Cosserat continuum model for layered materials. *Computers and Geotechnics*, 20(1):15–45, 1997.

[6] D.P. Adhikary, A.V. Dyskin, R.J. Jewell, and D.P. Stewart. A study of the mechanism of flexural toppling failure of rock slopes. *Rock Mechanics and Rock Engineering*, 30(2):75–93, 1997.

[7] T. Aste, T. Di Matteo, and A. Tordesillas. *Granular and Complex Materials*. World Scientific, Singapore, 2007.

[8] Zdenek P Bazant and Byung H Oh. Microplane model for fracture analysis of concrete structures. Technical report, NORTHWESTERN UNIV EVANSTON IL TECHNOLOGICAL INST, 1983.

[9] R. Burden and J. Faires. *Numerical Analysis*. Available Titles CengageNOW Series. Cengage Learning, 2004. ISBN 9780534392000.

[10] X. Chen and Z. P. Bažant. Microplane damage model for jointed rock masses. *International Journal for Numerical and Analytical Methods in Geomechanics*, 38(14):1431–1452, 2014.

[11] A. Cosserat and F. Cosserat. *Théorie des Corps Déformables*. Hermann, Paris, 1909.

[12] Peter A Cundall. UDEC-A generalised distinct element program for modelling jointed rock. Technical report, CUNDALL (PETER) ASSOCIATES VIRGINIA WATER (ENGLAND), 1980.

[13] Peter A Cundall and Otto DL Strack. A discrete numerical model for granular assemblies. *geotechnique*, 29(1):47–65, 1979.

[14] R. de Borst. Simulation of strain localization: A reappraisal of the Cosserat Continuum. *Eng. Comp*, 8(4):317–332, 1991.

[15] R. de Borst. A generalisation of J2-flow theory for polar continua. *Computer Methods in Applied Mechanics and Engineering*, 103(3):347–362, 1993.

[16] R. de Borst and H.B. Mühlhaus. Continuum Models for Discontinuous Media. In *RILEM Symp. on Fracture Mechanics of Brittle Disordered Materials*, Noordwijk (NL), 1991.

[17] R. de Borst and L.J. Sluys. Localisation in a cosserat continuum under static and dynamic loading conditions. *Computer Methods in Applied Mechanics and Engineering*, 90(1-3):805–827, 1991.

[18] V. A. Eremeyev, L. P. Lebedev, and H. Altenbach. *Foundations of micropolar mechanics*. Springer, 2013.

[19] A.C. Eringen. *Microcontinuum field theories*. Springer, New York, 1999.

[20] M. Godio, I. Stefanou, K. Sab, and J. Sulem. Dynamic finite element formulation for Cosserat elastic plates. *International Journal for Numerical Methods in Engineering*, 101(13):992–1018, 2015.

[21] Richard E Goodman, Robert L Taylor, and Tor L Brekke. A model for the mechanics of jointed rocks. *Journal of Soil Mechanics & Foundations Div*, 1968.

[22] Evert Hoek, (joint author.) Bray, John, Institution of Mining, and Metallurgy (Great Britain). *Rock slope engineering*. London : Institution of Mining and Metallurgy, revised 2nd ed edition, 1977. Previous ed.: 1974.

[23] A. Hudson and C. Fairhurst. Continuum models for layered and blocky rock. In *Comprehensive rock engineering*, volume 2, chapter 8, pages 209–230. Pergamon press, 1993.

[24] John A Hudson. *Engineering rock mechanics: part 2: illustrative worked examples*. Elsevier, 2001.

[25] Lanru Jing and JA Hudson. Numerical methods in rock mechanics. *International Journal of Rock Mechanics and Mining Sciences*, 39(4):409–427, 2002.

[26] W.T. Koiter. Couple-stresses in the theory of elasticity, i and ii. *Proc. Kon. Nederl. Akad. Wetensch*, 67:17–44, 1964.

[27] JCS Long, JS Remer, CR Wilson, and PA Witherspoon. Porous media equivalents for networks of discontinuous fractures. *Water Resources Research*, 18(3):645–658, 1982.

[28] P.B. Lourenço, R. De Borst, and J.G. Rots. A plane stress softening plasticity model for orthotropic materials. *International Journal for Numerical Methods in Engineering*, 40(21):4033–4057, 1997.

[29] H. Mühlhaus and E. C. Aifantis. A variational principle for gradient plasticity. *International Journal of Solids and Structures*, 28(7):845–857, 1991.

[30] H. Mühlhaus and I. Vardoulakis. The thickness of shear bands in granular materials. *Geotechnique*, 37(3):271–283, 1987.

[31] H.B. Muhlhaus. Exfoliation phenomena in pre-stressed rock. In C. Fairhurst, editor, *Rockbursts and Seismicity in Mines*.

[32] A. Needleman. Material rate dependence and mesh sensitivity in localization problems. *Computer Methods in Applied Mechanics and Engineering*, 67(1):69–85, 1988.

[33] M. Oda, H. Kazama, and J. Konishi. Effects of induced anisotropy on the development of shear bands in granular materials. *Mechanics of Materials*, 28:103–111, 1998.

[34] G Pande, Georgnot Beer, and J Williams. Numerical methods in rock mechanics. 1990.

[35] H. Ramézani, J. Jeong, and Z.-Q. Feng. On parallel simulation of a new linear Cosserat elasticity model with grid framework model assumptions. *Applied Mathematical Modelling*, 35(10): 4738–4758, 2011.

[36] R.A.Toupin. Theories of elasticity with couple-stress. *Archive for Rational Mechanics and Analysis*, 17:85–112, 1964.

[37] A. Riahi. 3D Finite Element Cosserat Continuum simulation of layered geomaterials, 2008. PhD thesis.

[38] A. Riahi and J. H. Curran. Full 3D finite element Cosserat formulation with application in layered structures. *Applied Mathematical Modelling*, 33(8):3450–3464, 2009.

[39] A. Riahi and J.H. Curran. Comparison of the Cosserat Continuum approach with finite element inteface models in a simulation of layered materals. *Scientia Iranica*, 17(1):39–52, 2010.

[40] J.W. Rudnicki and J.R. Rice. Conditions for the localization of deformation in pressure-sensitive dilatant materials. *Journal of the Mechanics and Physics of Solids*, 23(6):371–394, 1975.

[41] H. F. Schweiger, V. Galavi, and F. Scharinger. Application of a multilaminate model for soils to practical boundary value problems. In *12th International Conference on Computer Methods and Advances in Geomechanics 2008*, volume 1, pages 101–109, 2008.

[42] P. Steinmann. A micropolar theory of finite deformation and finite rotation multiplicative elastoplasticity. *International Journal of Solids and Structures*, 31(8):1063–1084, 1994.

[43] S. Timoshenko. *Theory of Elasticity*. Engineering societies monographs. McGraw-Hill, 1934.